

NASA/TM-2001-210846



Structural Testing of a Stitched / Resin Film Infused Graphite-Epoxy Wing Box

*Dawn C. Jegley and Harold G. Bush
Langley Research Center, Hampton, Virginia*

National Aeronautics and
Space Administration

Langley Research Center
Hampton, Virginia 23681-2199

April 2001

Available from:

NASA Center for AeroSpace Information (CASI)
7121 Standard Drive
Hanover, MD 21076-1320
(301) 621-0390

National Technical Information Service (NTIS)
5285 Port Royal Road
Springfield, VA 22161-2171
(703) 605-6000

Acknowledgements

The authors wish to express their thanks to William R. Doggett, William S. Small, and Cheri L. Bailey of NASA Langley Research Center and Byron L. Stonecypher of Wyle Laboratories for their support in the testing of the stitched semi-span wing.

Abstract

The results of a series of tests conducted at the NASA Langley Research Center to evaluate the behavior of an all-composite full-scale wing box are presented. The wing box is representative of a section of a 220-passenger commercial transport aircraft wing box and was designed and constructed by The Boeing Company as part of the NASA Advanced Subsonics Technology (AST) program. The semi-span wing was fabricated from a graphite-epoxy material system with cover panels and spars held together using Kevlar stitches through the thickness. No mechanical fasteners were used to hold the stiffeners to the skin of the cover panels. Tests were conducted with and without low-speed impact damage, discrete source damage and repairs. Up-bending, down-bending and brake roll loading conditions were applied. The structure with nonvisible impact damage carried 97% of Design Ultimate Load prior to failure through a lower cover panel access hole.

Introduction

One of NASA's goals is to reduce the cost of air travel by 50% in the next 20 years. To achieve this goal, NASA has been involved in the development of the technologies needed for future low-cost, light-weight composite structures for commercial transport aircraft. As a consequence of this effort, a stitched graphite-epoxy material system has been developed with the potential for reducing the weight and cost of commercial transport aircraft wing structure. By stitching through the thickness of a dry graphite-epoxy material system, the labor associated with wing cover panel fabrication and assembly can be significantly reduced. By stitching through the thickness of pre-stacked skin and then stitching together stringers, intercostals and spar caps with the skin, the need for mechanical fasteners is almost eliminated. This manufacturing approach reduces part count, and therefore, cost of the structure.

In order to explore fully the manufacturing aspects of this new material system, a 41-foot-long wing box was fabricated by the Boeing Company under contract NAS1-20546 as part of the NASA Advanced Subsonic Technology Program. A complete description of the wing box is presented in reference 1 and a summary of the NASA/Boeing program is presented in reference 2.

This wing box represents the load-carrying wing box of a 220-passenger commercial transport aircraft. Though originally conceived as a manufacturing development article since the stitched, resin-filled-infusion (RFI) process had never been used on a composite structure of this size and complexity, the wing was designed to withstand loads associated with several flight conditions. The most critical conditions to be examined were -1G downbending, 2.5G upbending and a brake roll runway condition where twist is applied through the simulated landing gear leg. The wing box was loaded in a series of tests covering all three load conditions and then loaded to failure at the NASA Langley Research Center. Included in the test series were tests to evaluate the behavior of the wing box when subjected to nonvisible impact damage, discrete source damage and repair. A photograph of the wing prior to testing is shown in figure 1. Nine load introduction locations are shown in the figure and load was applied by pushing up on the wing or pulling down on the wing, depending on the load case.

Wing-Box Test-Specimen Description

The wing box upper and lower cover panels and the front and rear spars were fabricated from stitched/resin film infused graphite-epoxy material, minimizing the number of mechanical fasteners needed to assemble the wing box. The composite upper cover skin and upper cover blade-stiffeners were composed of layers of graphite material forms that were prekitted in nine-ply stacks using Hercules, Inc. AS4 fibers. Each nine-ply stack had a $[45/-45/0_2/90/0_2/-45/45]_T$ laminate stacking sequence and was approximately 0.055-inches thick. The composite lower cover panel skin was composed of 0-degree layers of Hercules, Inc. IM7 fibers and ± 45 and 90 degree layers made from AS4 fibers. Prekitted stacks were assembled in the same way as for the upper cover panel skin. Several stacks of the prekitted material were used to build up the desired thickness at each location. Skin thickness ranged from 0.11 to 0.605 inches. Upper cover stringer blades ranged in thickness from 0.44 to 0.605 inches. Braided stringers, as described in reference 1, using AS4 fibers were used in the lower cover panel. Braided stringer blades ranged in thickness from 0.48 to 0.768 inches and contain ± 60 degree braids. All material was stitched together using E. I. DuPont de Nemours, Inc. Kevlar thread. Stiffener flanges for stringers in the spanwise direction, intercostals in the chordwise direction and spar caps along the forward and aft edges of the cover panels were stitched to the skin and no mechanical fasteners were used for joining. The composite wing box was fabricated using Hercules, Inc. 3501-6 epoxy in a Resin Film Infusion (RFI) process which is described in references 3 and 4. Stitched graphite-epoxy spars with the same stacking sequence and material as the upper cover panel skin were mechanically attached to the spar caps and tape-laid graphite-epoxy ribs were mechanically fastened to the intercostals to create the 41-foot-long wing box. Sketches of the upper and lower cover panels are shown in figures 2a and 2b, respectively. Eighteen ribs and ten stringers are identified by number and letter, respectively, in figure 2. Holes are identified by hole number starting with the most inboard hole.

The upper and lower cover panels each include five stringer terminations or runouts. The locations of these runouts are shown in figure 2. Details of the construction of these runouts are shown in figures 3 and 4. Blade and flange thicknesses are reduced by removing two stacks of material at a time, at three-inch intervals in all runouts. Runout locations are listed in table 1. The lower cover stringer terminating at rib 4 and the upper cover stringers terminating at ribs 4 and 15 have a constant height blade and terminate with the stringer by folding the last two stacks of material against the intercostal as shown in figure 3. Lower cover stringers terminating at ribs 8, 10, and 15 and the upper cover stringers terminating at rib 9 have a tapered height blade. The upper cover panel blade height is tapered from a maximum of between 2.5 and 3.25 inches to zero at a taper angle of 8 degrees. The lower cover panel blade height is tapered from a maximum of between 2.65 and 3.5 inches to zero at a taper angle of 11 degrees. A sketch of a tapered blade is shown in figure 4.

Finally, load introduction hardware was attached to the wing box prior to shipment to NASA Langley Research Center. The load introduction hardware included fixtures at each of the eight vertical actuator attachment locations, shown in figure 1 as locations 1-8. The purpose of these fittings was to distribute the actuator load over a sufficient area to eliminate the possibility of a load introduction failure. Metal landing gear doublers were added to the upper and lower cover panels to allow the distribution of shear load into the wing cover panels during the brake roll test condition. Finally, the root mount transition box was added to provide a method of attaching the wing box to the load wall in the test facility. Upon installation at the test facility, a simulated landing gear leg was attached to the doubler assembly through the use of two 9-inch diameter steel bolts. This simulated landing gear leg allowed the loads to be introduced into the wing box in a manner similar to the way they would be introduced on a real aircraft. The simulated landing gear leg assembly is shown as location 9 in figure 1.

Mounting and Loading Apparatus

Each actuator/load cell assembly 1-9 was connected to the floor and to the test article by use of swivels which would allow the actuator to rotate as the wing box deforms. This rotation prevented the introduction of localized bending loads into the wing lower surface at load introduction points 1-8 shown in figure 1. A sketch of the loading assembly for actuator 2 at the wing tip is shown in figure 5. All other vertical loading assemblies have the same arrangement as the one for actuator 2. The landing gear region includes three actuator assemblies as shown in figure 6. The actuator 9 assembly was initially located at an angle of 53.6 degrees to the floor and parallel to the test wall. One end was attached to the floor and the other was attached to the simulated landing gear leg. Swivels allowed the 53.6-degree angle to increase as load was applied. The actuator 10 assembly was parallel to the floor with one end attached to the test facility wall and one end attached to the simulated landing gear leg. Actuator 7 was positioned vertically underneath the lower cover doubler. At any given time, either actuator 7 or actuators 9 and 10 were connected to the test article.

Loading Sequence

The test article was subjected to eight tests with three load conditions as listed in table 2. These conditions are "brake roll," -1G and 2.5G. The brake roll load condition simulates a runway condition in which forces are applied primarily through the landing gear leg. A maximum load of 124,000 lb was applied to the simulated landing gear leg at location 9 while simultaneously applying smaller loads at locations 1-6 and 8 in figure 1. The -1G and 2.5G load conditions simulate extreme flight loading conditions. The wing tip is pulled down to simulate a -1G flight maneuver and pushed up to simulate a 2.5G flight maneuver. The values of load at Design Limit Load (DLL) for each of these load conditions are shown in table 3 for all the load introduction points. Positive values in the table refer to pushing up on the wing and negative values refer to pulling down on the wing. Since these values simulate flight conditions, a combination of pushing up and pulling down is required in each load condition to achieve the desired wing motion.

All actuators were active during all load conditions except the actuators at the landing gear region. These actuators, as shown in figure 6, are actuators 7, 9 and 10. Actuator 7 was active only in the flight condition loadings and actuators 9 and 10 were active only for the brake roll condition loadings.

A series of 8 tests were conducted as listed in table 2. First the test article was configured for ground condition testing, with actuators 9 and 10 attached to the simulated landing gear. The wing was subjected to two brake roll tests, a 50% DLL test to verify accurate function of all components and instrumentation, followed by a 100% DLL test. Then actuators 9 and 10 were disconnected and actuator 7 was connected to allow the flight condition loadings. Two more 50% DLL loadings were conducted to verify the accurate function of all components and instrumentation for the -1G and the 2.5G flight conditions. Then the wing was loaded to 100% DLL in each of these conditions.

After successful completion of all 100% DLL tests, discrete source damage was inflicted on the upper and lower cover panels of the wing. The wing was loaded to 70% DLL in the 2.5G upbending condition and unloaded. Finally, the discrete source damage was repaired, six nonvisible impacts were inflicted, and the wing was loaded to failure in the 2.5G upbending condition.

Controls and Data Acquisition

A computer control system and an independent computer data acquisition system were used during testing. The loading of the wing was controlled by a Labview/VXI control system. All actuators except actuator 10 were controlled to load at a specified load rate. Loading was increased slowly to a maximum with all actuators reaching the maximum loading simultaneously. Load rates varied among the different tests, but generally tests were planned to run for 15-30 minutes. Feedback signals were sent to the control system to keep the actuators loading evenly throughout each test.

Actuator 10 was controlled to keep its elongation a specified fraction of the elongation of actuator 9. This procedure was used because the simulated landing gear leg was not stiff enough to deform rigidly as actuator 9 extended. Therefore, actuator 10 was added in the horizontal position. The goal in adding actuator 10 was to keep the landing gear leg straight as the wing was twisted in the brake roll condition. The analysis described in reference 5 was used to determine that actuator 10 should shorten 0.238 inches when actuator 9 reached the predicted displacement of 2.81 inches at DLL.

A MODCOMP open-architecture data acquisition system with NEFF signal conditioners and a UNIX-based operating system was used to record data from all instrumentation. Data was recorded at the rate of once every second as load was applied during each test.

Instrumentation

Displacements were measured at each actuator location and at the two points on the lower surface where the root transition box connected to the composite box at the front and rear spar using displacement transducers. 466 strain gages were used to record strains all over the test article. Interior gages were positioned during assembly of the test article. Exterior gages were positioned after the test article was attached to the backstop in the test laboratory. General location of critical strain gages for the upper and lower cover panels are shown in figures 7 and 8 respectively. Details of gage locations are shown in figures 3 and 4 for stringer runouts, figure 9 for the main landing gear region, figure 10 for the front and rear spars, and figure 11 for ribs 1-10. Locations of gages in the vicinity of discrete source damage and impact damage sites are shown in figures 12 and 13, respectively. Locations of gages in the vicinity of upper and lower cover panel repairs are shown in figure 14. Strain gages shown at the access holes are on the edge of the hole at the midplane, not on the cover panel surface. All other gages were placed on the skin or blade surface. All strain gages were in place for multiple tests except those at the damage sites, repairs, and lower cover access holes.

Impact and Discrete Source Damage

An air-propelled steel projectile was used to inflict three impacts with an energy level of 83-84 ft-lb to the lower cover panel. The locations of these damage sites are shown in figure 2. A steel sphere with a 0.5-inch diameter was accelerated to a speed of approximately 545 ft/sec, resulting in the damage shown in figure 15. Impact damage at rib 4 is shown in figure 15a, impact damage at rib 8 is shown in figure 15b, and impact damage at rib 12 is shown in figure 15c. The dots surrounding the impact site are the limits of the damage, as determined by ultrasonic scans taken immediately after damage was inflicted and before loading. The damage was clearly visible to the eye and the extent of the damage as determined by using NDE was up to 2.75 inches in length, around the impact site. Dent depths up to 0.135 inches were measured. Details of the impacts are shown in table 4.

Impact damage was induced by the use of a dropped-weight and an air-powered projection mechanism. Impact damage was inflicted to the upper and lower surfaces of the wing. A dropped-weight impactor was used to inflict three impacts with an energy level of 100 ft-lb to the upper cover panel. The locations of these damage sites are shown in figure 2. A weight of 25 lb with a 1-inch diameter tup was dropped vertically from 4 feet, resulting in the damage shown in figure 16. Impact damage between ribs 4 and 5 is shown in figure 16a, impact damage at rib 9 is shown in figure 16b, and impact damage at rib 13 shown in figure 16c. The dots surrounding the impact site in each figure are the limits of the damage, as determined by ultrasonic scans taken immediately after damage was inflicted and before wing loading. The damage was barely visible to the eye and the extent of the damage as determined by using NDE ranged from 1.4 inches to 2.5 inches in diameter around the impact site. The depth of the damage was also measured and ranged from .01 to .05 inches. A description of the upper cover damage is given in table 5.

The wing was subjected to discrete source damage in the form of seven-inch-long sawcuts to the upper and lower cover. Each sawcut ran through two stinger bays and cut through a stringer, as shown in figure 12. Since the upper cover panel is loaded in compression in the 2.5G loading, the sawcut was widened to keep the edges from closing up and touching during the test. Sawcut width was not critical but the tip radius of 0.1 inches was required for both sawcuts. Photographs of the sawcuts are shown in figure 17.

Repairs

Metal patch repairs were used to restore the wing to full load-carrying capability after test 7 in which the test article was subjected to load in the presence of discrete source damage. The region of damage was removed then the repairs added. The repairs consisted of a metal plate which conformed to the wing surface on the outer surface of the cover panels and internally spliced stringers. All parts of the repair were attached to the wing with mechanical fasteners. Sketches of the repairs are shown in figure 14. Photographs of the repairs are shown in figure 18.

Results and Discussion

Results are shown herein for all load conditions. Results for the 50% DLL tests, identified as tests 1, 3 and 4 in table 2, are not presented since these tests provide information that is already captured in the 100% DLL tests, identified as tests 2, 5 and 6 in table 2. Results are shown first for the brake roll condition (test 2 in table 2), then the -1G flight condition (test 5), then the 2.5G flight conditions (test 6, 7, and 8). The final failure of the test article is then described. Not all results from all gages are presented; however, results for all gages that either recorded high strains or indicated a nonlinear behavior of the test article are shown.

In all the figures, loads less than zero indicate pulling down on the test article and loads greater than zero indicate loads pushing up on the test article. Similarly, displacements less than zero and greater than zero indicate downward and upward displacements, respectively. However, this motion up or down is the elongation or contraction of the actuator rather than a measurement perpendicular to the floor. Since the initial position of all actuators except for actuators 9 and 10 is vertical, the difference between the displacement upward or downward perpendicular to the floor and the stroke of the actuator is dependent upon the rotation of the actuator during loading. The largest displacement (and largest rotation) is for actuator 2 at the wing tip. The measured deflection is 40 inches and the initial position of the intersection of the actuator assembly and the test article is 168 inches above the floor. The angle between the initial vertical position of the actuator and the final tilted position can be calculated to be less than 2 degrees, resulting in a negligible difference between vertical displacement and stroke (see ref 5). Strain results

presented herein follow a similar convention in that negative is compressive and positive is tensile. All strain results are plotted against the largest load in that test, i.e., from actuator 9 in the brake roll condition and actuator 2 in the -1G and 2.5G conditions.

Brake Roll Loading

Load corresponding to DLL in the brake roll configuration was applied to the test article. The loads presented in table 3 are the programmed loads at DLL. A comparison between this load and the actual applied load is shown in figure 19. The error at each load introduction location is also shown. The applied load in the most heavily loaded actuator was greater than the programmed load by approximately 3.9 percent due to an initial calibration error. The calibration error only effected the actuator 9 load cell. The applied load in each of the more lightly loaded actuators was within 10% of its programmed load and within 1% of the maximum load cell capacity (maximum error of 200 lb).

The loads for the brake roll condition induce twist into the test article as can be seen from the displacements along the front and rear spars at DLL as shown in figure 20. Dashed lines represent the displacement of the rear spar and solid lines represent the displacement of the front spar. Displacements were measured at each active vertical actuator location and at the root rib. All measurement locations are shown in figure 2b except at the landing gear leg which is shown in figure 5. The curves shown are a spline fit between the measured data points.

These displacements are approximately vertical (normal to the floor). The largest measured displacement was at actuator 9 and was 3.9 inches. This dimension represents the elongation of the actuator, as the angle to the floor changed from 53.6 degrees to approximately 54 degrees, as described in reference 5. At 54 degrees the wing moved vertically approximately 3.1 inches. All displacements increased linearly as load was applied, except at the landing gear leg, as shown in figure 21. The load-displacement relationship at the base of the landing gear leg, location 9, is nonlinear with a magnitude more than three times that of any other actuator. The displacement measured at actuator 10 is also shown. This displacement is perpendicular to the test wall and parallel to the floor. The maximum value of this displacement is 0.01 inches.

Nonlinear or large strains measured during brake roll loading are shown in figures 22-30. All measured strains not shown are linear and do not exceed 0.005 in./in. Measured strains at the edges of the lower cover panel access holes indicate that high strains occur at these locations. These strains are shown in figure 22 and the gage locations are shown in figure 7. In the figure strains at hole 1 are represented by the solid lines and strains at hole 3 are represented by long dashed lines. Strains at holes further outboard are represented by progressively shorter dashes. Strains at inboard corners are represented by open symbols and strains at the outboard corners are represented by filled symbols. The maximum measured strain is -0.0049 in./in. at DLL and is at access hole 1, between ribs 2 and 4. All access hole edge strains increase linearly as load is increased.

The test article contains five upper cover stringer runouts and five lower cover stringer runouts as shown in figures 2 and 3. Each stringer runout terminates as it approaches the front or rear spar. These runouts are identified by the rib at which they terminate and their location front or aft. Measured strains at lower and upper cover stringer runouts are shown in figures 23 and 24, respectively. In these figures the length of the dashes is used to differentiate among runout locations. Symbols represent locations at each runout. Open symbols represent gages on the interior surface of the test article. Filled symbols represent strains on the exterior surface of the test article. The strain gage locations are shown in figures 3 and 4. The largest runout strains are at the rear spar at rib 9 in the upper and at rib 8 in the lower cover

panel. These runouts are just outboard of the landing gear doubler plates. Measured strains are less than 0.001 in./in. in magnitude.

Measured strains in the Main Landing Gear (MLG) region are shown in figures 25-27. Strains in the upper and lower cover panels are shown in figures 25 and 26, respectively. Strains in the main landing gear doublers are shown in figure 27. From the strain gage locations shown in figure 9, strain data on the upper cover panel at locations A-E are shown in figure 25, on the lower cover panel at locations F-K are shown on figure 26 and data from doubler gages A-H are shown on figure 27. Interior strains are represented by open symbols while exterior strains are represented by filled symbols. Most gages in this region record small strain and the strain increases linearly with load. The largest upper cover strain measured in the MLG region is in a rosette on the external skin surface 1.5 inches inboard from the doubler plate midway between stringers F and G. This rosette is shown as location A in figure 25. The largest strain is from the 45-degree branch of the rosette, shown as gage A1. Strain does not exceed 0.0025 in./in. in magnitude, however strains in all branches of the rosette display nonlinear behavior in the form of discontinuities in the slope of the load-strain curve at a loads greater than 70 kips.

Strain does not exceed 0.0025 in./in. in magnitude in the MLG region of the lower cover panel. Gages F1, F2, G, and I are on the intercostals. Gages F1, G and I are at an angle of 45 degrees to the edge of the intercostal. Only the strain gage on the intercostal of rib 5, location G, displays nonlinear behavior in the lower cover in this region.

Strains in the doubler plates remain less than 0.0005 in./in. in magnitude but strains at locations B, C, E, F, and G are erratic. Upper doubler strains are represented by dashed lines and lower doubler strains are represented by solid lines. All gages on the doublers are on the external surface.

Measured strains in the upper and lower cover splice between the root transition box and the composite box are shown in figure 28. The strain gage locations are shown in figures 7 and 8. Open symbols represent lower cover panel strains, filled symbols represent strains on upper cover panel and half-filled symbols represent strains on the root transition box. Strains are nonlinear in the lower cover panel between the spar cap and stringer J and in the lower splice at the rear spar and in the upper splice at stringer I. Strains shown on the root transition box are near the rear spar. Strains measured at these splice locations are small but nonlinear.

Measured strains in all ribs and both spars are small and linear except for the ribs near the wing root and the root region of the rear spar. Strains for ribs 1-3 and the rear spar are shown in figures 29 and 30, respectively. Strain gage locations for the ribs are shown in figure 11. Open symbols represent strains measured on rib 2. Filled symbols represent strains measured on rib 3 and half-filled symbols represent strains on rib 1. Continuous and dashed lines are used to indicate strain gage positions. Strain gage locations for the rear spar are shown in figure 10. Nonlinear behavior is seen at gages in the rib web in the 45-degree direction in ribs 1 and 2 and at the edge of the access hole in rib 3. Strains in the rear spar near the MLG are nonlinear near the upper and lower edges of the spar near the root. The strain at the spar vertical center at rib 5 is typical of the measured strains in the spar and is shown for comparison. Measured strains in these ribs and the spars are less than 0.001 in/in.

No evidence of permanent damage was observed due to brake roll loading to DLL.

-1G Flight Loading

Load corresponding to DLL in the -1G configuration was applied to the test article. A photograph of the test article loaded in this manner is shown in figure 31. The loads presented in table 3 are the programmed loads at DLL. A comparison between this load and the actual applied load is shown in figure 32. The error at each load introduction location is also shown. The applied (measured) load in the most heavily loaded actuator was 2.0 % greater than the programmed load (an error of 600 lb). The applied loads in all the more lightly loaded actuators were within 12% of the programmed load and are within 2% of the maximum load capacity (a maximum error of 300 lb).

These loads cause the wing tip to bend downward and induce a small twist into the test article as can be seen from the displacements along the front and rear spars at DLL as shown in figure 33. These displacements are approximately vertical. Dashed lines represent the displacement of the rear spar and solid lines represent the displacement of the front spar. Maximum measured displacement was at actuator 2 and was 13 inches downward. All displacements increased linearly as load was applied, as shown in figure 34. Displacements are shown at each actuator location and at the root rib. All measurement locations are shown in figure 2b.

Strain data measured during the -1G loading are shown in figures 35-44. All strains for the -1G load condition are plotted against the load in actuator 2. All measured strains not shown are linear and do not exceed 0.005 in./in.

Measured strains at the edges of the lower cover panel access holes indicate high strain occur at these locations. These strains are shown in figure 35. Strain gage locations are shown in figure 7. In the figure strains at hole 1 are represented by the solid lines and strains at hole 3 are represented by long dashed lines. Holes further outboard are represented by shorter dashes. Strains at inboard corners are represented by filled symbols and strains at the outboard corner are represented by open symbols. The largest measured strain is at access hole 4 between ribs 8 and 9 and was approximately -0.0032 in./in. at DLL. These strains increase linearly as load is increased.

Measured strains at lower and upper cover runouts are shown in figures 36 and 37, respectively. These runouts are identified by the rib at which they terminate and by their front or aft location. In the figure the length of the dashes is used to differentiate among runout locations. Symbols represent locations at the runouts. Open symbols represent gages on the interior surface of the test article. Filled symbols represent strains on the exterior surface of the test article. Strain gage locations are shown in figures 3 and 4. The lower cover is loaded in compression in this loading condition, so all measured strains at runout locations are negative. All lower cover strains at runouts are approximately linear and no strain exceeds -0.003 in./in. in magnitude, indicating no damage occurred in the runouts during this loading. The maximum strains are in the runout at the rear spar at rib 8. The upper cover is loaded in tension in this loading condition, so all measured upper cover strains at runout locations are positive. All upper cover strains at runout locations are approximately linear and no strain exceeds .002 in./in. in magnitude, indicating no damage occurred in the runouts during this loading. The maximum strains are at the runout location at the rear spar at rib 9.

Measured strains in the main landing gear (MLG) region are shown in figures 38-40. Strains in the upper and lower cover panels are shown in figures 38 and 39, respectively. Strains in the main landing gear doublers are shown in figure 40. Strain gage locations are shown in figure 9. In the figure open symbols represent strain on the internal surface of the test article. Filled symbols represent strain on the external surface of the test article. All measured strains in the upper cover MLG region are linear and

none exceed 0.0015 in./in. However, strains at location F on the lower cover intercostal at rib 5 (figure 38) and at location E on the upper cover doubler (figure 40) are nonlinear and show discontinuities in the slope of the load-strain curve. Upper cover doubler strains are represented by dashed lines and lower doubler strains are represented by solid lines.

Measured strains in the upper and lower cover splice between the root transition box and the composite box are shown in figure 41. Strain gages locations are shown in figures 7 and 8. Strain gages are located on the composite and metal parts and on the inside and outside of the test article. Upper cover strains are represented by filled symbols, lower cover strains are represented by open symbols and root transition box strains are represented by half-filled symbols. Strain in the upper cover panel stringer I displays nonlinear behavior. However, strain gages are also present at stringers A and F and near the rear spar and these gages do not display nonlinear behavior. All measured strains in the root splice region of the lower cover are linear except at the blade of stringer D.

Measured strains in all ribs are small but some rib strains display nonlinearity. Strains measured in ribs 4 and 5 indicate bending of these ribs, as shown in figures 42 and 43. In these figures gage locations are distinguished using line type. Back-to-back strain gages show separation from the onset of loading, indicating the rib is bending locally. The location of these gages is on the rib surface adjacent to central access holes, as shown in figure 11. All rib strains remain between -0.001 and +0.001 in./in. Measured strains in the front and rear spars are linear and with maximum values between -0.002 and 0.004 in./in.

No evidence of permanent damage was apparent due to -1G loading to DLL.

2.5G Flight Loading

Loading

Three loadings of the test article in the 2.5G load condition are discussed herein. Load corresponding to DLL in the 2.5G configuration was applied to the undamaged test article in test 6. Load corresponding to 70% DLL in the 2.5G configuration was applied to the sawcut-damaged test article in test 7. Load corresponding to DUL, or 150% DLL, was programmed into the control system to be applied to the repaired test article in test 8. A photograph of the test article at maximum load is shown in figure 44. The loads presented in table 3 are the programmed loads at DLL.

A comparison between the programmed loads at DLL and the actual applied loads is shown in figure 45. The error at each load introduction location is also shown. The applied load in the most heavily loaded actuator was 3 % greater than the programmed load (an error of 2000 lb). The applied loads in the more lightly loaded actuators were all within 4% of the programmed load and with an error of no more than 2% of the actuator capacity (maximum error of approximately 600 lb).

A comparison between the actual applied load at test article failure and the programmed loads at that load level for the most heavily-loaded actuator is shown in figure 46. The error at each load introduction location is also shown. The applied load in the more lightly-loaded actuators are within 3 % of the programmed load corresponding to the maximum load at actuator 2 and with an error of no more than 2% of the actuator capacity (maximum error of approximately 500 lb).

Displacement

The applied loads cause the wing tip to bend upward and induce a small twist into the test article as can be seen from the displacements presented in figure 47 along the front and rear spars for DLL condition. Displacements are shown at each actuator location and at the front and rear spars at the root rib. Maximum measured displacement at DLL was at actuator 2 and was 30 inches upward.

Displacements at the outboard six actuator locations are shown in figure 48 for tests 6, 7 and 8. Solid lines represent deflection of the undamaged structure loaded to DLL. Long and short dashed lines represent deflection of the sawcut and repaired structure, respectively. Measured displacements for these three tests are shown in table 6 for a load in actuator 2 of 47 kips (maximum load for the 70% DLL loading). Percentage differences were calculated based on the deflection of the undamaged structure. The largest difference in deformation between the undamaged and sawcut damaged structure was 8% at actuator 8. In addition, the largest difference in deformation between the undamaged and repaired structure was 6% at actuator 7. Actuator 7 is located at the rear spar at the landing gear doubler and actuator 8 is located at the front spar at rib 5, as shown in figures 1 and 2. At the comparison load of 47 kips in actuator 2, the locations of actuators 7 and 8 displace less than 1 inch while the wing tip displaces 20 inches. At the wing tip, the damaged and repaired structure deflects within 0.5 percent of the undamaged structure, which indicates that the damage and repair had an insignificant effect on the global behavior of the test article.

Strain

Undamaged Structure

Nonlinear or large strains measured during the 2.5G loading are shown in figures 49-55 for the loading to DLL. All strains for the 2.5G load condition are plotted against the load in actuator 2. All measured strains not shown are linear and do not exceed 0.005 in./in.

The strain gages at the edges of the lower cover panel access holes indicate high strains at these locations. These strains are shown in figure 49. The strain gage locations are shown in figure 7. In the figure strains at hole 1 are represented by the solid lines and strains at hole 3 are represented by long dashed lines. Holes further outboard are represented by progressively shorter dashes. Strains at inboard corners are represented by filled symbols and strains at the outboard corner are represented by open symbols. Nonlinearity in the load-strain behavior is can be seen at access holes 3, 4, 5 and 6. The most significant nonlinearity is at the outboard corner of access hole 4 between ribs 8 and 9. The largest measured strain is at this location and is approximately 0.0096 in./in. at DLL.

Strains measured in strain gages on the upper cover panel midway between ribs 8 and 9 at the rear spar cap and at stringers B, D, F, H and J are shown in figure 50. The gage locations are shown in figure 7 as locations U4-U9. These strains show the difference between external surface strains and internal strains at stringer blades. Each pair of gages is back-to-back and would read the same strain in the absence of bending or buckling behavior. However, as can be seen from the figure, the internal and external strains in all stringers differ from the onset of loading, but remain linear throughout the load range. Similar results can be seen for the lower cover panel between ribs 7 and 8 for gages at stringer C in figure 51. The fact that this separation between internal and external strains occurs in both cover panels in many pairs of gages indicates a global bending behavior of the test article.

Measured strains at lower and upper cover runouts are shown in figures 52 and 53, respectively. These runouts are identified by the rib at which they terminate and their position front or aft. In the figure the length of the dashes is used to differentiate among runout locations. Symbols represent locations at the runouts. Open symbols represent strains on the interior surface of the test article. Filled symbols represent strains on the exterior surface of the test article. Strain gage locations are shown in figures 3 and 4. The lower cover is loaded in tension in this load condition, so all measured lower cover runout strains are positive. Similarly, the upper cover is loaded in compression in this loading condition, so all measured upper cover runout strains are negative. All runout strains are approximately linear except in the lower cover near the rear spar at rib 8. Strains do not exceed 0.004 in./in in magnitude except at that rear spar runout. At that runout location, gage E records a linear load-strain relationship up to approximately 0.004 in./in. strain, then it records significantly higher strain as load is increased, indicating some damage may have occurred at this location. However, post-test visual and ultrasonic evaluation could not identify any damage at this runout. Strain gage B at that runout displays a small discontinuity in the slope of the load-strain curve at a load of approximately 62 kips. The maximum strains in any upper cover runout location are in the runout at the rear spar at rib 9 as shown in figure 53.

Measured strains in the main landing gear region are shown in figures 54-56. Strains in the upper and lower cover panels are shown in figures 54 and 55, respectively. Strains in the main landing gear doublers are shown in figure 56. Strain gage locations are shown in figure 9. All measured strains in the upper cover MLG region are linear except at stringer I. None of these strain values exceed 0.0035 in./in. The strain measured at stringer I shows discontinuities in slope at the load-strain curve for loading greater than approximately 50 kips. Strains at the lower cover intercostal at rib 5 show a discontinuity in the load-strain curve at a load of approximately 45 kips, as shown in figure 55. Strain in stringer I at rib 6 is linear for load less than about 65 kips, then decreases instantaneously. Several strains in the MLG doublers display nonlinear behavior. Strains near the edges of the upper and lower cover doublers are nonlinear and show discontinuities in the slope of the load-strain curve.

Measured strains in the upper and lower cover splice between the root transition box and the composite box are shown in figure 57. Strain gage locations are shown in figures 7 and 8. Open symbols represent lower cover panel strains, filled symbols represent strains on upper cover panel and half-filled symbols represent strains on the root transition box. All measured strains in the root splice region of the cover panels are approximately linear with increasing load except at location U2 where the load-strain curve is nonlinear. No strain exceeds 0.0035 in./in. in magnitude.

Measured strains in all ribs are less than 0.002 in./in. in magnitude. However, strains in ribs 2 through 15 display nonlinear behavior. Measured strain in ribs 2 and 3 are shown in figure 58. Measured strains in ribs 4, 5 and 6 are shown in figure 59. Measured strains in ribs 7, 8 and 9 are shown in figure 60 and are typical of ribs 10 through 15. Strain gage locations for ribs are shown in figure 11. For each figure, gage location is distinguished by line type and symbol. Even though strains are small, back-to-back strain gages show separation from the onset of loading, indicating the ribs are bending locally at the access hole in ribs 3 and 4 and globally in ribs 6-15. No back-to-back gages were placed on the rib away from the access hole in ribs 4 or 5 which could be used to determine if this bending behavior is restricted to the hole region.

Measured strains in the front and rear spars are linear and with maximum values between -0.008 and 0.004 in./in. Strains measured in the front spar are shown in figure 61.

No evidence of permanent damage was apparent due to 2.5G loading to DLL.

Sawcut Structure

Discrete source damage in the form of sawcuts was inflicted to stringer H in the upper cover panel and to stringer C in the lower cover panel. The upper cover sawcut is half way between ribs 10 and 11 and the lower cover sawcut is half way between ribs 8 and 9. The location of the upper and lower cover panel sawcut damage is shown in figure 2.

The effect of the sawcut on the behavior of the test article can be seen by comparing the strains measured in test 6 when the wing was loaded to DLL to the strains measured in test 7 in the presence of the sawcut. Axial strain gages were located on the internal and external skin at the sawcut tips and on the adjacent (uncut) stringers. These gage locations are shown in figure 12. Strain measured near the sawcut in the lower cover panel is shown in figure 62a and strains measured near the sawcut tips in the upper cover panel are shown in figure 62b. Internal strain is represented by solid lines and external strain is represented by dashed lines in the figures. Open symbols represent strain in the sawcut-damaged structure. Filled symbols represent strain in the undamaged structure. Strains at the sawcut tips are more than twice the strains at the same location in the undamaged structure. Strains remain linear for the full load range for the lower cover sawcut but sudden increases in strain occur in the upper cover panel sawcut tips internal surface. However, post-test ultrasonic inspection indicated no damage at the tips.

Strains in the same stringer bay as the sawcut but away from the sawcut tips are shown in figure 63a for the lower cover panel and figure 63b for the upper cover panel. Strains in the lower cover panel between ribs 8 and 9 at stringers B and D, at the access hole, and in the wide skin bay region outboard of stringer J are shown. Strain gage locations are shown in figure 7. Strains in the sawcut structure are 4 to 6 percent greater than strains in the undamaged structure at the access hole and approximately the same elsewhere in that bay.

Strains in the upper cover panel between ribs 10 and 11 at stringers F, G and I, and at the front and rear spar caps are shown. Strain gage locations are shown in figure 8. Strains in the sawcut structure are 6 to 55 percent greater than in the undamaged structure. However, strains in the 70% DLL test remain less than 0.0025 in./in. The most significant increase in strain is in stringer G.

Repaired Impact-Damaged Structure

Both sawcuts were repaired prior to the final test (test 8). The strains measured in the lower cover panel repair are shown in figure 64. The solid line represents strain in the metal component of the spliced blade. The short dashed line represents the strain in the metal repair plate. The long dashed lines represent the strain at the edges of the repair bole. The alternating long and short dashes represent the strain in the composite skin immediately outboard of the metal plate. The location of these strain gages is shown in figure 14. Strains on the composite structure in the vicinity of the repair are linear and do not exceed 0.005 in./in. Strains in the metal repair components display nonlinearity but remain less than 0.003 in./in.

The effect of the lower cover panel repair on the behavior of the lower cover panel strains can be seen by comparing the strains measured in test 6, when the wing was loaded to DLL, to the strains measured in the final test. Measured strains at six locations between ribs 8 and 9 in the lower cover panel are shown in figure 65. These locations are shown in figure 8 as L4 (skin outboard from stringer J), L5 (stringer D) and L6 (stringer B) and at the corners of access hole 4. Solid lines represent strain in the skin outboard of stringer J. Dashed lines with progressively shorter dashes represent strains moving toward the front spar. Open symbols represent data from test 6 and filled symbols represent data from test 8. The repair causes

an increase in strain in the blades of the stringers adjacent to the spliced stringer. At the load values corresponding to DLL, an increase of 45% in stringer B, 2% at the outboard corner of the access hole and 7% at the inboard corner of the access hole is seen. No increases in strain are seen in the skin near the rear spar in this bay. Significant local effects are seen but there is little effect away from the repair site. The effect of the repair on the strains at the access holes in the lower cover is presented in table 7 where strains measured at DLL in test 6 and in test 8 are shown.

The strains measured in the upper cover panel repair are shown in figure 66. The solid line represents strain in the metal component of the spliced blade. The short dashed line represents the strain in the metal repair plate. The long dashed lines represent the strain at the edges of the repair hole. The alternating long and short dashes represent the strain in the composite skin immediately outboard of the metal plate. The location of these strain gages is shown in figure 14. Strains on the composite structure in the vicinity of the repair are linear and do not exceed 0.005 in./in. Strains in the metal repair components display nonlinearity but remain less than 0.003 in./in.

Measured strains at eight locations in the upper cover panel between ribs 10 and 11 are shown in figure 67. These locations are shown in figure 7 as U4 (rear spar cap), U5 (stringer I), U6 (stringer G), U7 (stringer F), and U8 (front spar cap). The solid lines represent the strain in the front spar cap. Long dashed lines represent strain in stringers G and I which are adjacent to the spliced stringer. Short dashed lines represent strain in stringer F. Open symbols represent data from test 6 and filled symbols represent data from test 8. The repair causes an increase in strain in the blades of the stringers to the rear of the spliced stringer and a decrease in strain in the blades of the stringers forward of the repair. At the load values corresponding to DLL, a decrease of 50% and an increase of 40% are seen in the adjacent stringers forward and aft stringers, respectively. The repair causes an increase in strain of 2% at the rear spar and has no effect on the front spar. The strain in the skin is effected little by the repair.

The test article was impacted at the six locations shown in figure 2. Internal strain gages at the planned impact sites were positioned during wing box assembly, however some interior strain gages were damaged during the impact event. External strain gages were added after impacts were inflicted. Strain gage locations are shown in figure 13. Strains measured at the impact sites are shown in figures 68-73. When available, data from test 6 and test 8 are shown in the figures to identify the effect of the impact damage on the behavior of the test article. Symbols are added to the curves of the strains in the undamaged structures. In each figure solid lines represent the strain on the external surface and dashed lines represent the strain on the internal surface.

Strains in the upper cover panel at impacts at rib 4, at rib 9 and at rib 13 are shown in figures 68, 69 and 70, respectively. Internal skin strains are represented by long dashed lines and external skin strains are represented by solid lines. Blade strains are represented by short dashed lines. The lines with filled symbols represent strain of the undamaged structures. The lines with no symbols represent strain in the damaged structure. Strains at the rib 13 impact and the rib 4 impact remain linear as load is increased. At the load values corresponding to DLL, the strain increases at these two locations by no more than 4% due to the presence of the impact and strain does not exceed 0.005 in./in. in magnitude. The percentage increase in strain at each location is show on the figures.

The impact site at rib 9 is at the location that stringer J terminates. Long dashes represent the strain on the internal skin surface and short dashes represent the strain in the stringer blade. This region was more heavily strain gaged than others to capture strain gradients due to the presence of the runout. Strain gage locations are show in figure 3. Strain gages on the stringer blade record an increase in strain of up to 5%. The most significant increase in strain is near the termination point of the blade, location G in figure 69

and the closest point to the impact site. An increase of 15% is seen at the interior gage closest to the impact site but there is no increase in strain at the closest exterior skin gage location

The nonlinearity shown in this plot is not significant for load less than DLL, but becomes quite obvious for load greater than DLL. However, this nonlinearity appears to be more due to the presence of the runout than the influence of the impact.

Strains in lower cover panel with impacts are shown in figures 71, 72 and 73 for impact sites at rib 4, rib 8 and rib 12, respectively. Internal strains are shown with dashed lines and external strains are shown with solid lines. The lines with filled symbols represent strain of the undamaged structures. Strains within 1 inch of the impact site remain linear and increase by less than 4 percent compared to strains in the undamaged structure for the impacts at the three impact sites. The impact at rib 12 was originally intended to be at rib 13 (shown in figure 1), so the test article was strain gaged with the corresponding gage pattern. However, the impact site had to be moved because it was impossible to impact the lower cover so close to the rib 13 load saddle. Internal gages could not be moved or added to the rib 12 location. So strains at the rib 12 impact site can only be compared to one gage on the undamaged structure, as shown in figure 73.

The effects of the repairs and impacts on the rib strains are shown in figure 74 by presenting results from tests 6 and 8. Strain gage locations are shown in figure 11. The magnitude of the rib strains is small for all ribs. Strains are decreased in ribs 2 and 3 by approximately 25 and 18%, respectively. Strains are nonlinear in these ribs in test 6 but are linear in these ribs in the final test. Strains in ribs 4, 5 and 6 increase but remain less than 0.001 in./in. in magnitude. A sudden increase in strain is seen at a gage on rib 6 near the upper cover intercostal occurs at a load in actuator 2 of 91 kips.

Strains in ribs 8, 9, 10, 11, 12 and 13 remain less than 0.001 in./in. in magnitude but back-to-back strain gages indicate that the ribs are bending from the onset of loading. In addition, sudden increases in strain are seen in some strain gages at a load of 91 kips in actuator 2. No significant effect of repair and impacts is apparent.

Failure

The test article supported 97% of its Design Ultimate Load (DUL) prior to failure. This load corresponds to the actuator load values shown in figure 46. A photograph of the test article loaded at 95% DUL is shown in figure 44. The primary failure location is across the lower cover panel through access hole 4. This region of the lower cover panel after final failure is shown in figure 75. The failure goes through all stringers but primarily remains between ribs 8 and 9. Both spars were also damaged, as shown in figures 76 and 77. Other minor damage was found but appears to be unrelated to the initial failure event. The discussion of the failure will be limited to the regions between ribs 6 and 10, the impact sites and the repairs.

Even though the impacts caused strains in the immediate vicinity of the damage to increase, as shown in figures 68-73, the wing failure did not go through any inflicted damage sites and post-failure ultrasonic scanning found no growth in damage at any damage site. The upper cover repair had an effect only on the rear spar region outboard of rib 10, well away from the failure site and so was uninvolved with the failure. The lower cover repair was in the region of failure but strains in the repair itself remained less than 0.005 in./in.

However, the strain at the edge of the access holes may also have been influenced by the repair. Strains recorded at access holes 3, 4, 5 and 6 are shown in figure 78 for the undamaged structure and the repaired structure. A comparison of strains indicates that the largest increase in strain due to repair is at access hole 4. Since strains at the corners of this hole were greater than expected in preliminary tests, additional gages were added to the skin surface prior to the final test. New gages were located 0.13 and 0.39 inches from the hole edge on the interior surface and 0.3 inches from the edge on the exterior surface. As shown in figure 79, the strains at this access hole are not linear for load greater than approximately 50% DUL. Strains measured during the undamaged test to DLL and the final test to failure are shown for gages in the most critical corner of the hole at the midplane. Also shown in figure 79 is a projection of what the strain would have been if the DLL test had gone to DUL. The projection is based on a 4th order polynomial fit to the DLL data. This projection indicates that the damage and repair had little influence on the strain at the access hole. For loads greater than 84 kips in actuator 2, the midplane strain gage fails to record increasing load, indicating a failure at the edge of the hole. The surface strain gages continue to record linear strain for load up to 91 kips. Video recorded during the test does not show damage until the catastrophic failure at 97% DUL, however, such damage might not be visible to the camera due to inadequate lighting or distance from the structure. In addition, gages at holes 5 and 6 fail or record nonlinear behavior. Strain gages at access hole 6 indicate failure at a load as low as 76 kips, however, there is no evidence of damage propagation. Maximum strains recorded before apparent failure at each hole strain gage location are shown in table 8.

In addition to the global bending behavior illustrated in figure 50, local nonlinear behavior occurred in the upper cover panel to the rear of the rear spar between ribs 8 and 10. An overhang of the cover panel with a width of approximately four inches behind the rear spar left an unsupported edge along the length of the test article. This region is shown on figure 7 as the "critical overhang region." Two back-to-back gages on the skin at the edge of the overhang midway between ribs 8 and 9 indicate that significant local bending occurred. Strains in the upper cover near the rear spar between ribs 8 and 9 are shown in figure 80 for the repaired structure. Open symbols represent strains on the upper skin surface on the cover panel. Filled symbols represent strains on the blade of stringer H and on the lower skin surface of the overhang. For a load less than 70 kips in actuator 2, the local bending effects do not occur (only the global bending effects are seen). However strain reversal is seen in the gages located in the overhang region as load approaches DUL. No other gages were in the overhang region.

A small initial geometric imperfection in the form of a kink in the upper cover panel was present in the manufactured structure. This kink is centered half way between ribs 9 and 10 and has a maximum depth of 0.1 inches. A sketch of this kink is shown in figure 81. The kink was initially deemed minor enough to have no influence on structural behavior. However, since the kink is in close proximity to a stringer runout and in the region of the upper cover panel which displays local nonlinear behavior in the final test, the possibility that the kink influenced the behavior of the overhang region must be acknowledged. Since only two strain gages were in this region, there is not enough experimental data to explain fully the influence of the kink and the interaction of all components in this region. A detailed finite element analysis which accounts for this imperfection is needed for that. That analysis is beyond the scope of the present paper.

Concluding Remarks

A 41-foot-long graphite-epoxy stitched wing box was tested in three load conditions and ultimately loaded to failure. The test article is representative of a 220-passenger commercial transport wing. The structure was fabricated using advanced manufacturing techniques to reduce cost, weight and improve damage tolerance capability. The test article sustained 100% Design Limit Load in a brake roll ground

loading, a -1G flight loading and a 2.5G flight loading with no evidence of damage. The wing then sustained 70% Design Limit Load in the 2.5G condition with severe discrete source damage in the form of a severed stringer in the upper and lower cover panels. Following the installation of a simple patch repair at each broken stringer, the wing was subjected to barely visible impact damage and loaded to failure. The test article sustained 97% of Design Ultimate Load prior to failure through a lower cover access hole which resulted in the loss of the entire lower cover panel. Post-test ultrasonic scanning of the impact sites indicates that no damage growth occurred from the impact sites. In addition to the high strains at the lower cover panel access holes, strain gage results indicate that local nonlinear deformations occurred in the upper cover panel in an unsupported region behind the rear spar.

NASA Langley Research Center
Hampton, VA 23681-2199
January 24, 2001

References

1. Hawley, A.: "Preliminary Design of a Transport Aircraft Composite Wing," Proceedings of the Fifth NASA/DoD Advanced Composites Technology Conference. NASA CP-3294, Volume 1, Part 2, pp. 717-772.
2. Karal, Michael: "AST Composite Wing Program - Executive Summary," NASA CR 2001-210650.
3. Markus, A.; Thrash, P.; and Grossheim, B.: "Manufacturing Development and Requirements for Stitched/RTM Wing Structure," NASA CP 3229, 1993, pp. 503-523.
4. Rohwer, K.; Ghumman, A.; and Markus, A.: "Stitched/Resin Film Infusion (S/RFI) Manufacturing Technology Development," Proceedings of the 11th DOD/NASA/FAA Conference on Fibrous Composites in Structural Design. Report number WL-TR-97-3009 pp. XIII-93-116.
5. Lovejoy, Andrew: "Finite Element Analysis of a Composite Semi-Span Test Article With and Without Discrete Damage," NASA CR 2000-210308, August 2000.

Table 1. Stringer Runouts

Location			Configuration
Upper cover stringer*	Rib	Adjacent spar	
A	4	Front	Straight
B	9	Front	Tapered
I	9	Rear	Tapered
C	15	Front	Straight
J	15	Rear	Straight
Lower cover stringer**			
A	4	Front	Straight
J	8	Rear	Tapered
B	10	Front	Tapered
C	15	Front	Tapered
I	15	Rear	Tapered

* Rib and stringer numbering system shown on figure 2a.

** Rib and stringer numbering system shown on figure 2b.

Table 2. Test Sequence

Test number	Loading condition
1	50% DLL, brake roll
2	100% DLL, brake roll
3	50% DLL, -1G
4	50% DLL, 2.5G
5	100% DLL, -1G
6	100% DLL, 2.5G
7	70% DLL 2.5G
8	Failure/DUL 2.5G

Table 3. Design Limit Load Values for Three Load Conditions

Actuator position*	Brake roll, lb**	-1 G, lb**	2.5 G, lb**
1	-1000	-6000	27000
2	-2000	-30000	66500
3	-1000	-22000	-2000
4	-2000	8000	14000
5	-8000	-6000	10000
6	-11500	11500	-30000
7	0	-3000	30000
8	10000	-9500	4000
9	124450	0	0

*Actuator locations shown in figure 1.

** Positive load is due to pushing up and negative load is due to pulling down.

Table 4. Lower Cover Impacts With Specimen Penetration Device

Location	Speed (ft/sec)	Energy (ft-lb)	Dent depths (inches)	NDE area (inches)
Rib 4	546	84	0.13	1.2 x 1.5
Rib 8	544	83	0.08	1.5 x 1.8
Rib 12	543	83	0.09	1.9 x 2.7

Table 5. Upper Cover Impacts With Drop Weight

Location	Weight (lb)	Height (inches)	Energy (ft-lb)	Dent depths (inches)	NDE area (inches)
Rib 13	26.43	45.4	100	0.01	1.4 x 1.9
Rib 4	26.41	45.4	100	0.05	2.5 x 2.4
Rib 9	25.24	47.5	100	0.01	1.7 x 1.9

Table 6. Effect Of Damage and Repair on Displacement

Actuator	Test 6 loads (kips)	Test 7 loads (kips)	Test 8 loads (kips)	% difference tests 6 and 7	% difference tests 6 and 8
1	20.2	20.0	20.2	-1.2	0.1
2	20.6	20.3	20.6	-1.5	-0.1
3	8.1	7.9	8.1	-2.2	-0.8
4	8.3	8.1	8.2	-1.5	-0.6
5	2.6	2.5	2.5	-3.2	-4.5
6	1.4	1.4	1.4	-3.2	-3.2
7	0.9	0.9	0.8	-5.9	-6.4
8	0.7	0.8	0.7	7.9	2.3

Table 7. Effect of Repair on Access Hole Strains at DLL

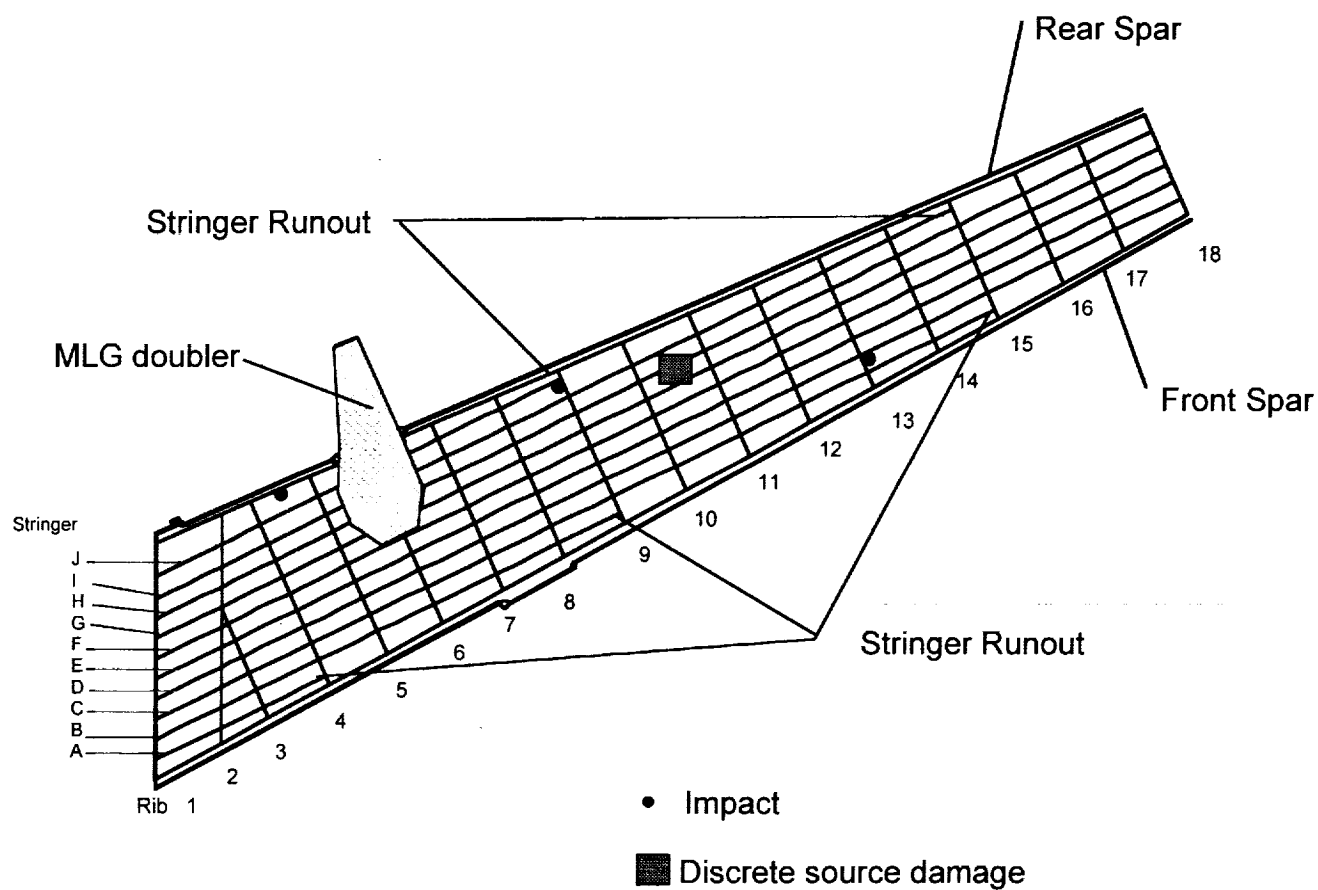
Access hole	Location	Test 5 strain (in./in.)	Test 8 strain (in./in.)	% difference tests 5 and 8
1	outboard	0.0039	0.0038	-2.8
1	inboard	0.0033	0.0033	-1.2
3	outboard	0.0061	0.0063	2.1
3	inboard	0.0038	0.0037	3.6
4	outboard	0.0096	0.0098	2.3
4	inboard	0.0064	0.0068	6.9
5	outboard	0.0052	0.0053	2.5
5	inboard	0.0049	0.0050	3.1
6	outboard	0.0079	0.0080	1.1
6	inboard	0.0076	0.0077	1.9

Table 8. Maximum Strain and Load at Actuator 2 at Access Hole Edges for Hole Failure Locations

Access hole	Location	Load kips	Strain in./in.
4	outboard	84	0.0132
5	outboard	96	0.0104
6	outboard	76	0.0096
6	inboard	92	0.0112

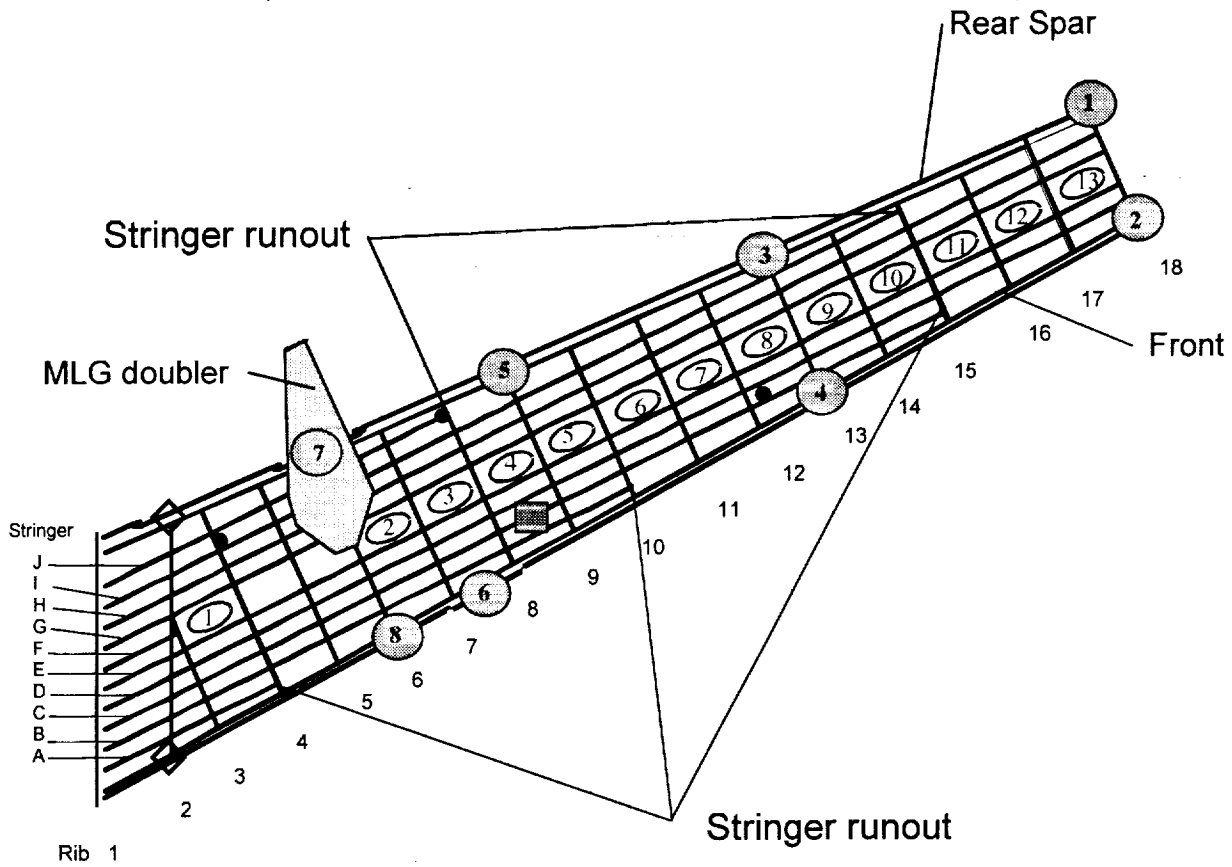


Figure 1. Stitched semi-span wing prior to testing.



a) Upper cover panel

Figure 2. Wing cover panel configuration.



- ① Actuator and displacement measurement locations
- Impact locations
- Discrete Source Damage
- ◇ Additional displacement measurement locations

b) Lower cover panel

Figure 2. Concluded.

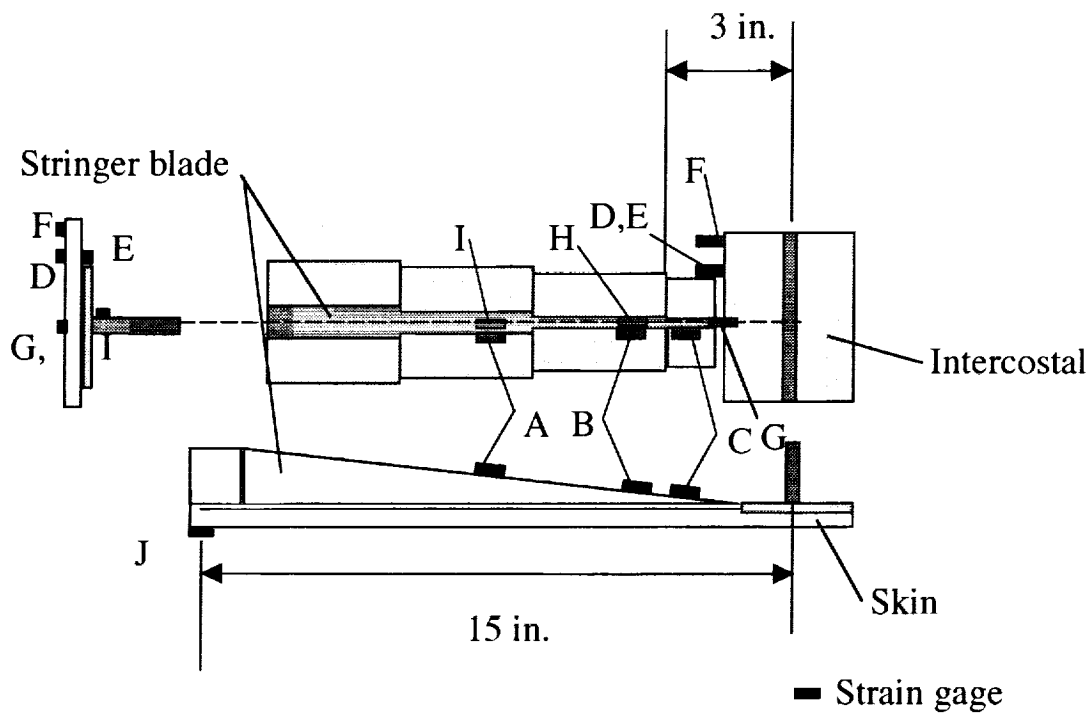


Figure 3. Tapered height stringer runout.

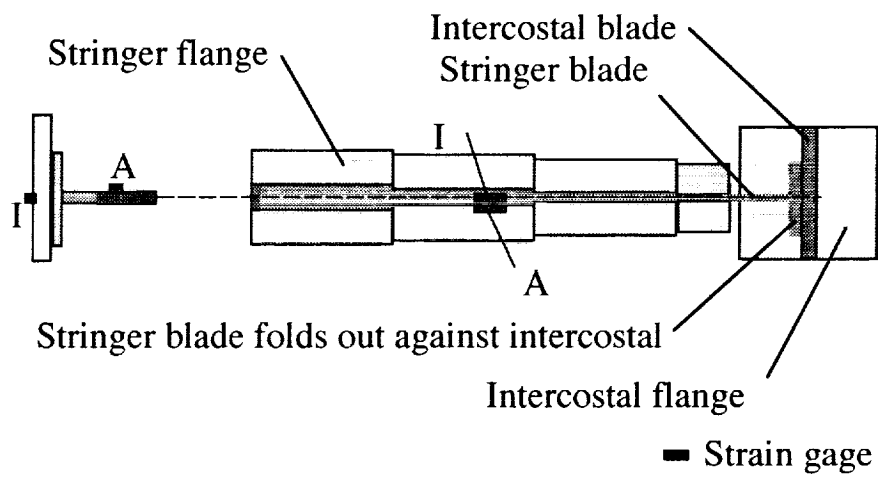


Figure 4. Constant height stringer runout.

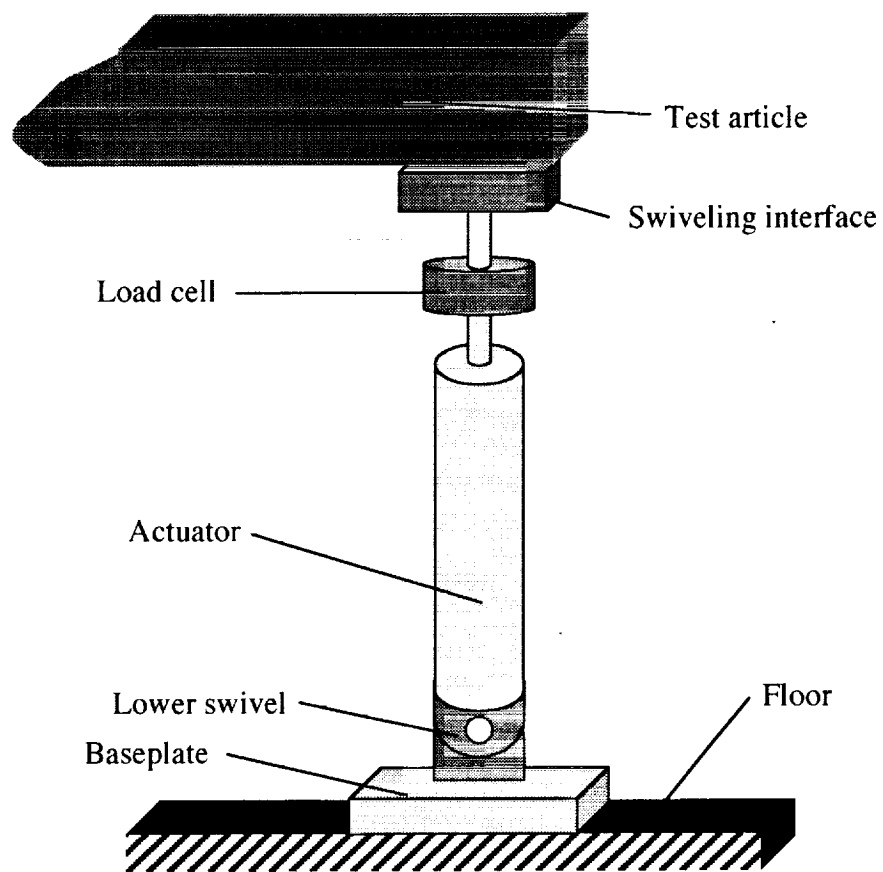


Figure 5. Configuration of vertical actuator assembly.

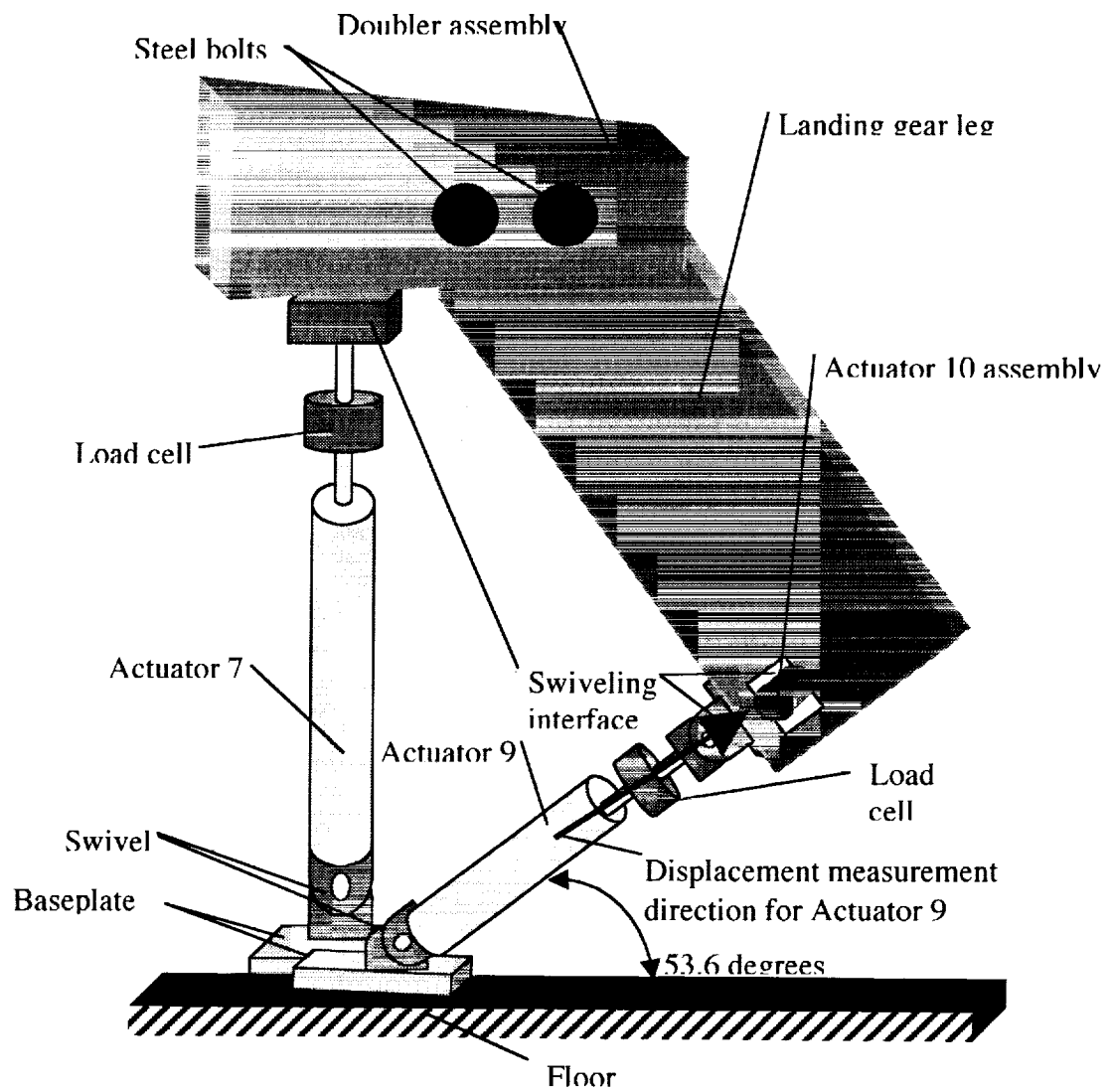


Figure 6. Configuration of landing gear leg actuator assembly.

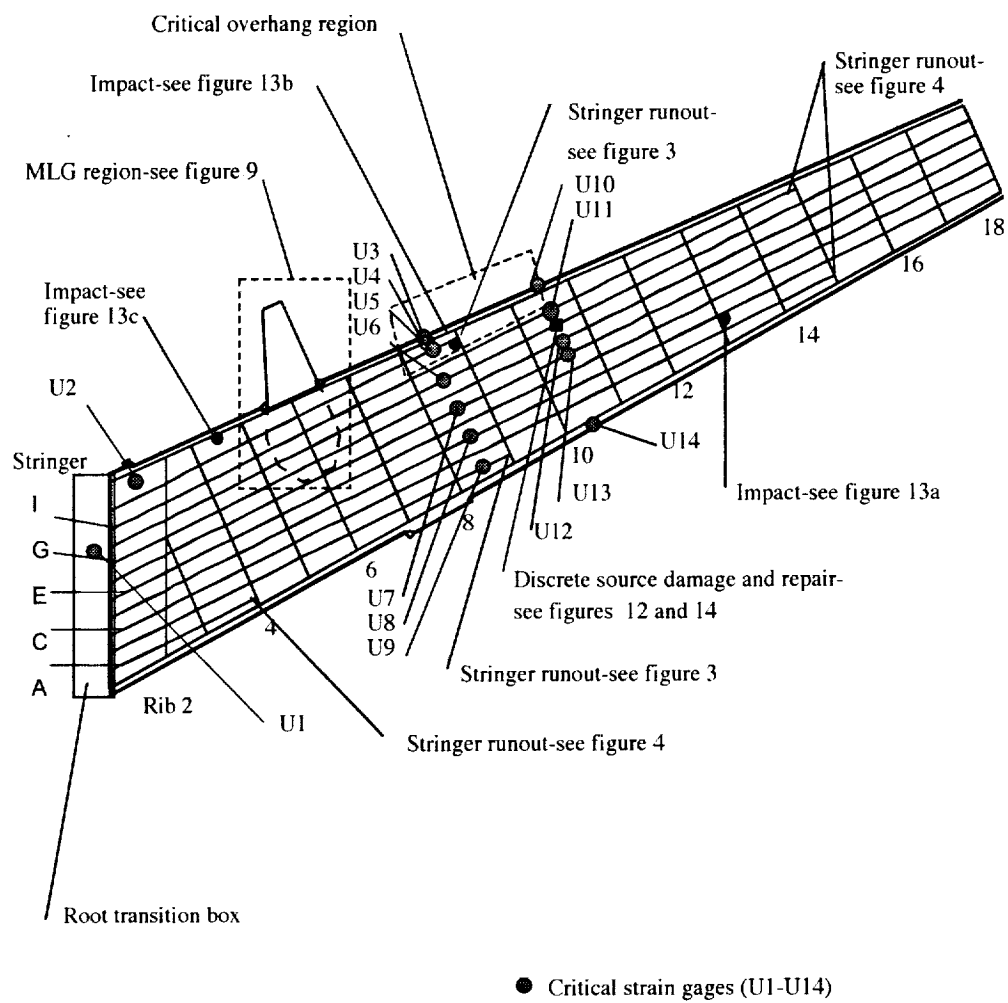


Figure 7. Upper cover panel strain gage locations

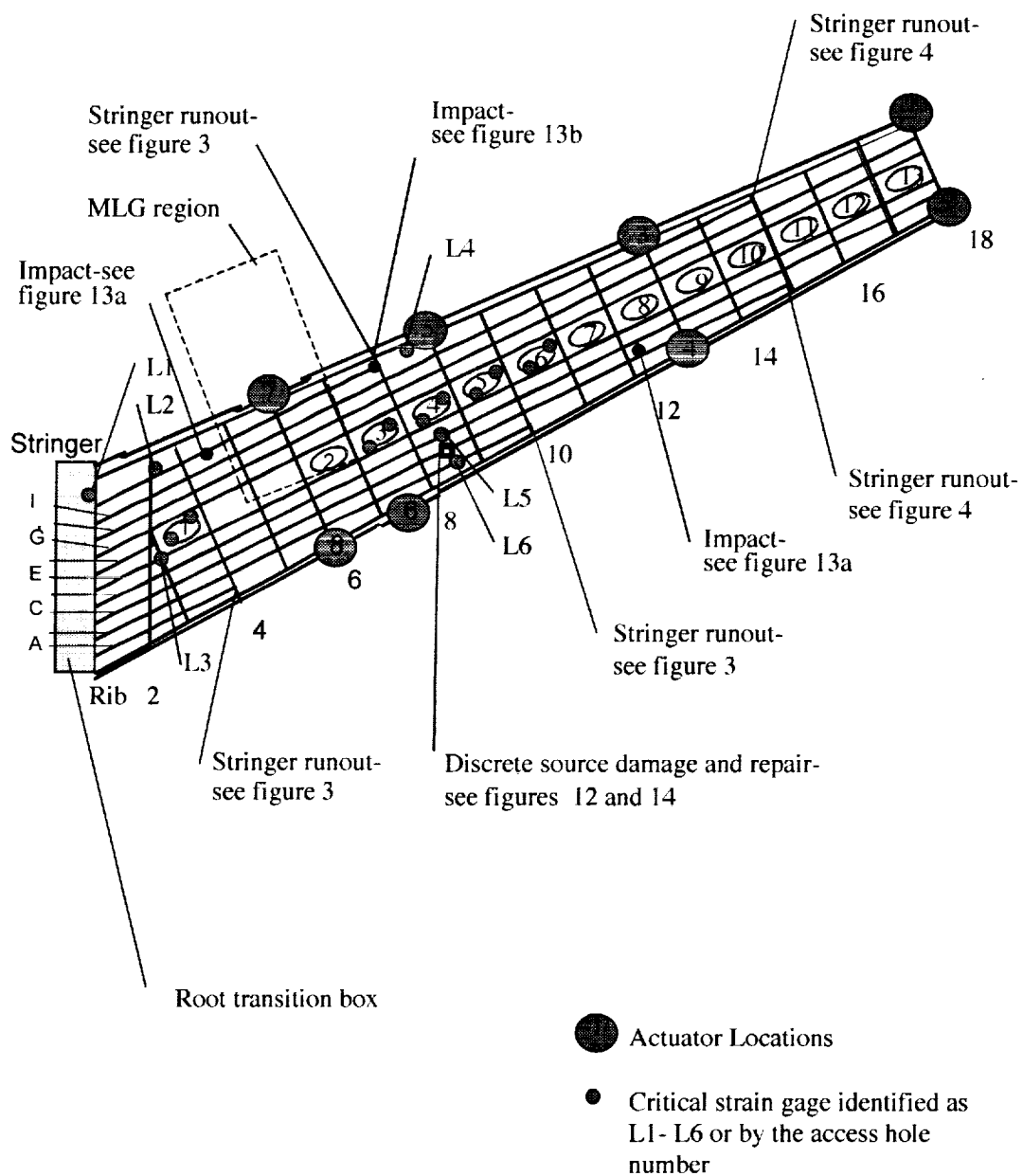
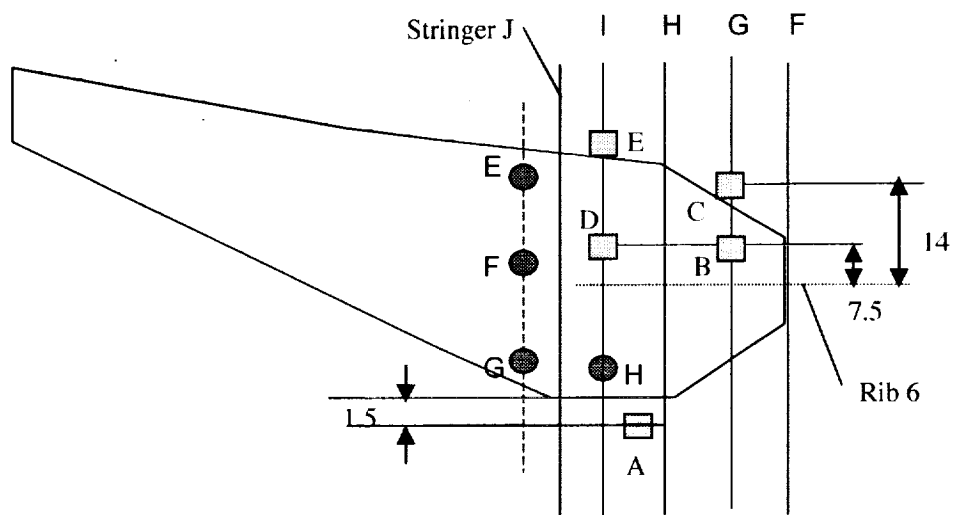
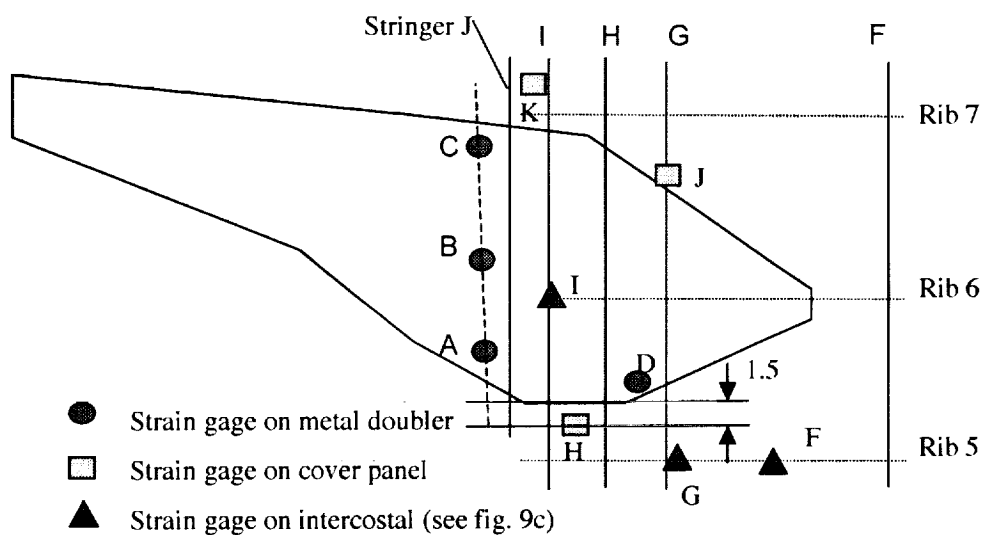


Figure 8. Lower cover panel strain gage locations.



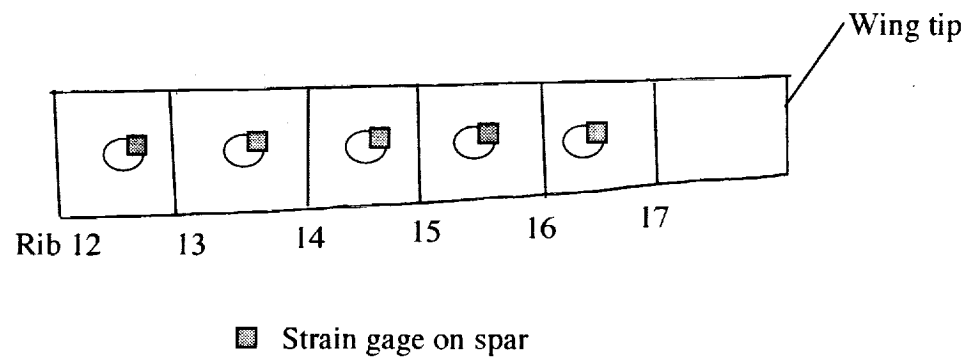
a) Upper cover

Figure 9. Strain gages in main landing gear region. Stringers identified in figures 7 and 8.



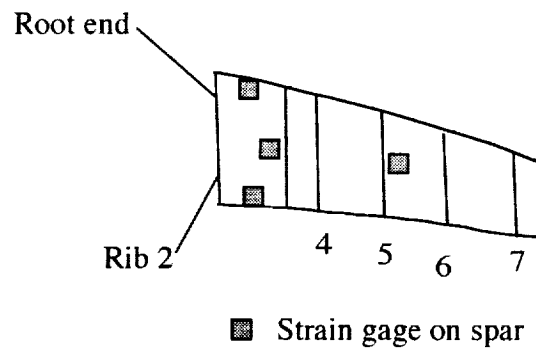
b) Lower cover

Figure 9. Continued.



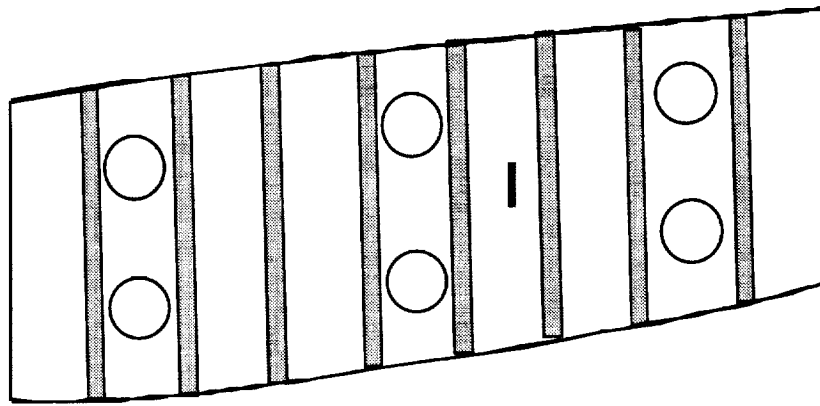
a) Front spar

Figure 10. Strain gages on spars.



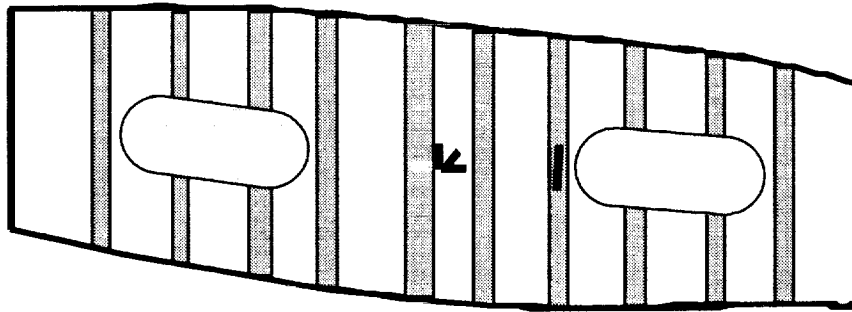
b) Rear spar

Figure 10. Concluded.



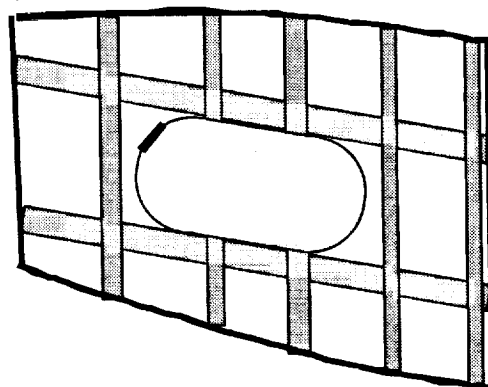
a) Rib 1

Figure 11. Strain gage locations on ribs.



b) Rib 2

Figure 11. Continued.



c) Rib 3

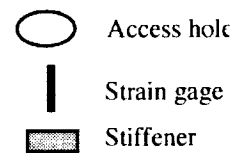
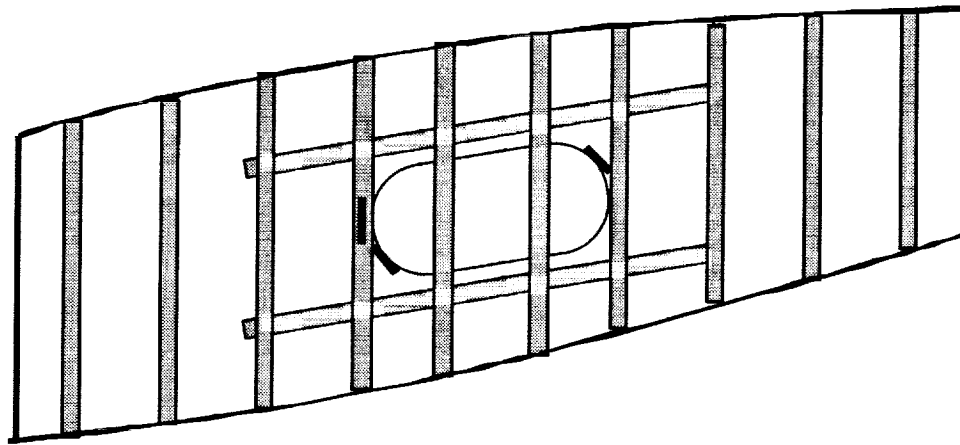
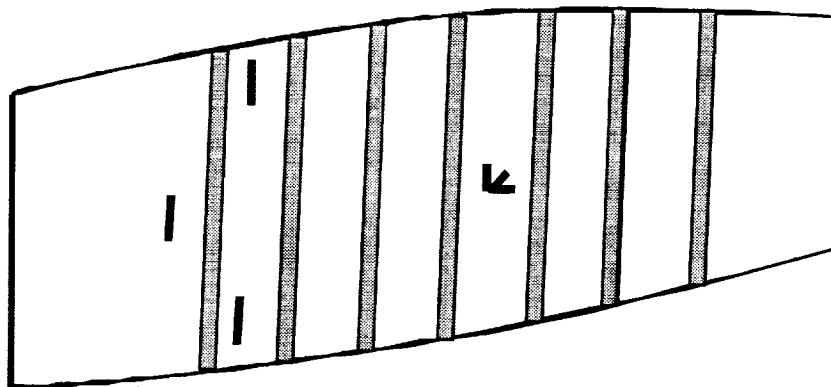
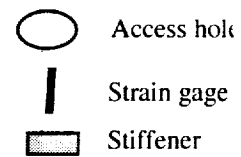


Figure 11. Continued.



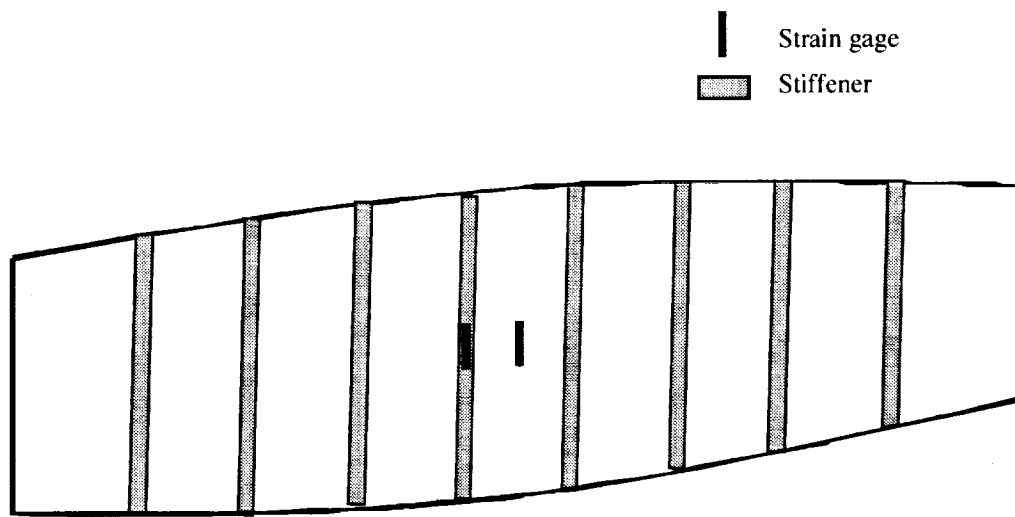
d) Ribs 4 and 5

Figure 11. Continued.



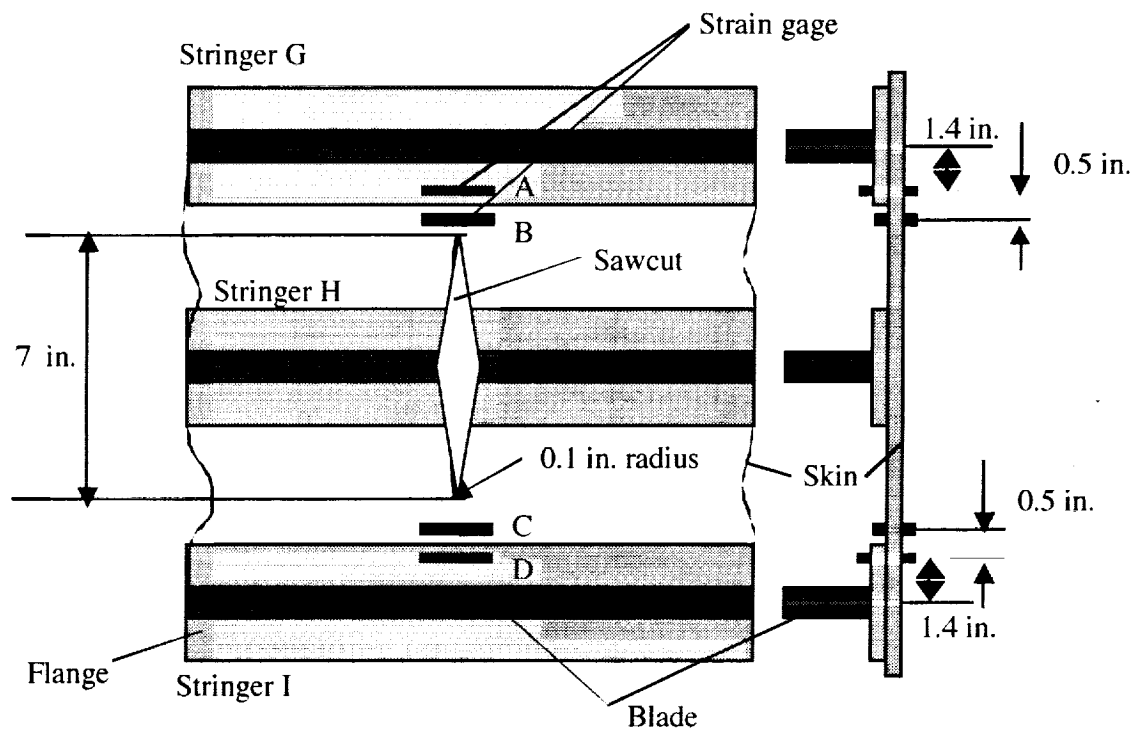
e) Strain gage locations on rib 6

Figure 11. Continued.



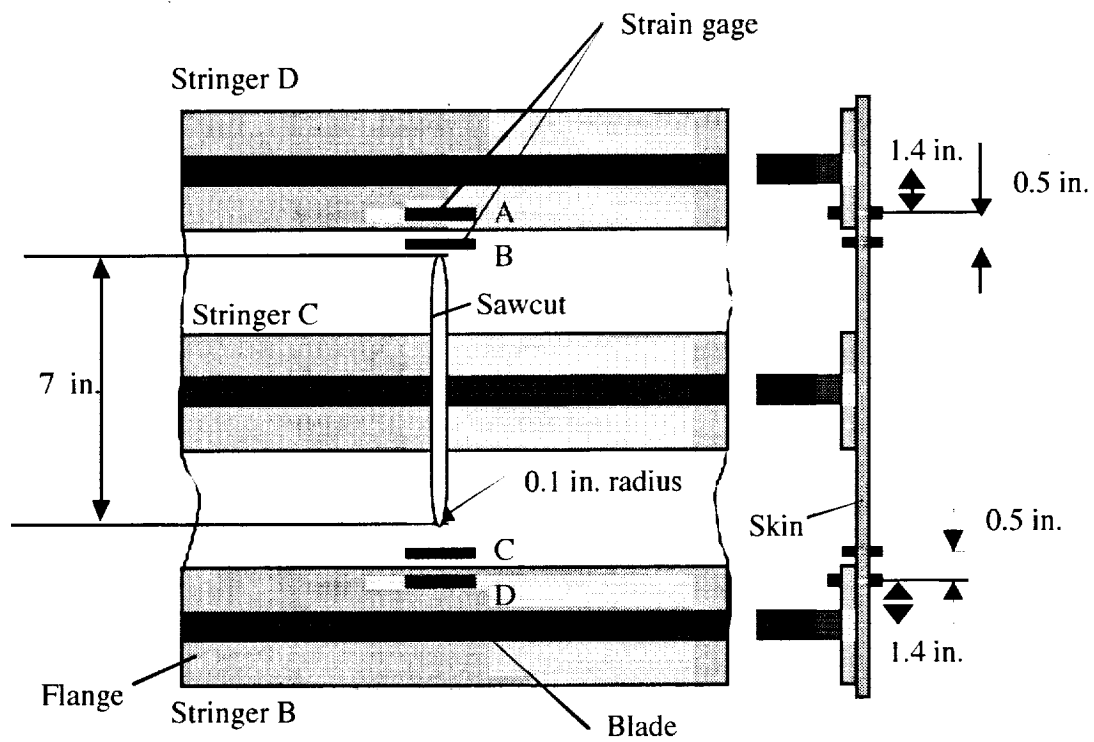
f) Ribs 7, 8, 9, and 10

Figure 11. Concluded.



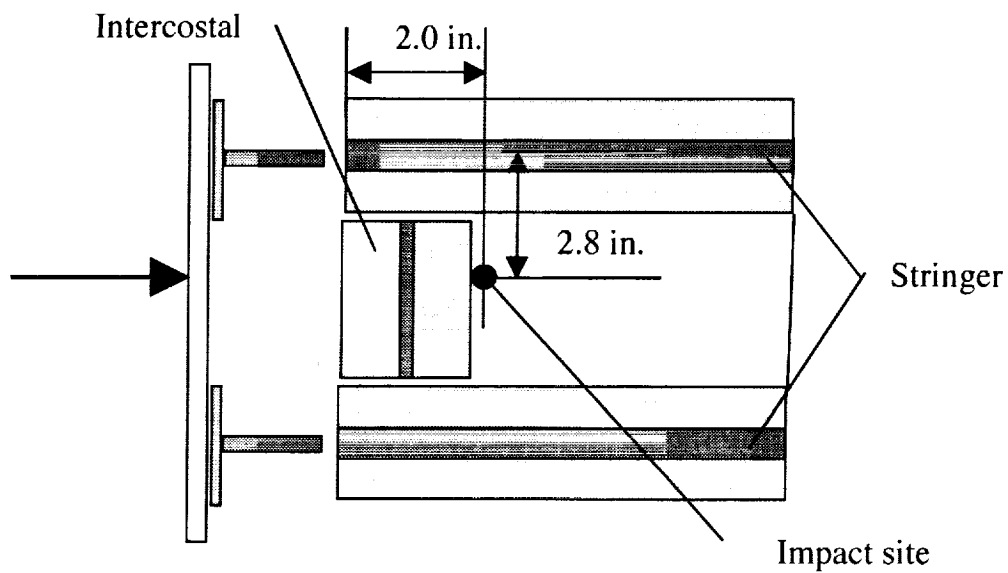
a) Upper cover panel sawcut

Figure 12. Strain gage locations near sawcuts.



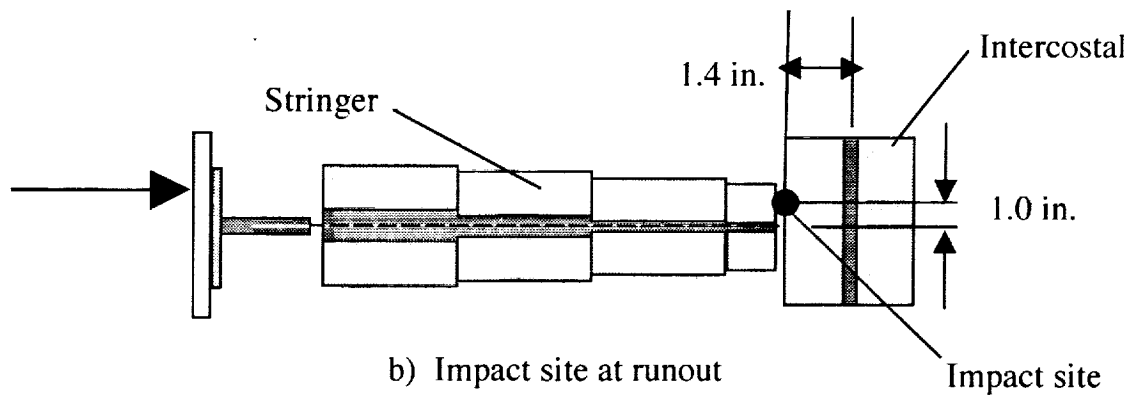
b) Lower cover panel

Figure 12. Concluded.



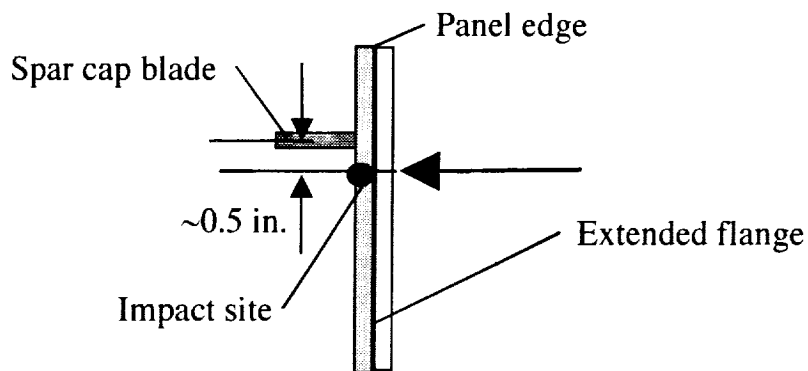
a) Impact site away from stringer

Figure 13. Impact sites.



b) Impact site at runout

Figure 13. Continued.



c) Impact site at spar cap

Figure 13. Concluded.

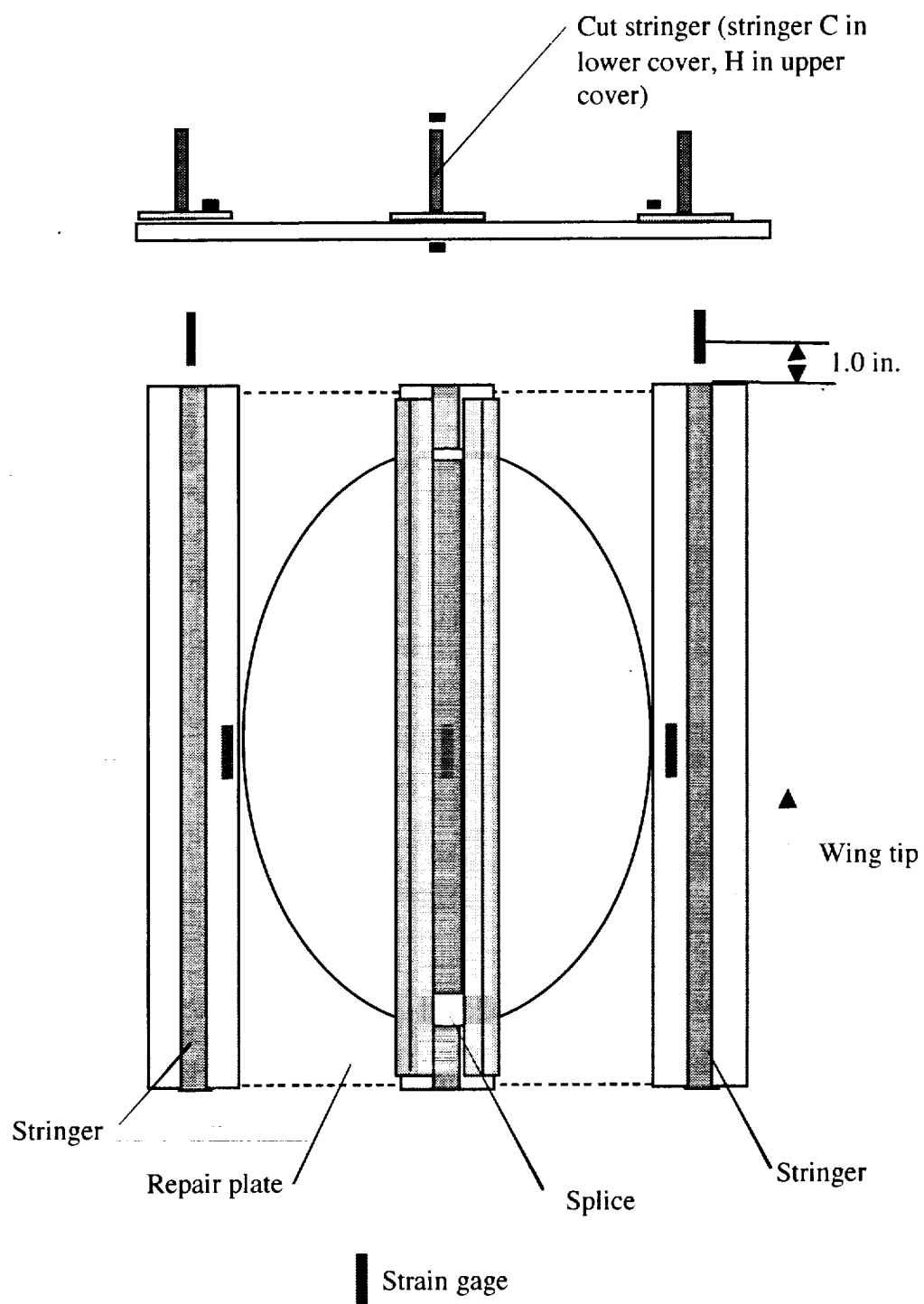
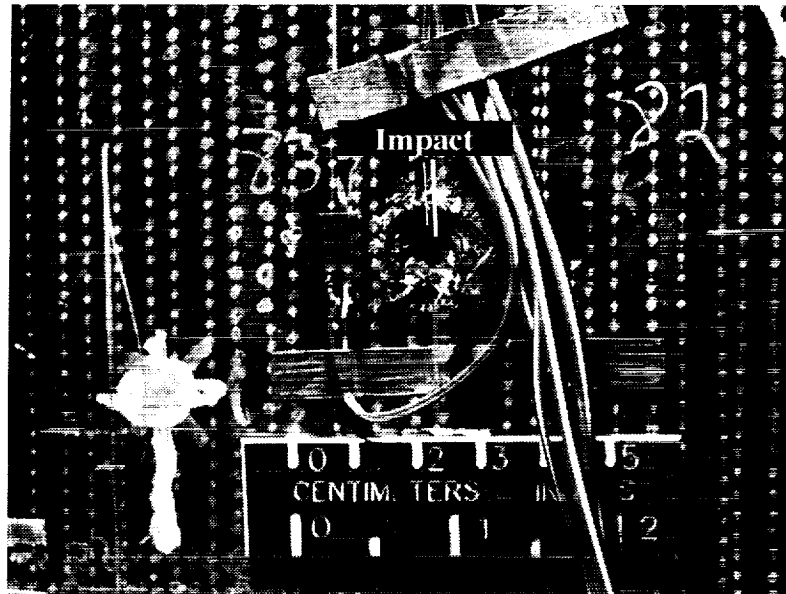
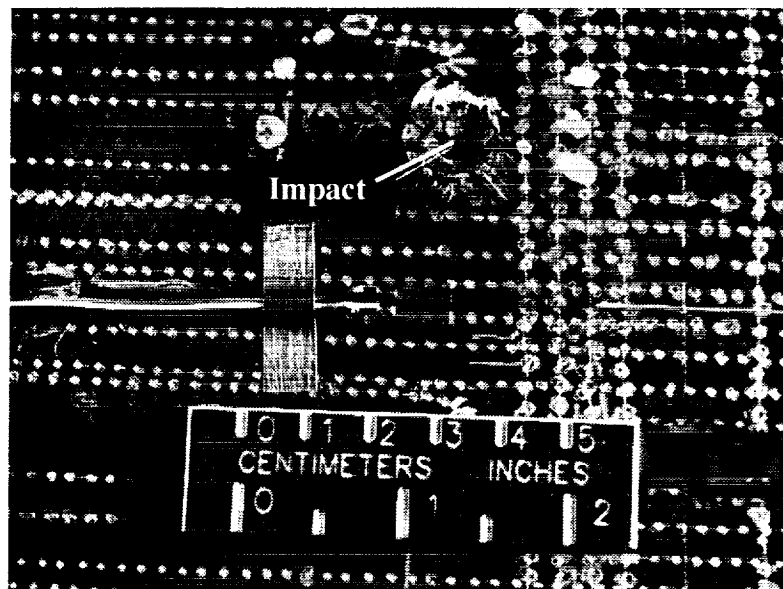


Figure 14. Strain gages at repair sites.



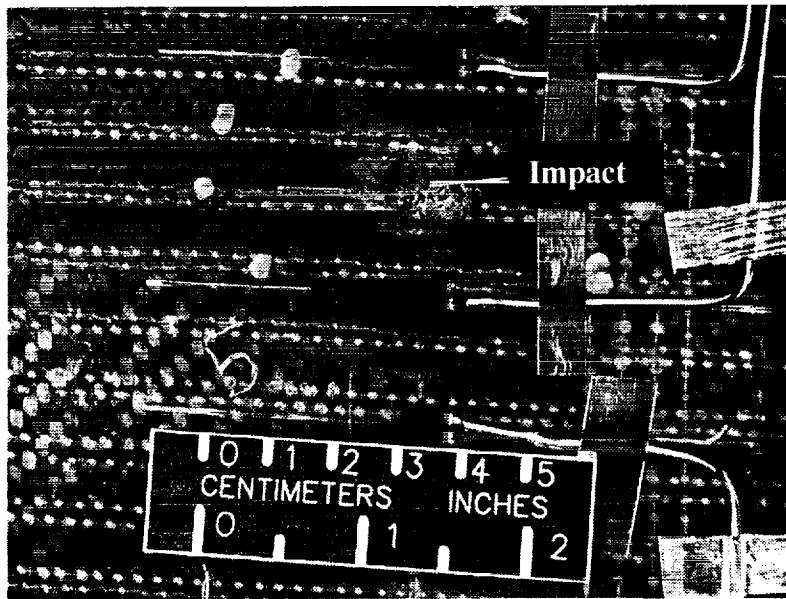
a) Site at rib 4

Figure 15. Lower cover impact damage locations.

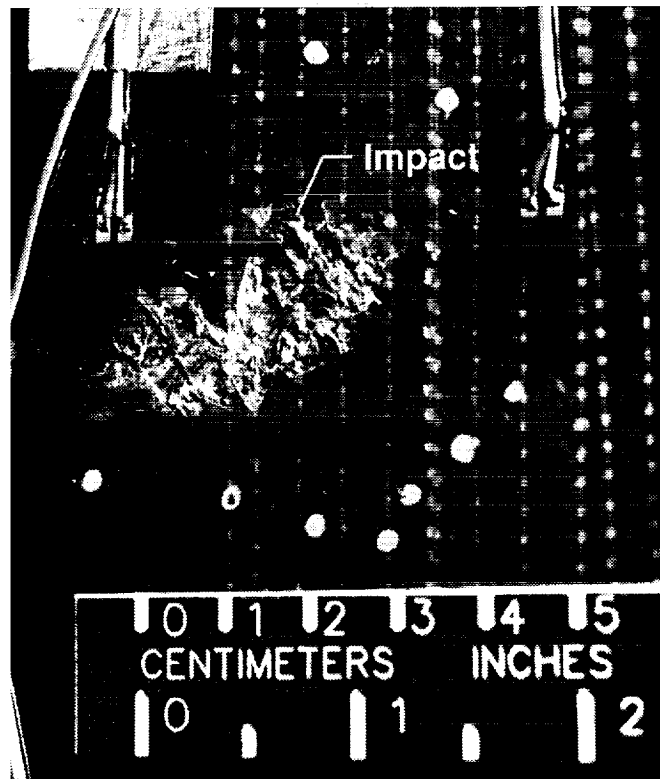


b) Site at rib 8

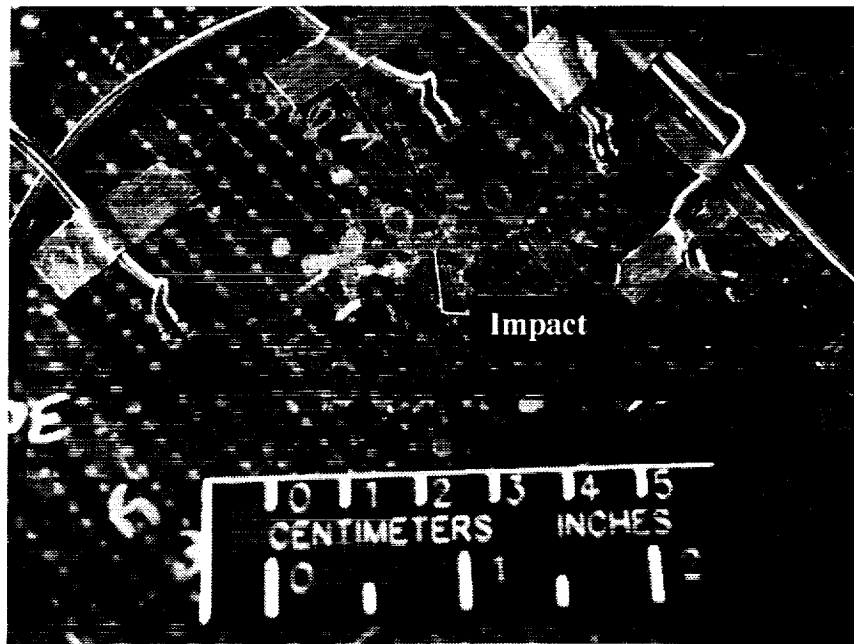
Figure 15. Continued.



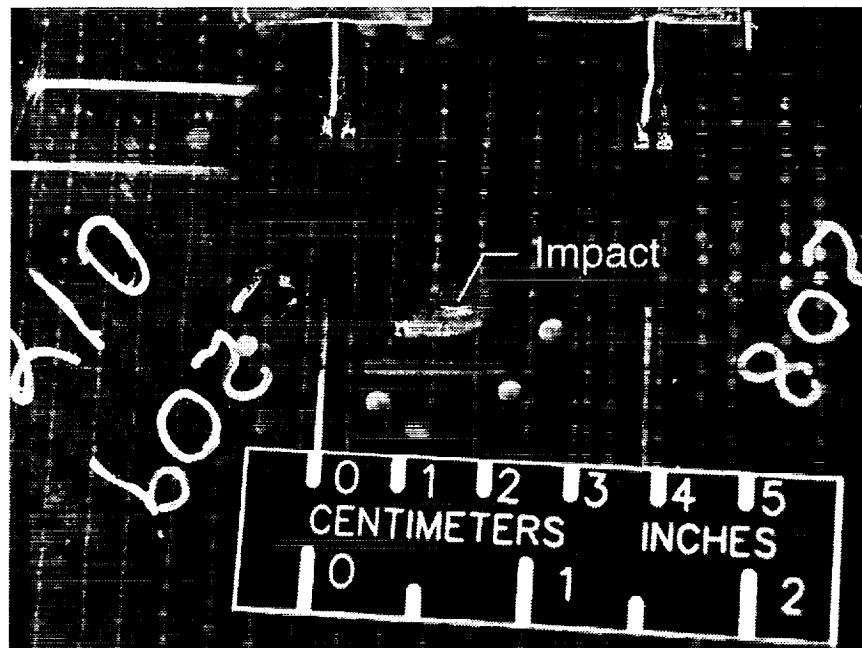
c) Site at rib 12
Figure 15. Concluded.



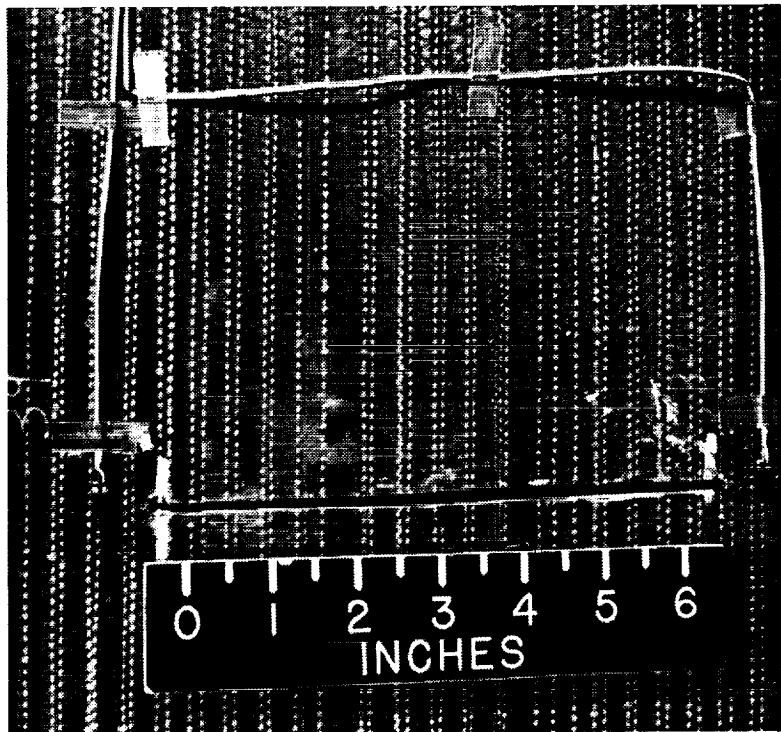
a) Site at rib 4
Figure 16. Upper cover impact damage locations.



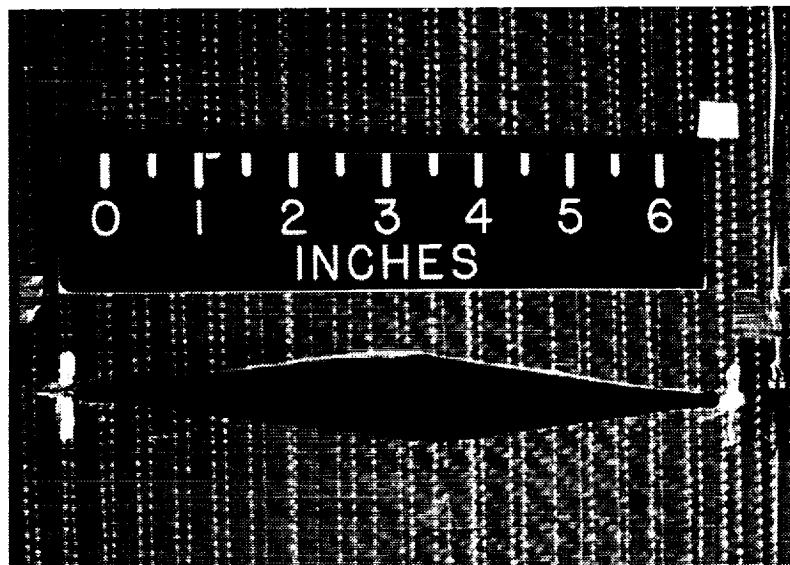
b) Site at rib 9
Figure 16. Continued.



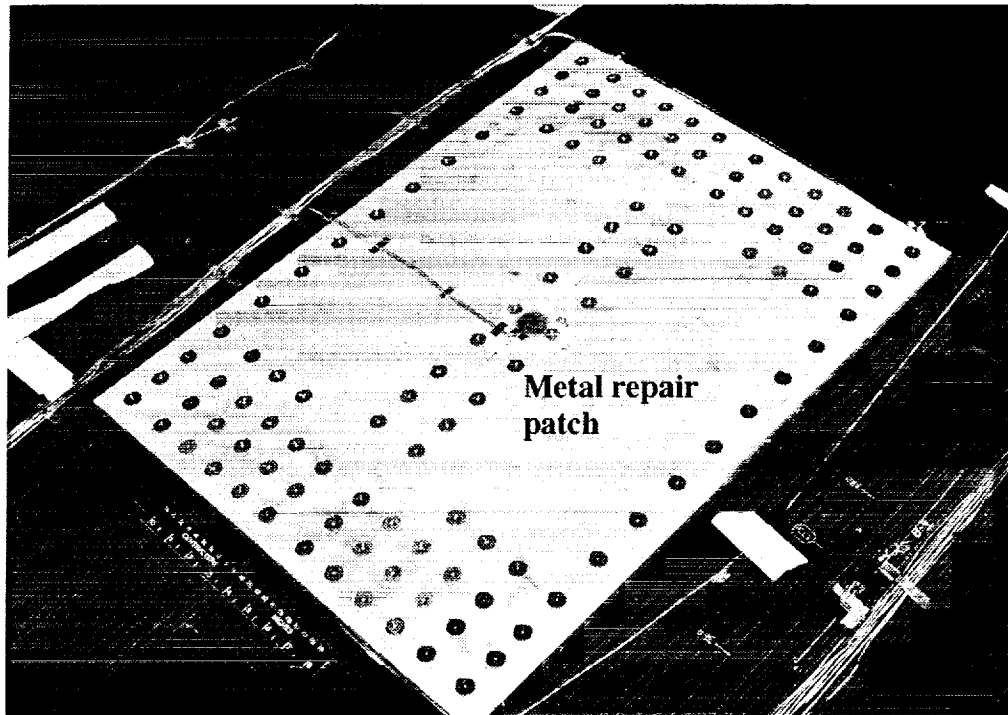
b) Site at rib 13
Figure 16. Concluded.



a) Lower cover panel
Figure 17. Sawcuts.

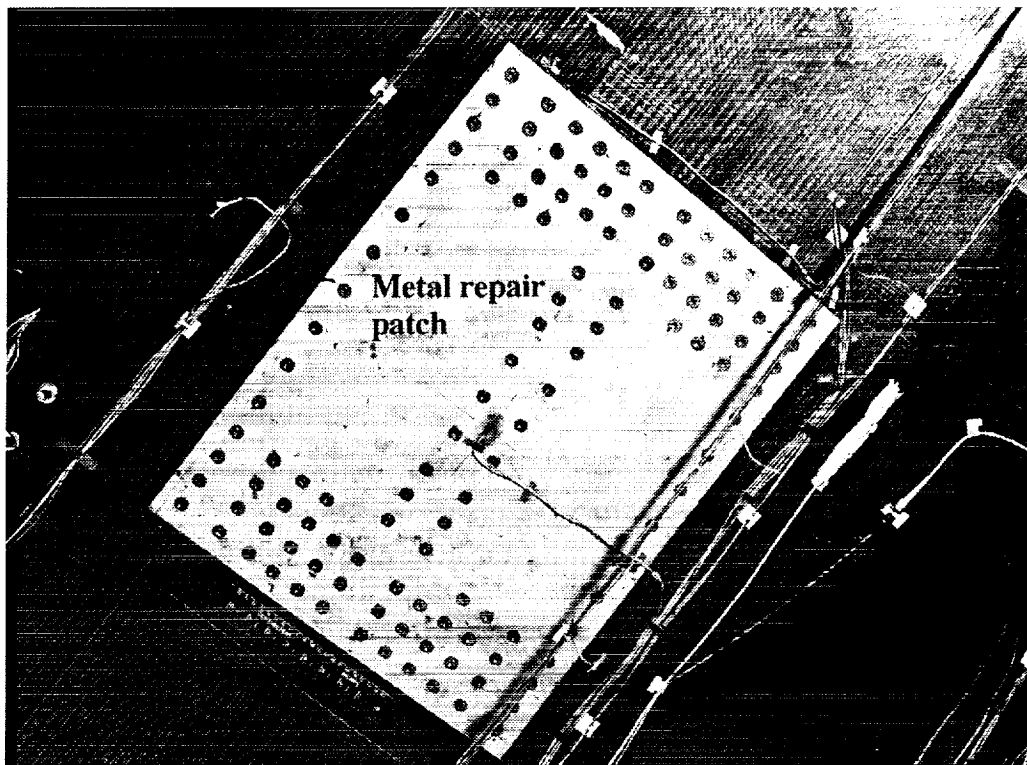


b) Upper cover panel
Figure 17. Concluded.



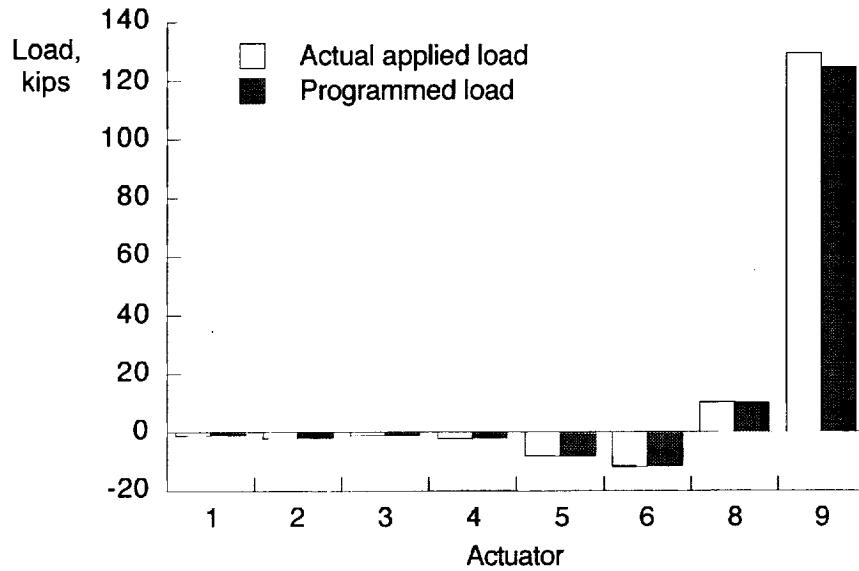
a) Upper cover panel

Figure 18. Repairs to cover panels.



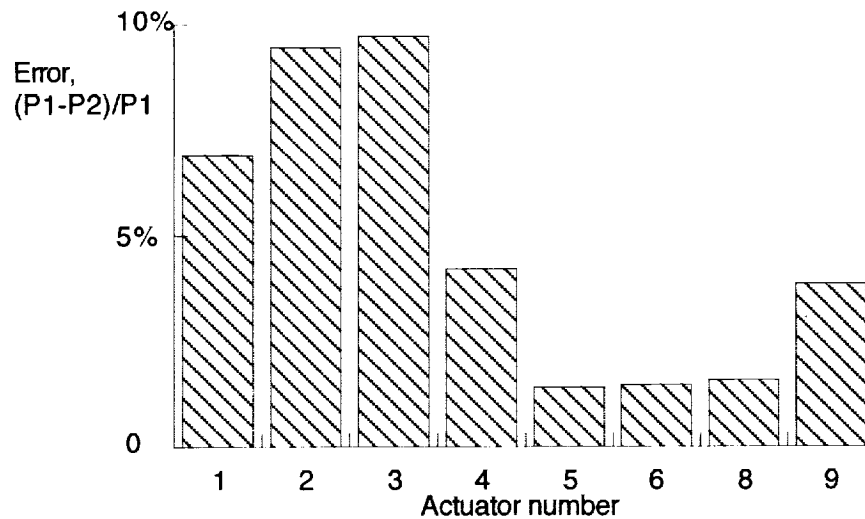
b) Lower cover panel.

Figure 18. Concluded.



a) Programmed and actual load at actuator positions

Figure 19. Brake roll load conditions.



b) Error in applied load where P1=actual load and P2=programmed load at DLL.

Figure 19. Concluded.

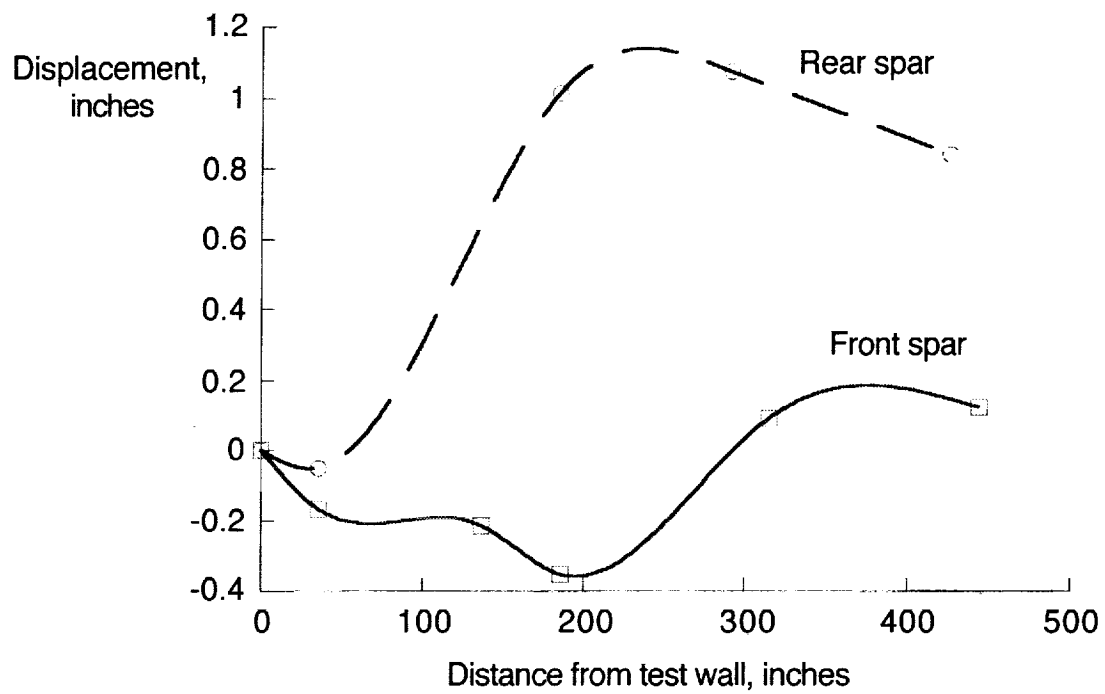


Figure 20. Displacements along front and rear spars of test article when loaded to DLL in the brake roll condition.

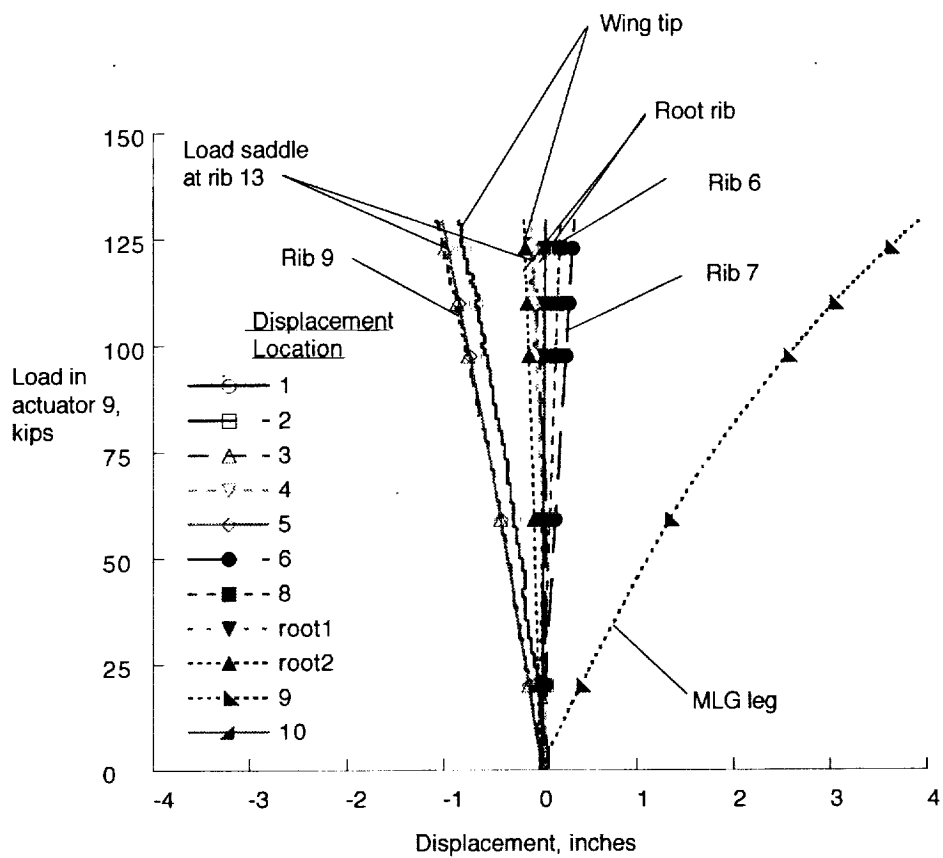


Figure 21. Measured displacements for loading to DLL in the brake roll condition. Displacement locations shown on figure2b.

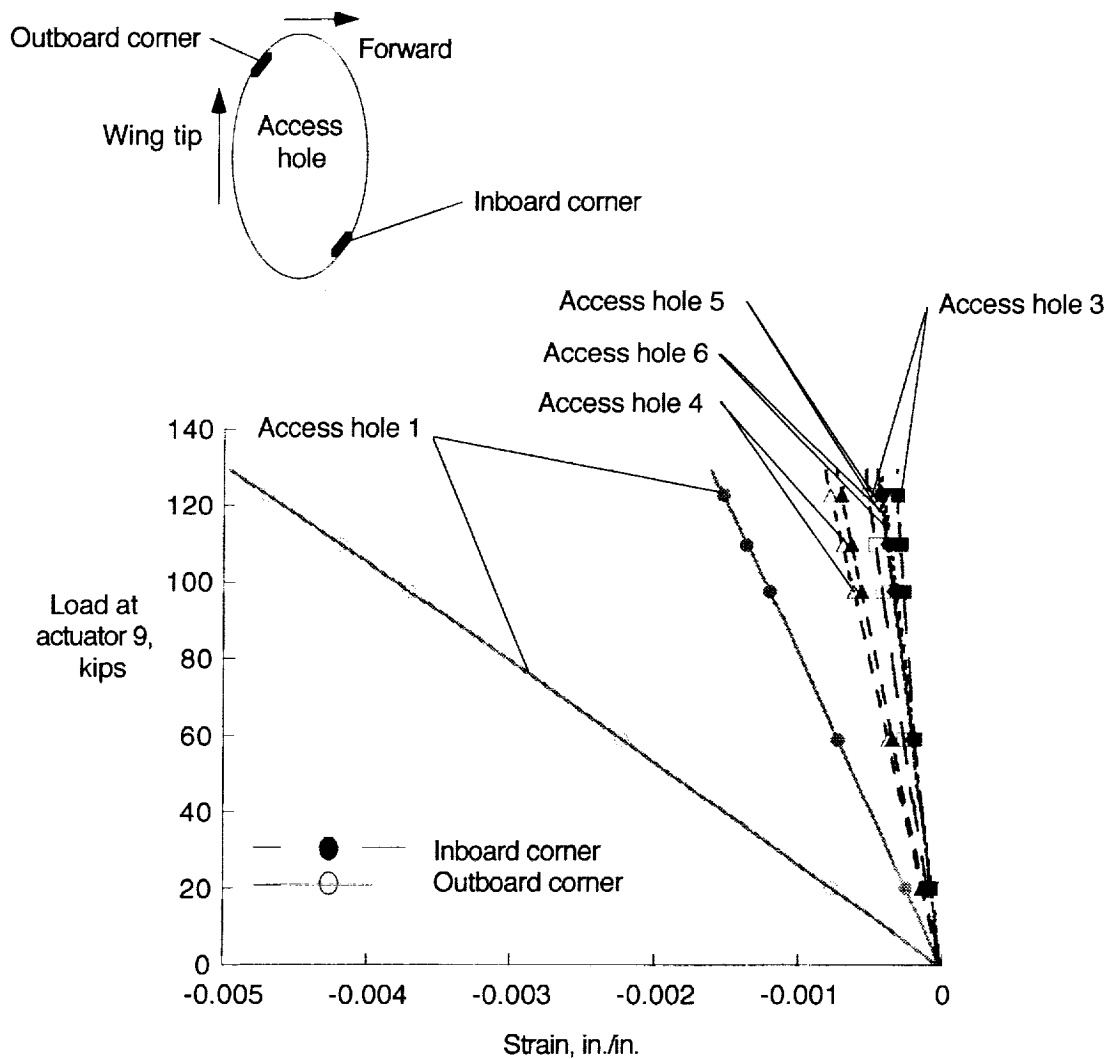


Figure 22. Measured strain at access hole edges for load to DLL in brake roll condition. Access hole locations are shown in figure 2.

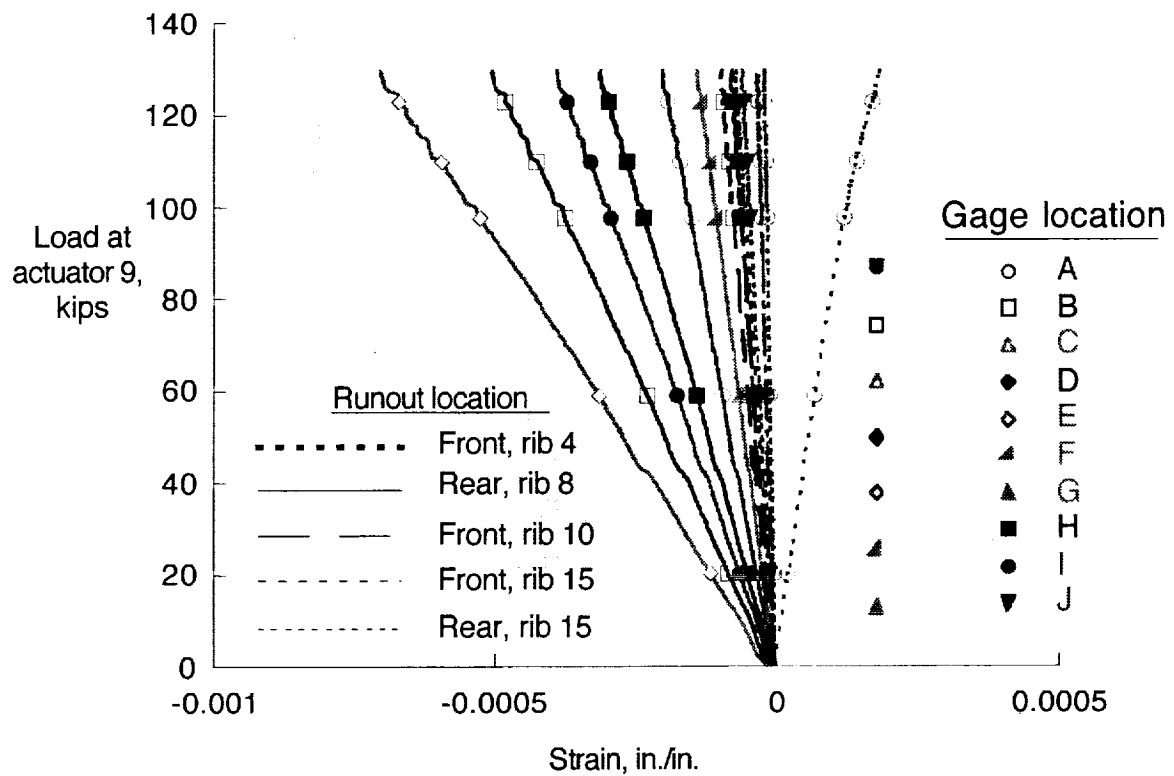


Figure 23. Measured strain at lower cover stringer runouts at DLL for brake roll load condition. Strain gage locations are shown in figures 3 and 4.

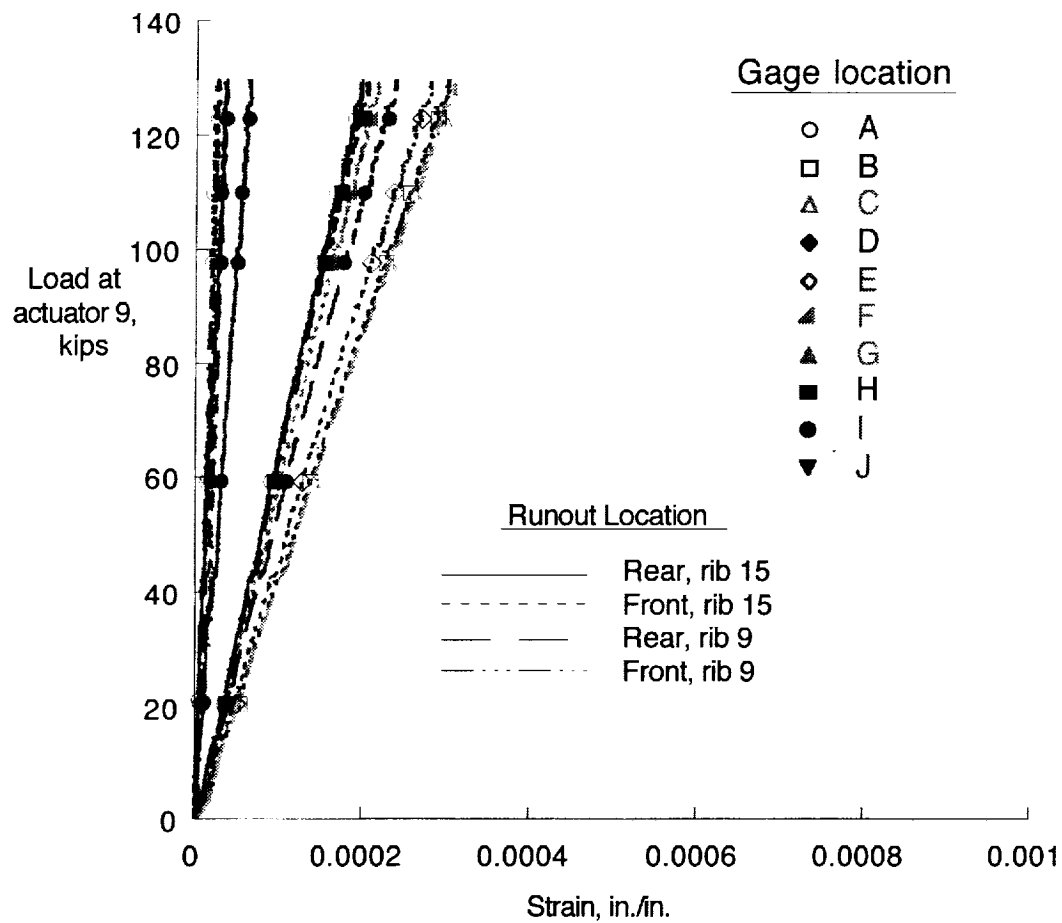


Figure 24. Strain in upper cover stringer runouts for loading to DLL in the brake roll load condition. Strain gage locations are shown in figures 3 and 4.

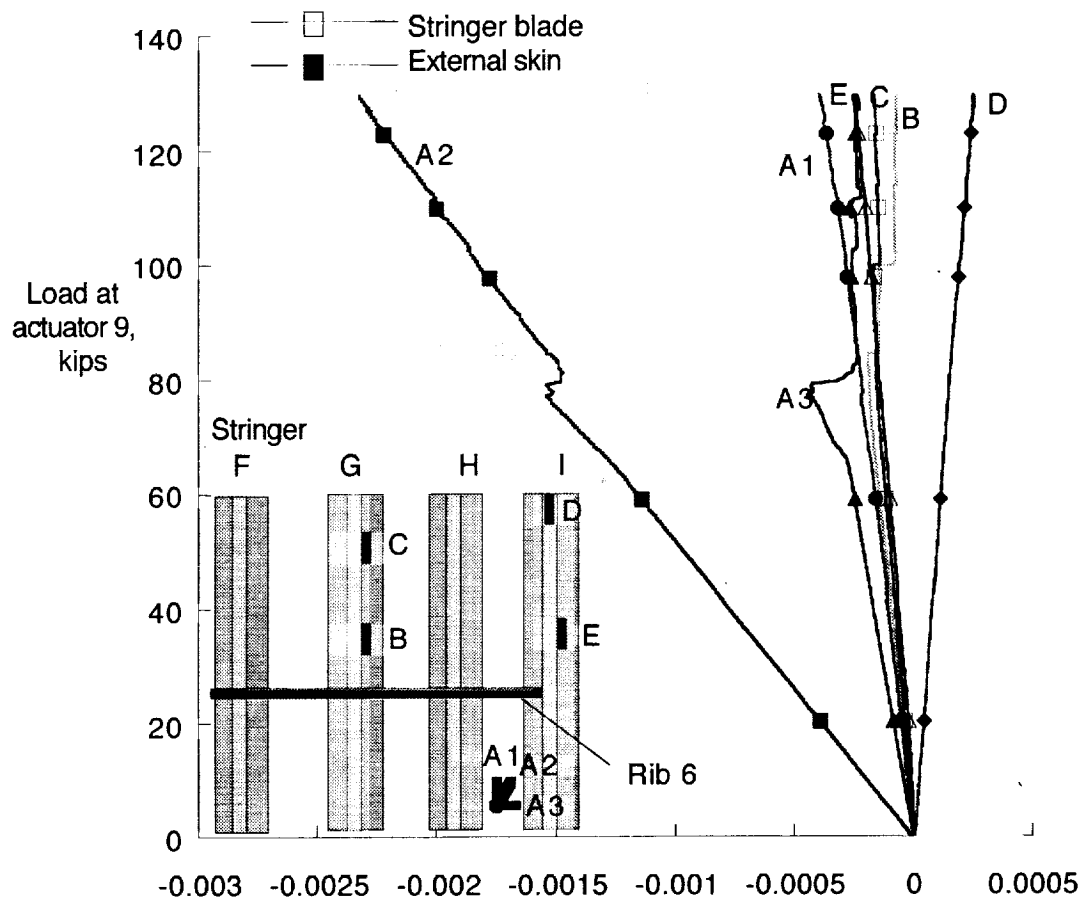


Figure 25. Strain in upper cover main landing gear region for loading to DLL in the brake roll load condition. Strain gage locations are shown on figure 9.

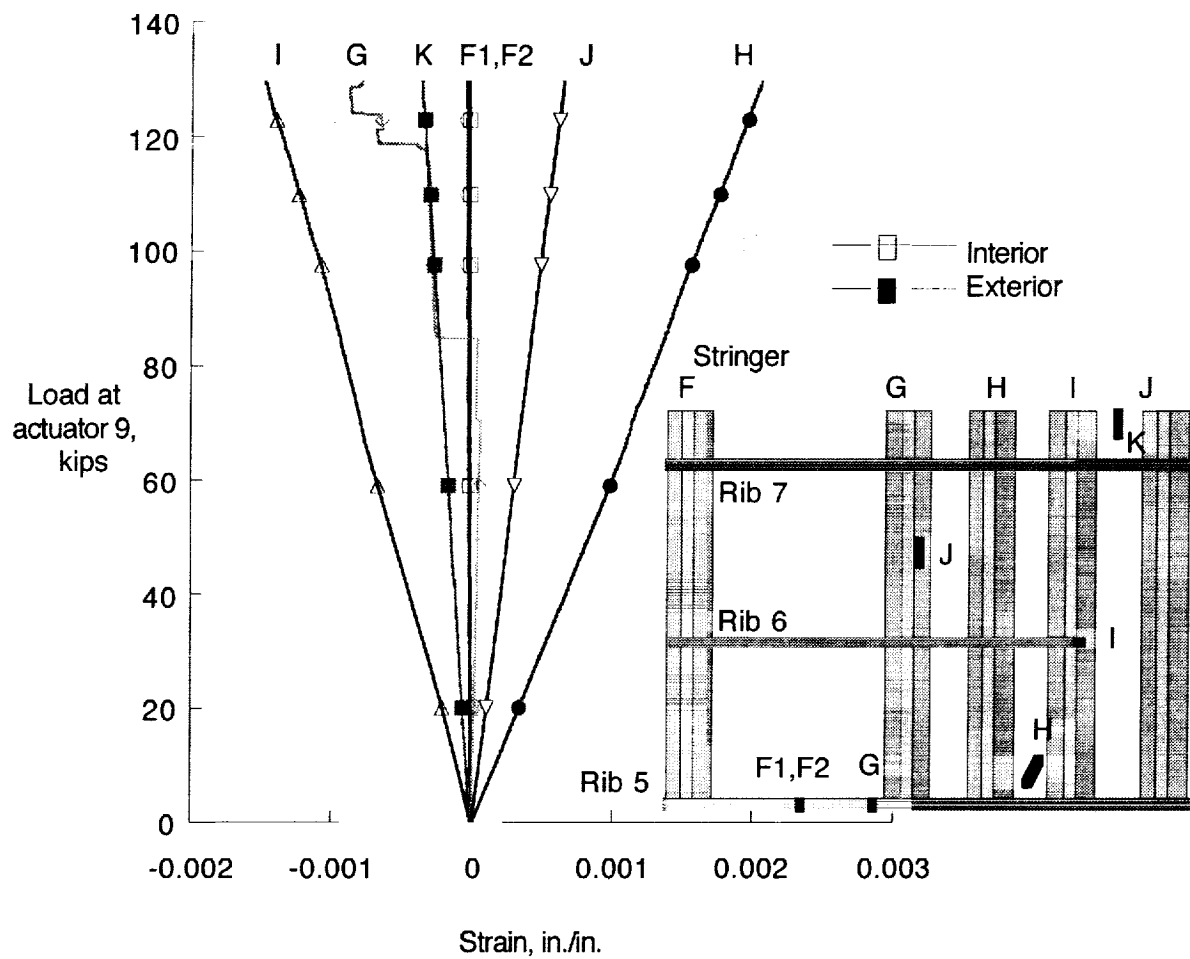


Figure 26. Strain in main landing gear area of the lower cover for loading to DLL in the brake roll load condition. Strain gage locations are shown on figure 9.

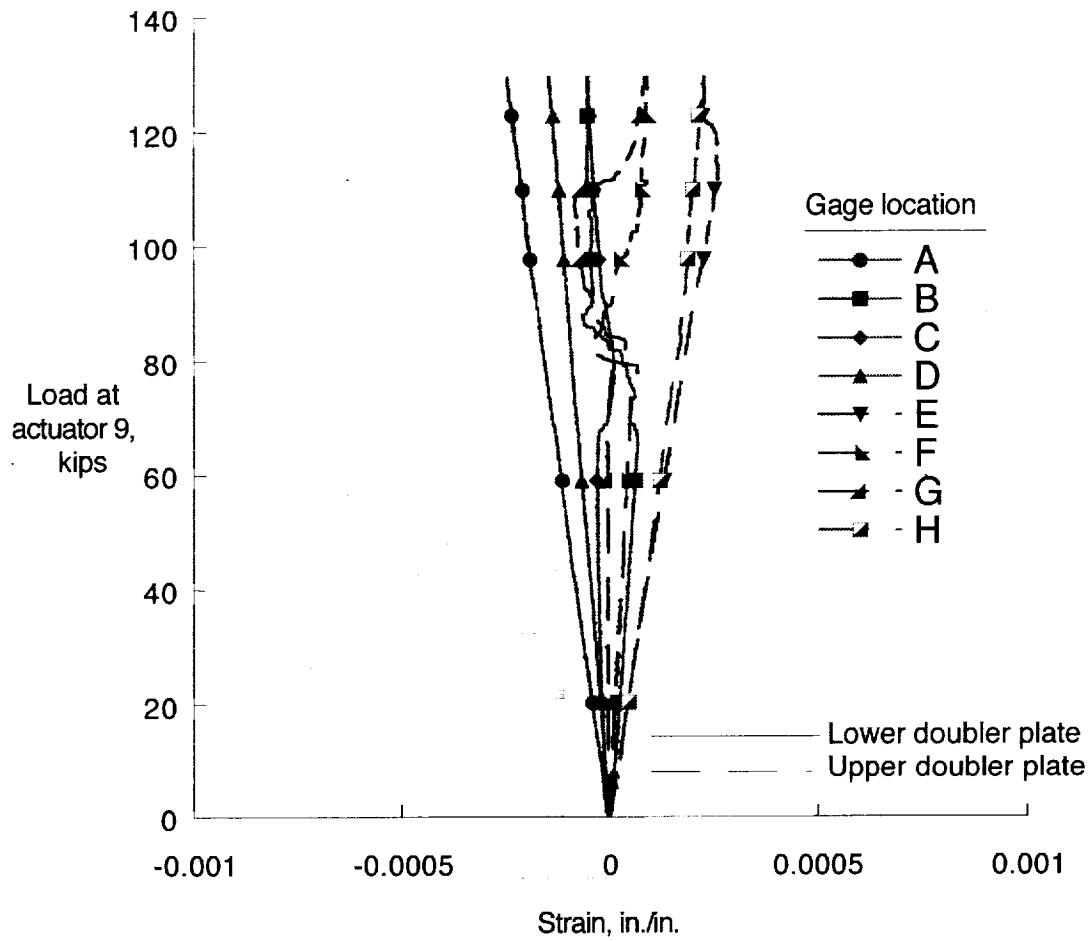


Figure 27. Strain in MLG plates for loading to DLL in the brake roll load condition. Strain gage locations are shown on figure 9.

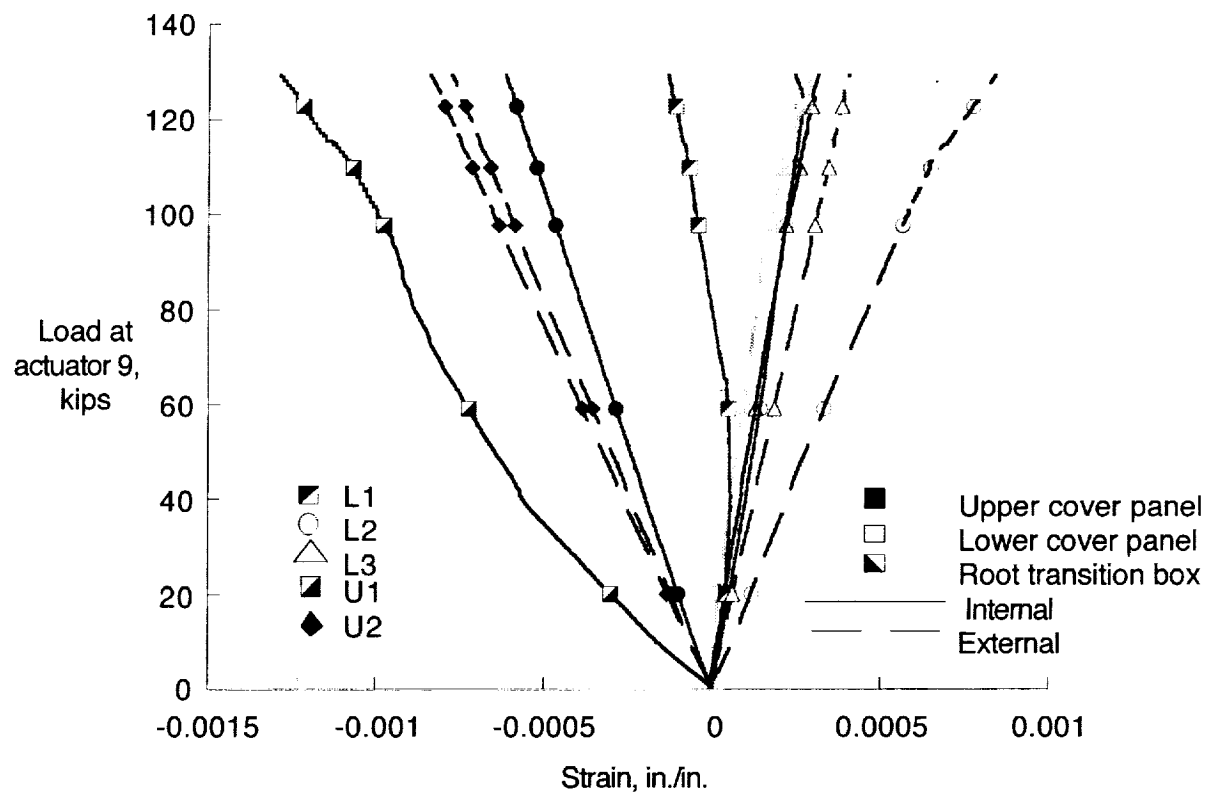


Figure 28. Strain in root region at DLL for brake roll load condition. Strain gage locations are shown in figures 7 and 8.

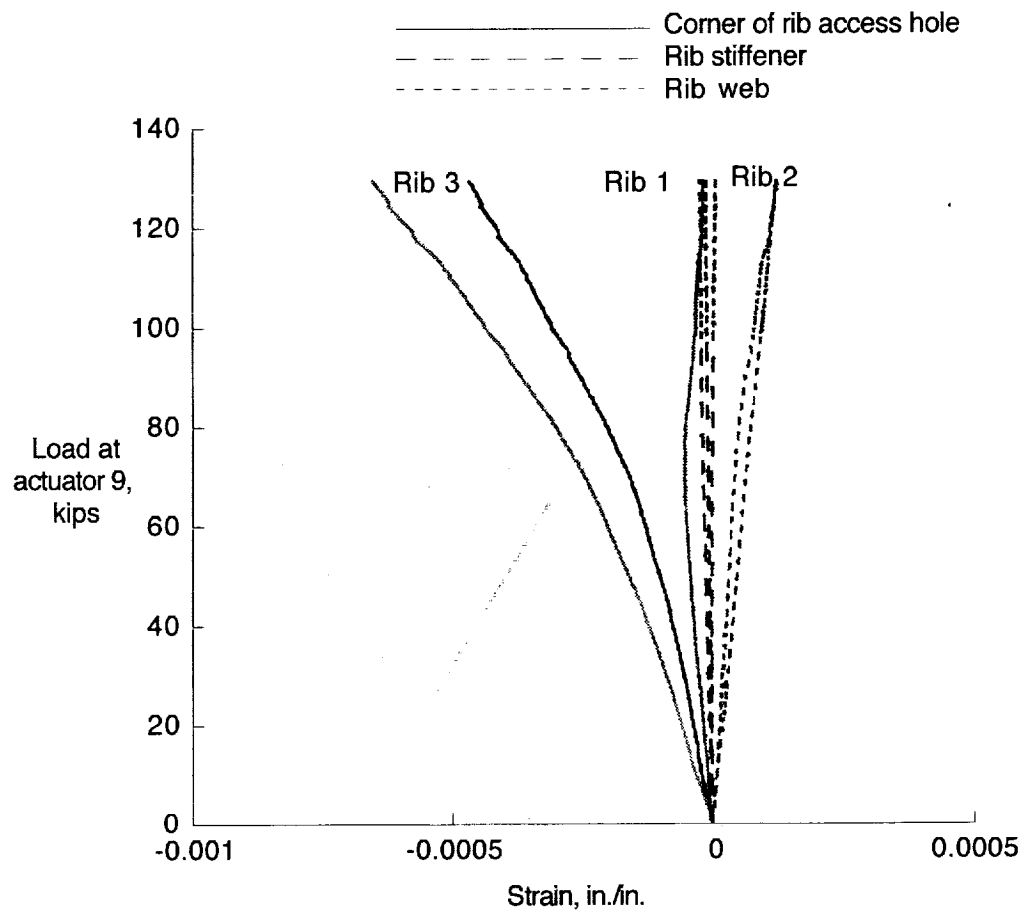


Figure 29. Measured strain in ribs 1, 2, and 3 at DLL for brake roll load condition. Strain gage locations are shown in figures 11a, 11b and 11c.

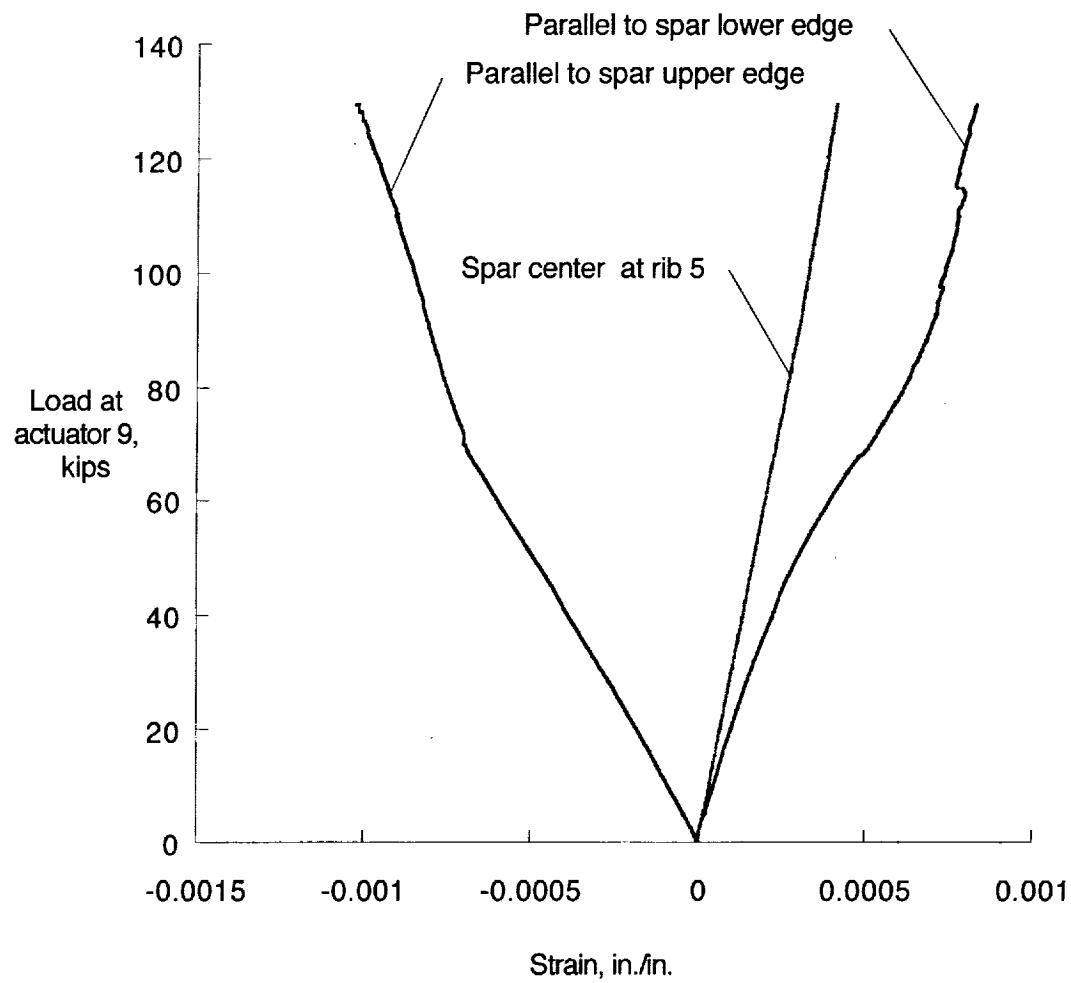


Figure 30. Strain in rear spar for loading to DLL in the brake roll load condition. Strain gage locations are shown in figure 10.

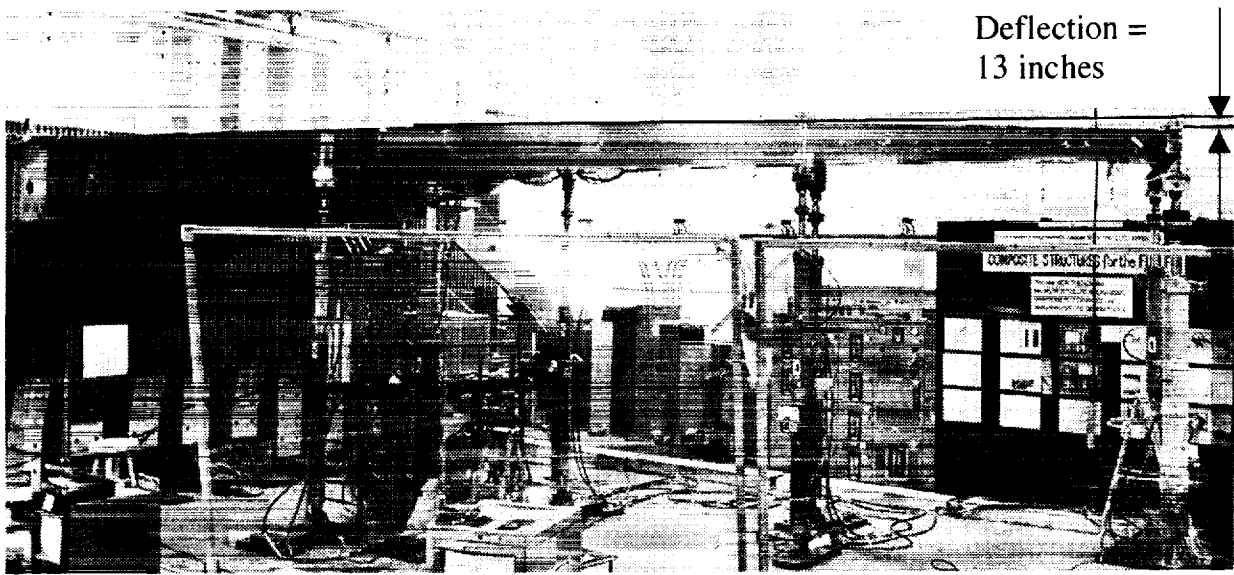
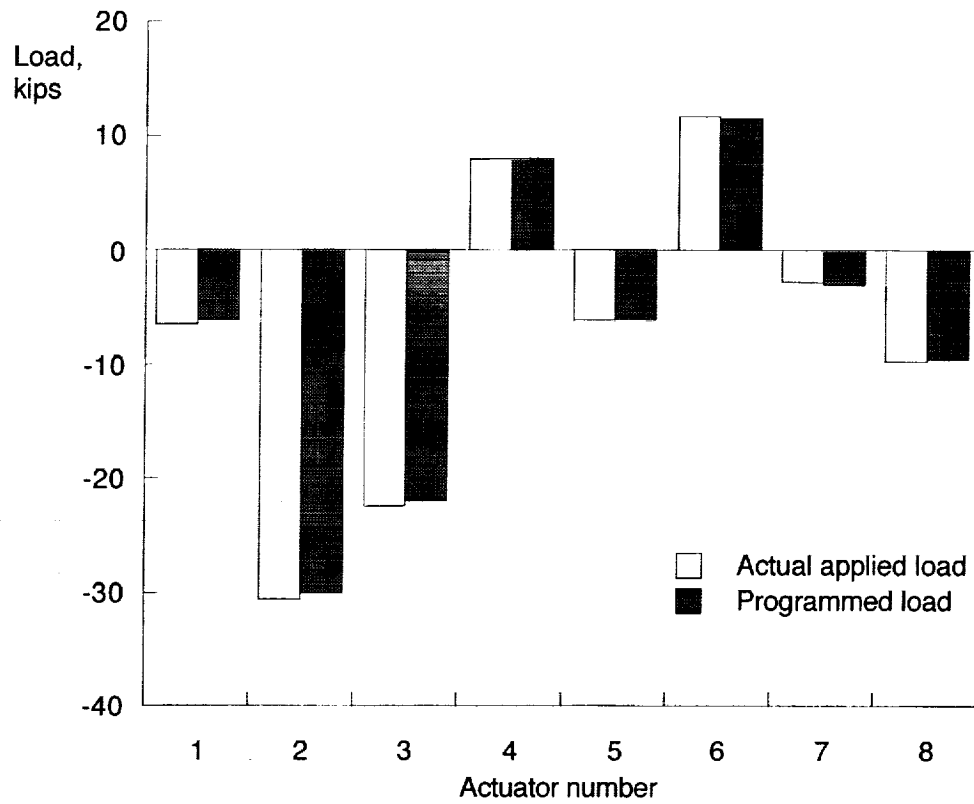
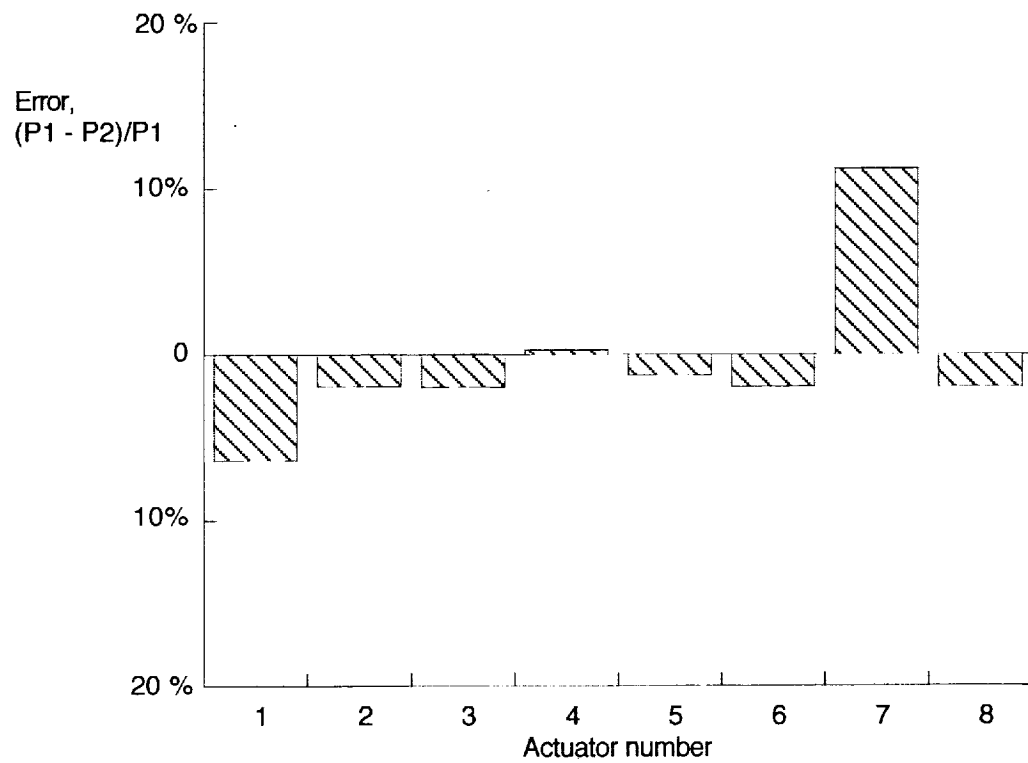


Figure 31. Deformed test article loaded to DLL in -1G condition.



a) Programmed and actual applied load at actuator positions.

Figure 32. Load in -1G condition.



b) Error in applied load where P1= actual load, and P2=programmed load at DLL.

Figure 32. Concluded.

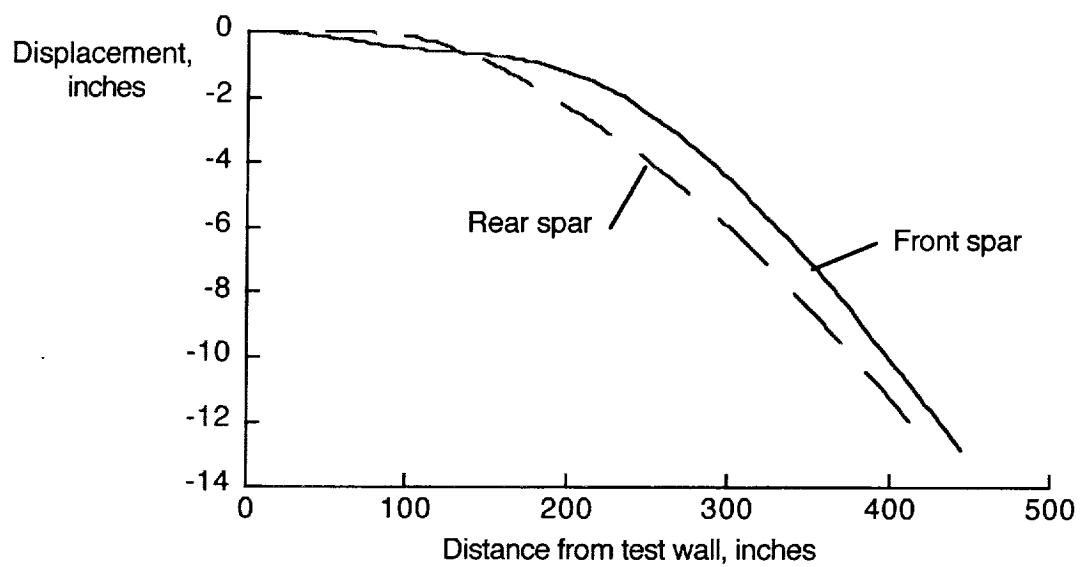


Figure 33. Displacements along front and rear spars of test article when loaded to DLL in the -1G condition.

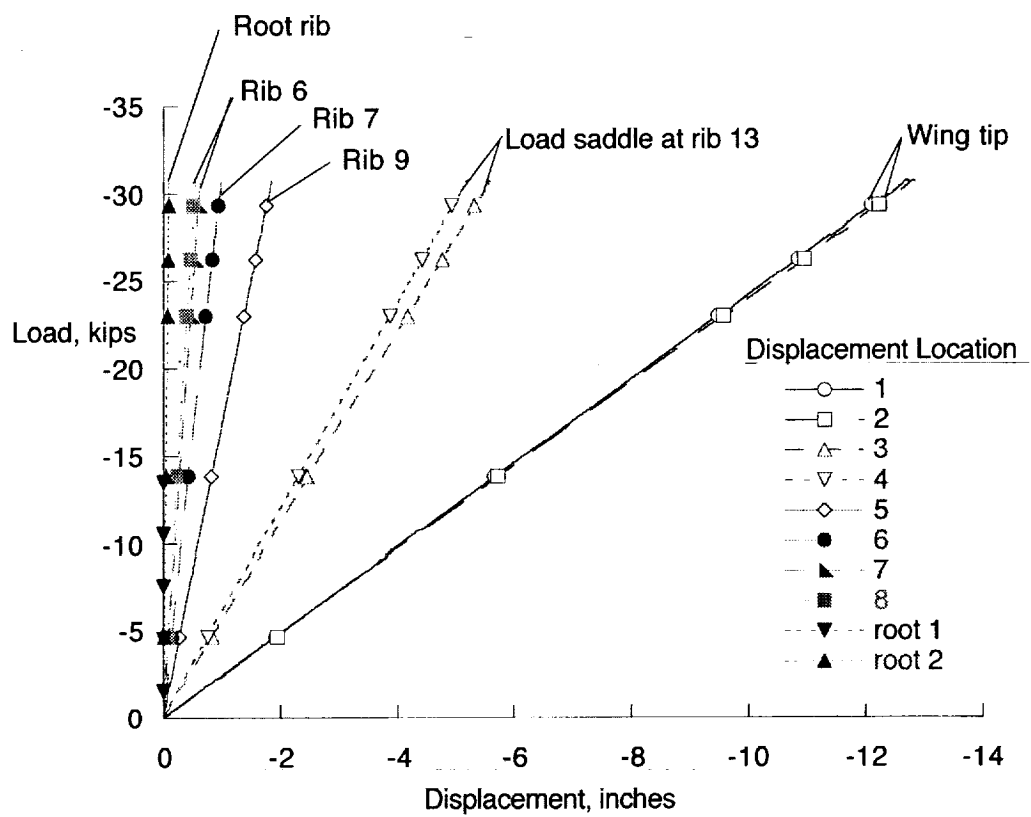


Figure 34. Measured displacements for loading to DLL in -1G condition. Displacement locations are shown on figure 2b.

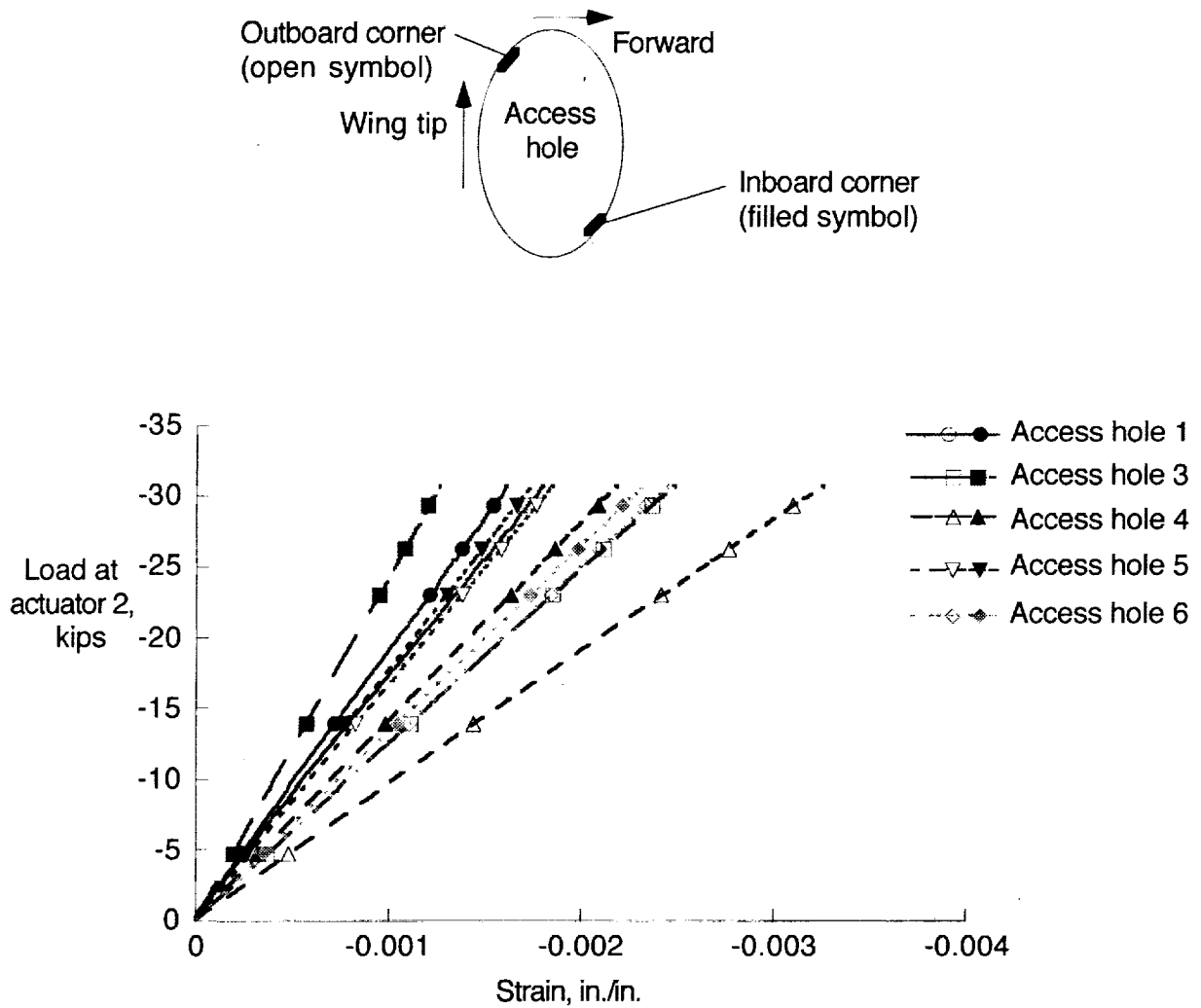


Figure 35. Measured strain at access hole edges for load to DLL in -1G load condition. Access hole locations are shown in figure 2.

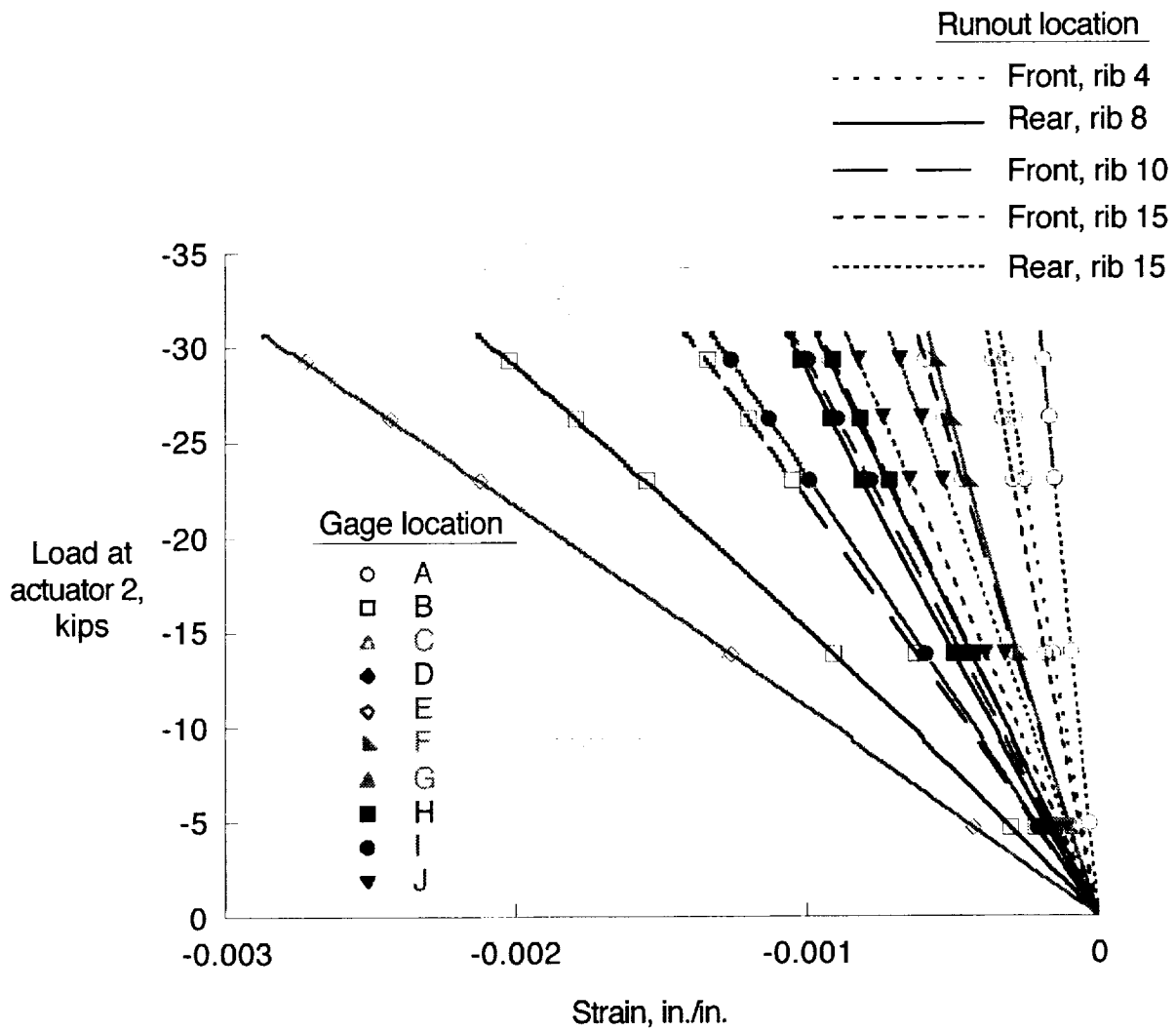


Figure 36. Measured strain at lower cover stringer runouts at DLL for -1G load condition. Strain gage locations are shown in figures 3 and 4.

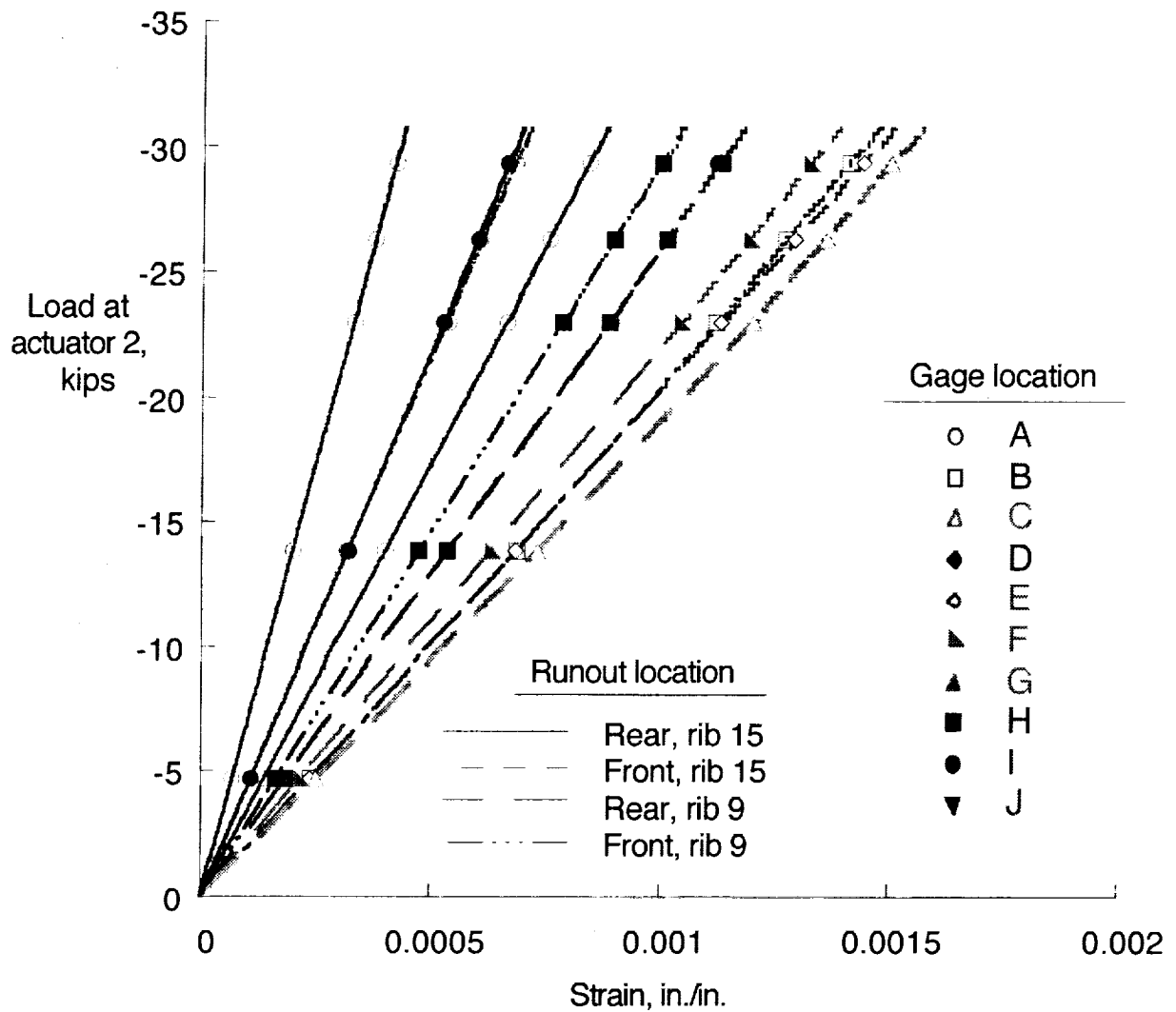


Figure 37. Strain in upper cover stringer runouts for loading to DLL in the -1G load condition. Strain gage locations are shown in figures 3 and 4.

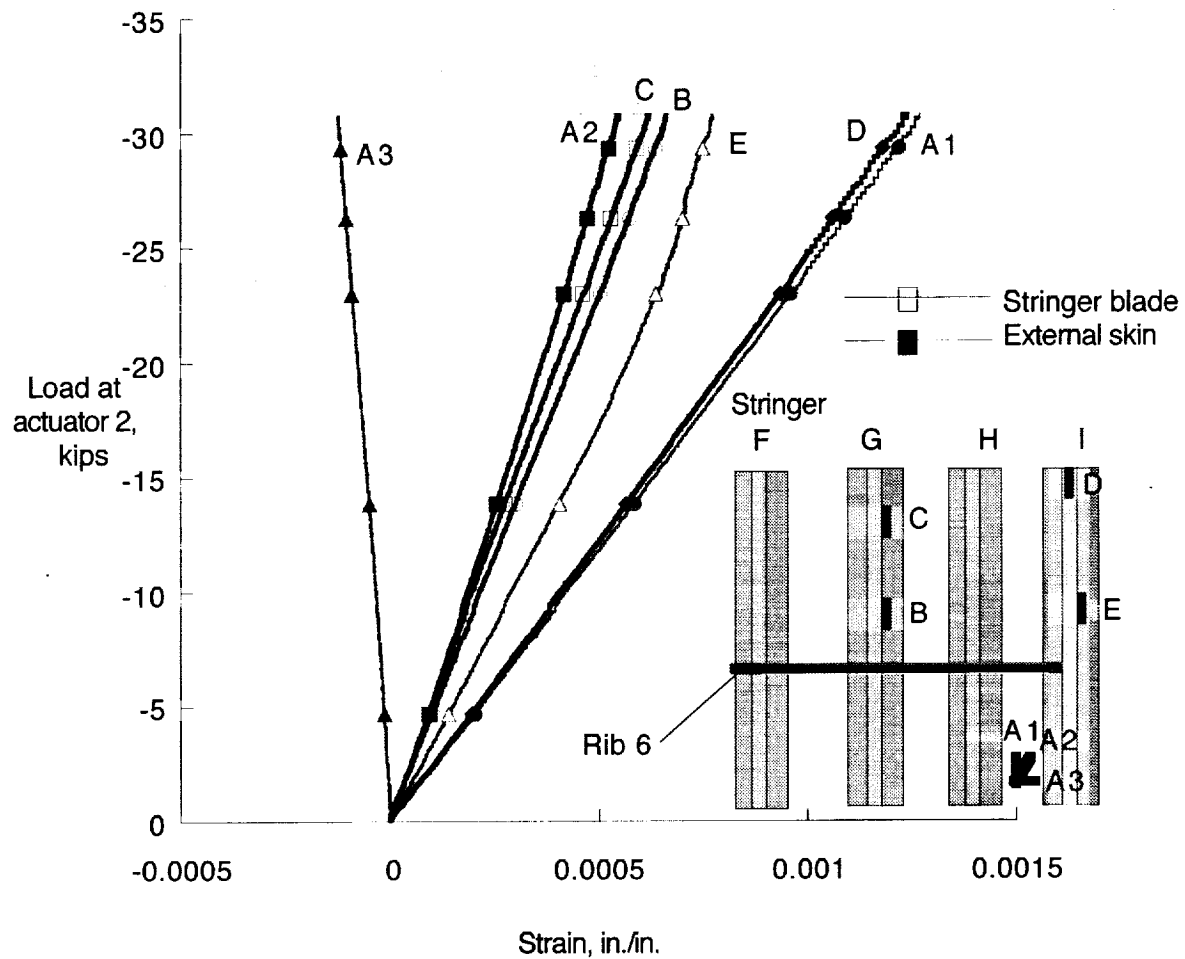


Figure 38. Strain in upper cover main landing gear region for loading to DLL in the -1G load condition. Strain gage locations are shown on figure 9.

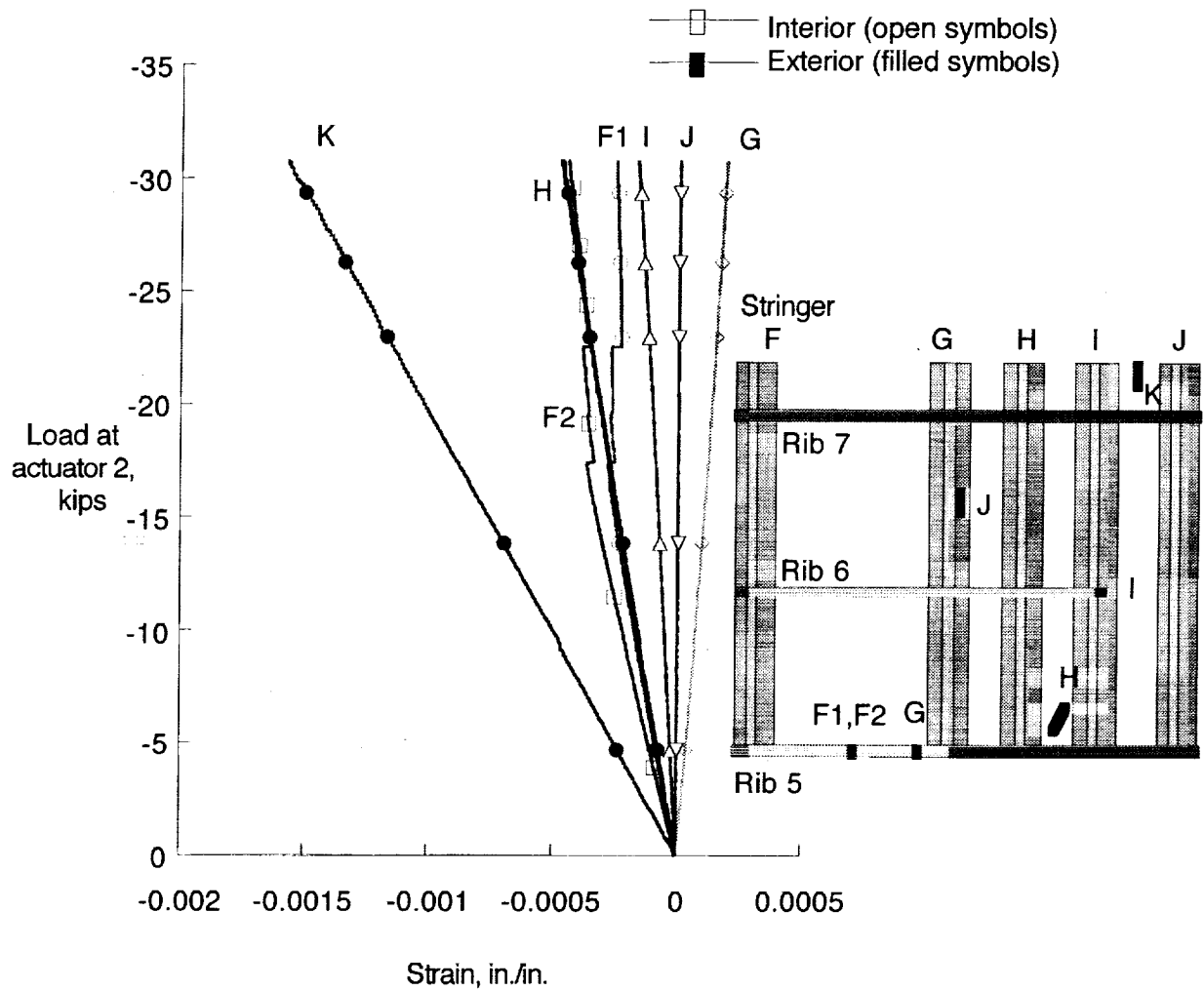


Figure 39. Strain in main landing gear area of the lower cover for loading to DLL in the -1G load condition. Strain gage locations are shown on figure 9.

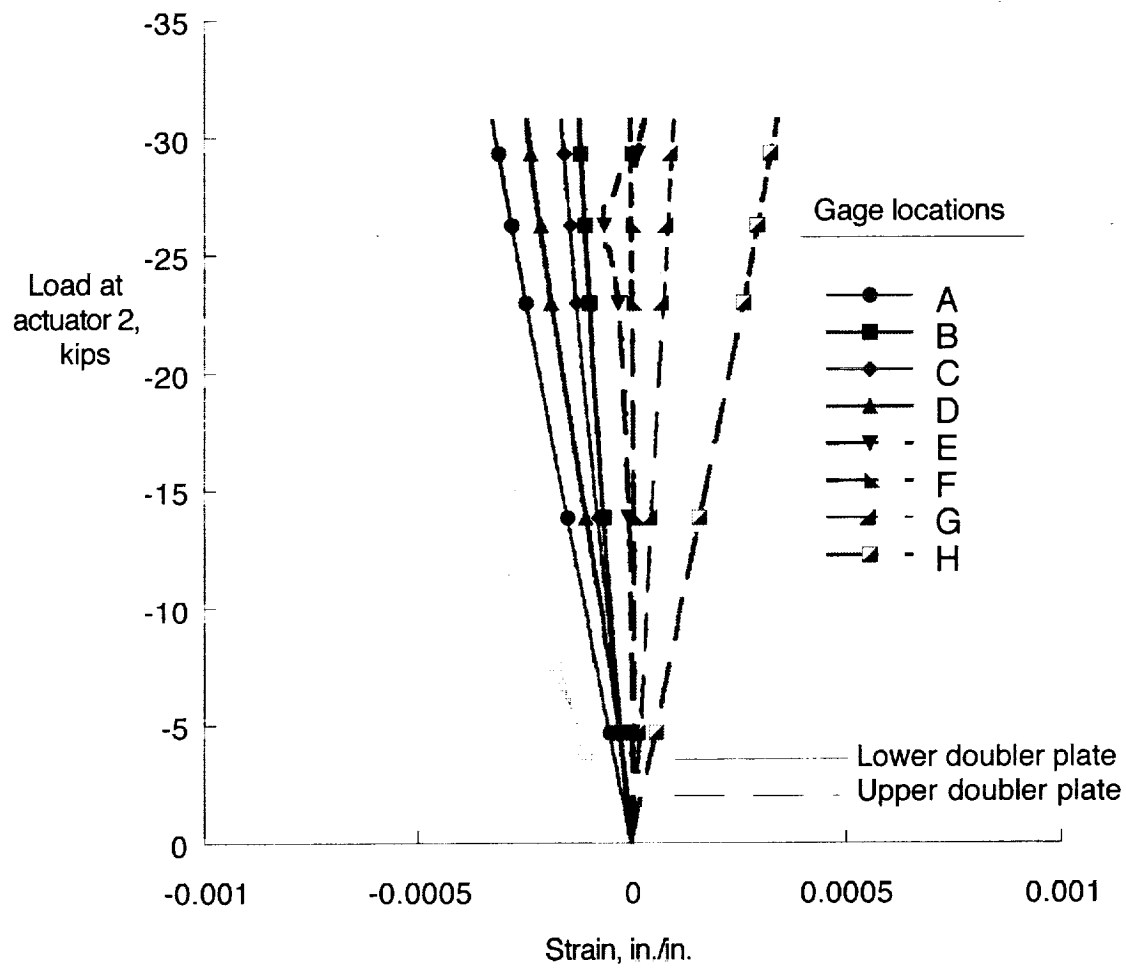


Figure 40. Strain in MLG doublers for loading to DLL in the -1G load condition. Strain gage locations are shown on figure 9.

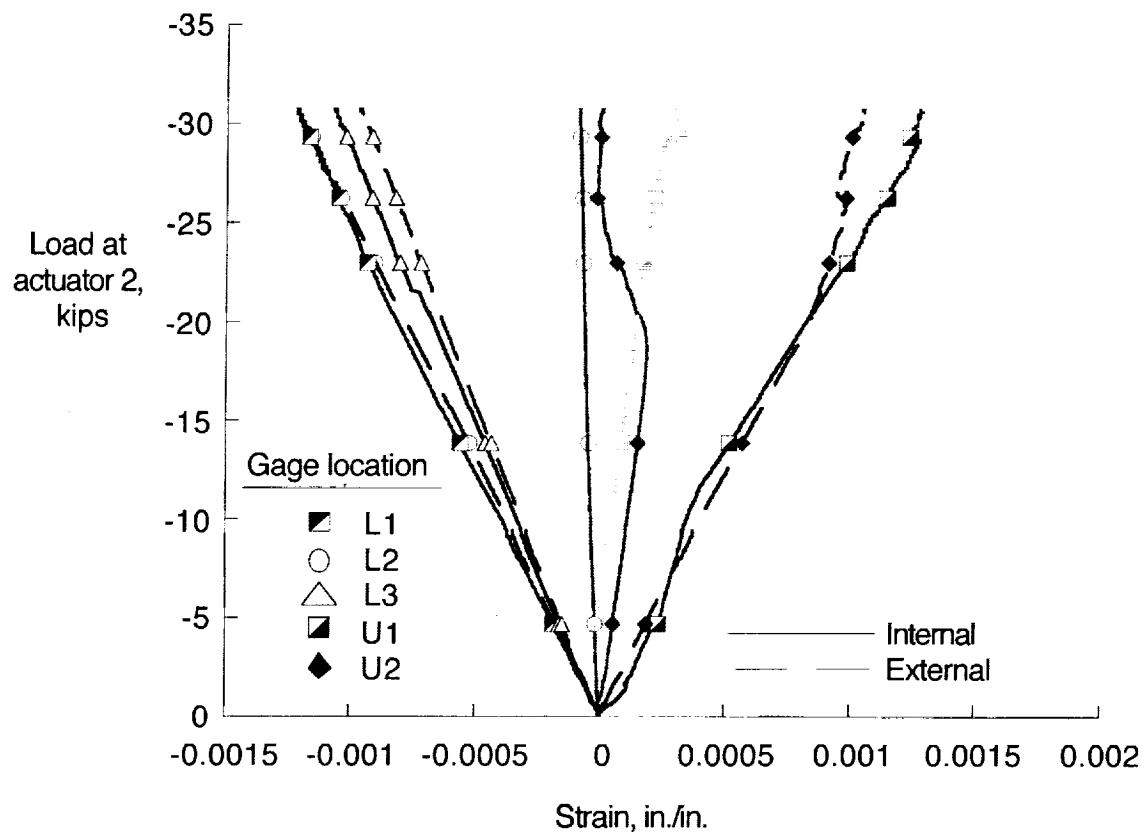


Figure 41. Strain in root region at DLL for -1G load condition. Strain gage locations are shown in figure 7 and 8.

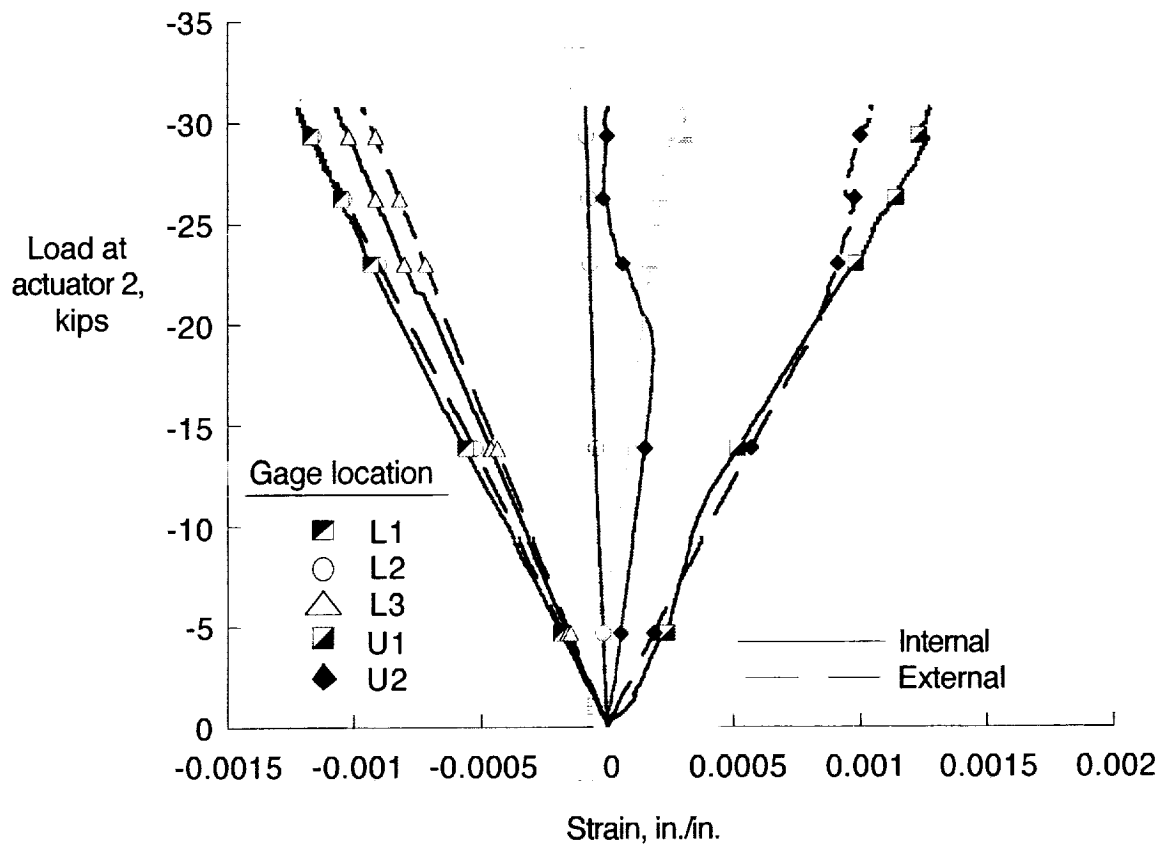


Figure 41. Strain in root region at DLL for -1G load condition. Strain gage locations are shown in figure 7 and 8.

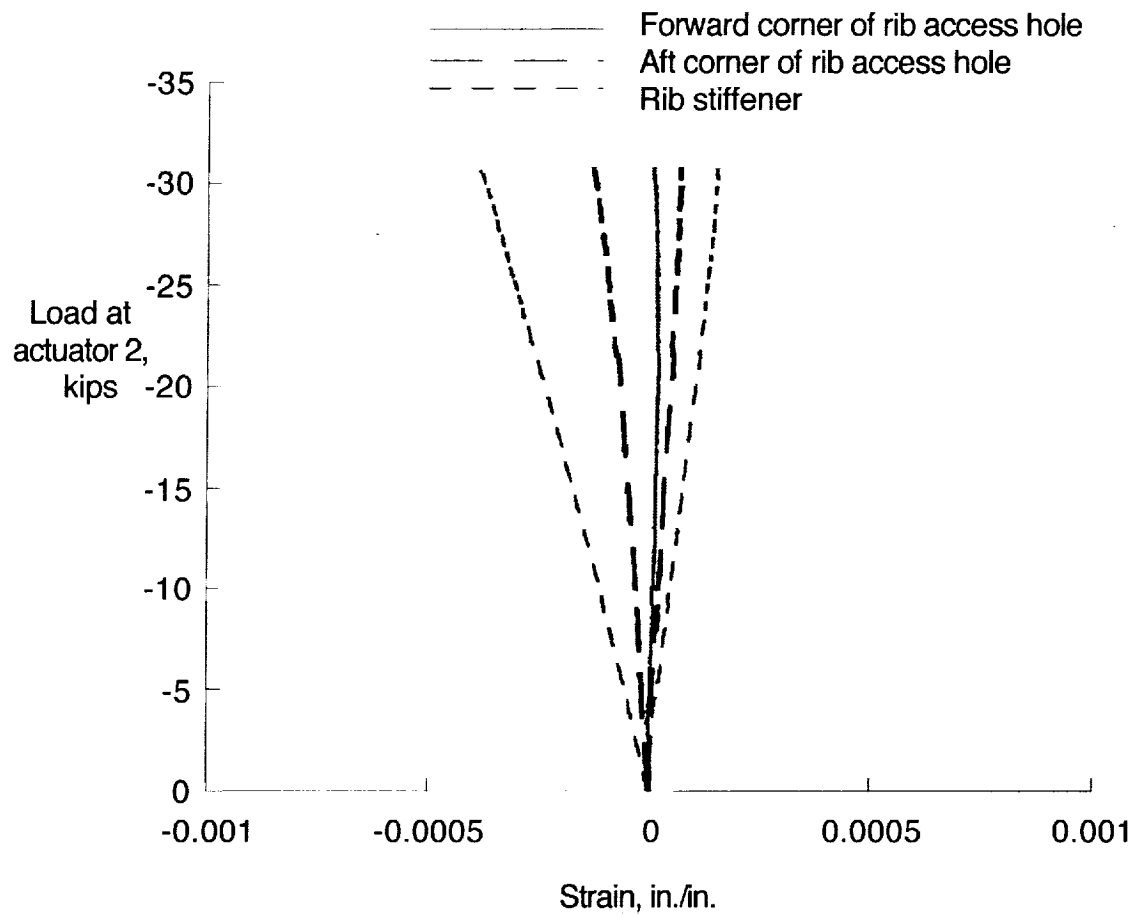


Figure 42. Strain in rib 4 for loading to DLL in the -1G load condition. Strain gage locations are shown in figure 11d.

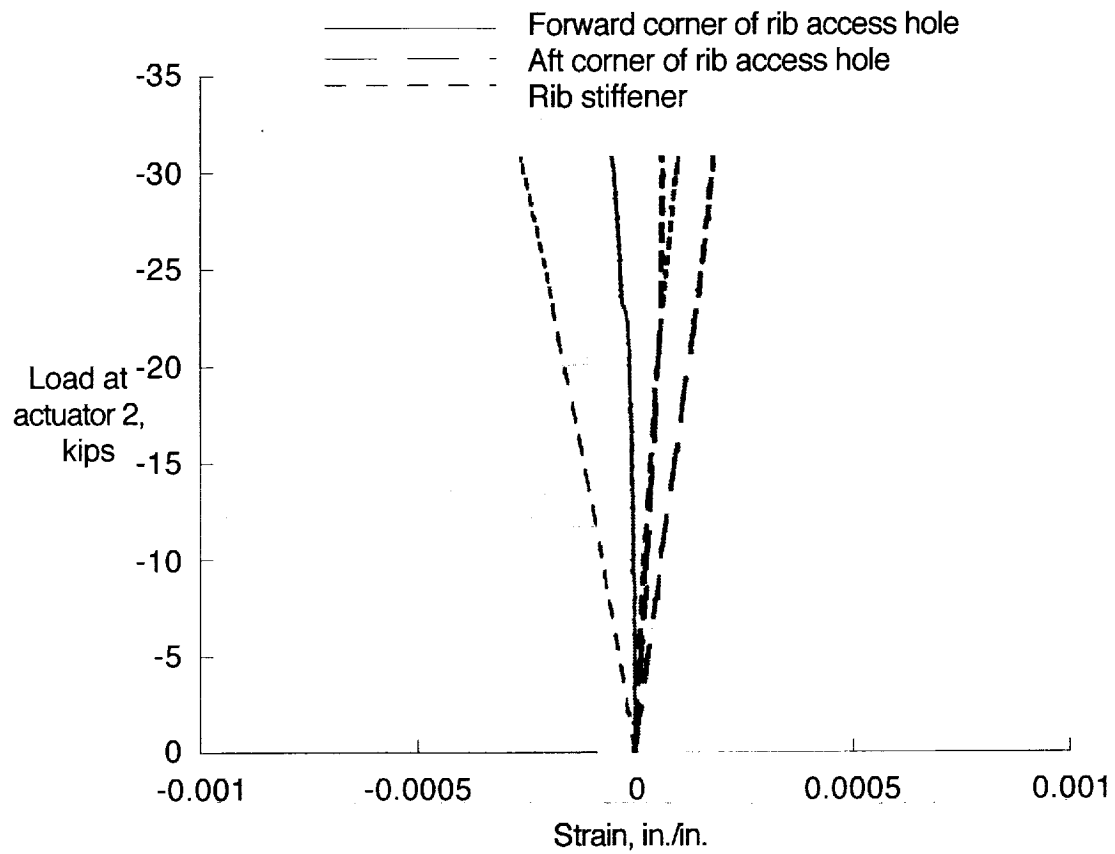


Figure 43. Strain in rib 5 for loading to DLL in the -1G load condition. Strain gage locations are shown on figure 11d.

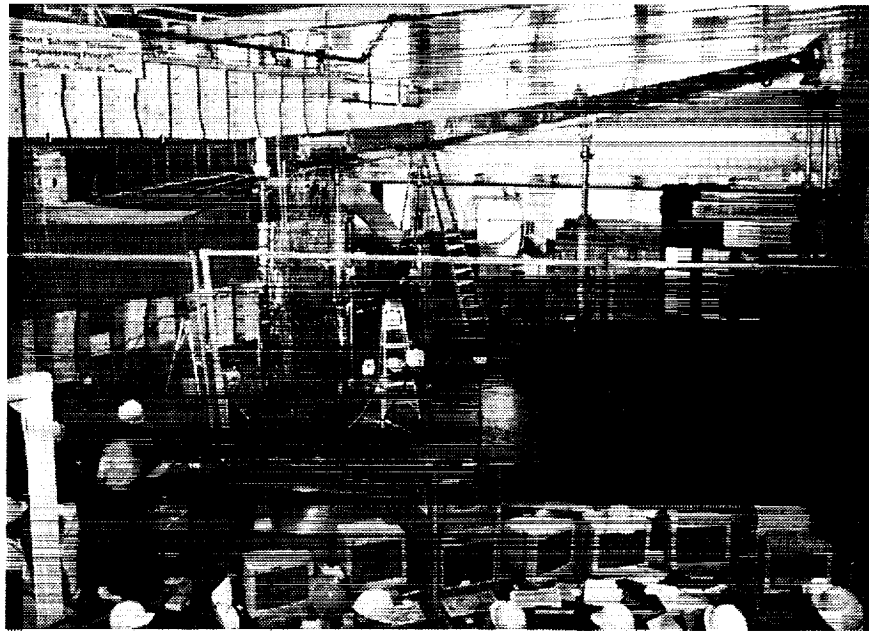
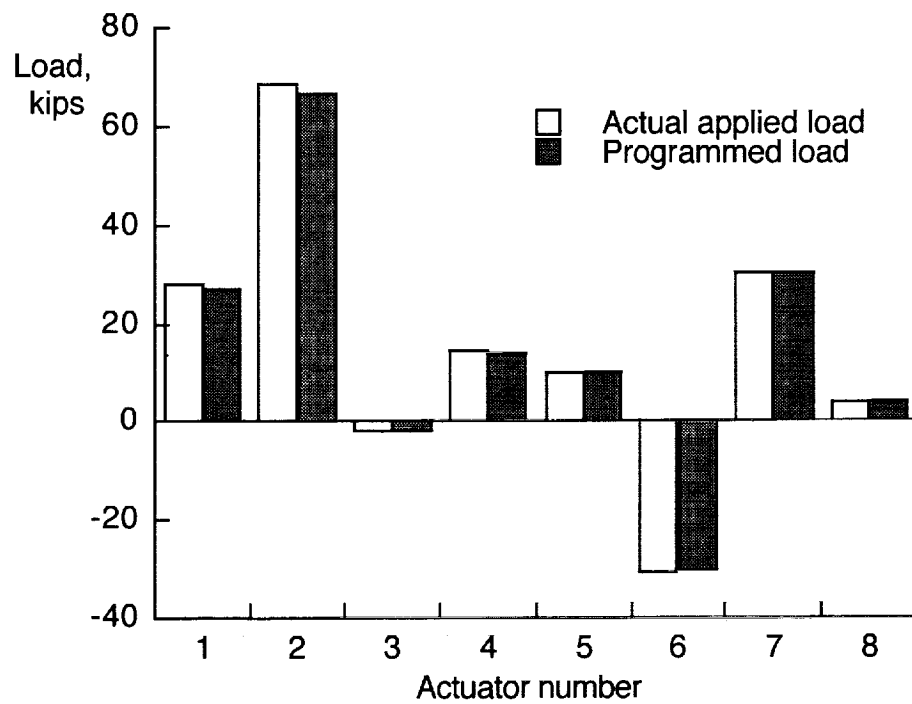
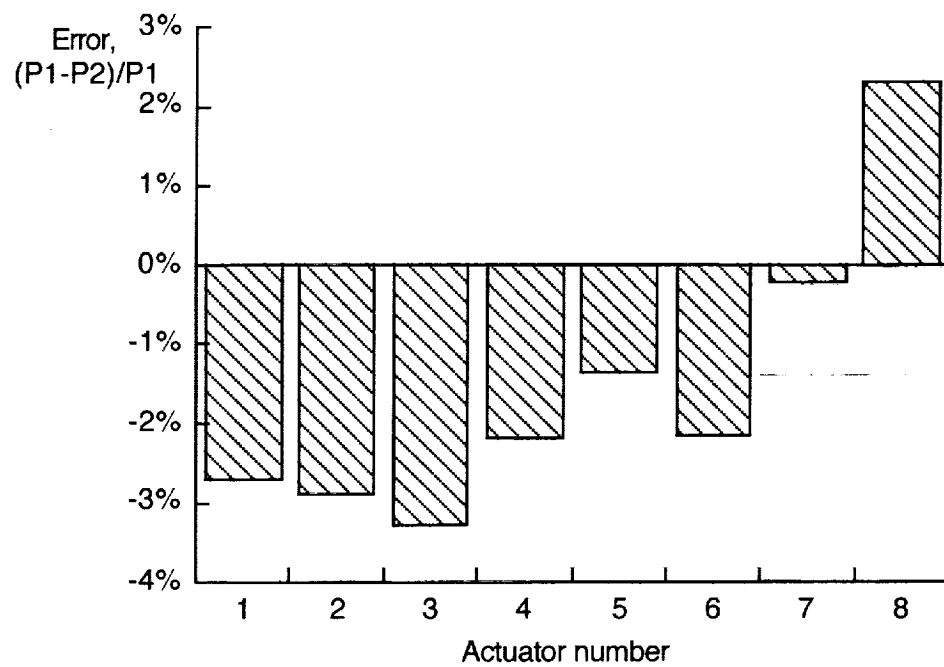


Figure 44. Test article loaded to 95% DUL in 2.5G load condition.



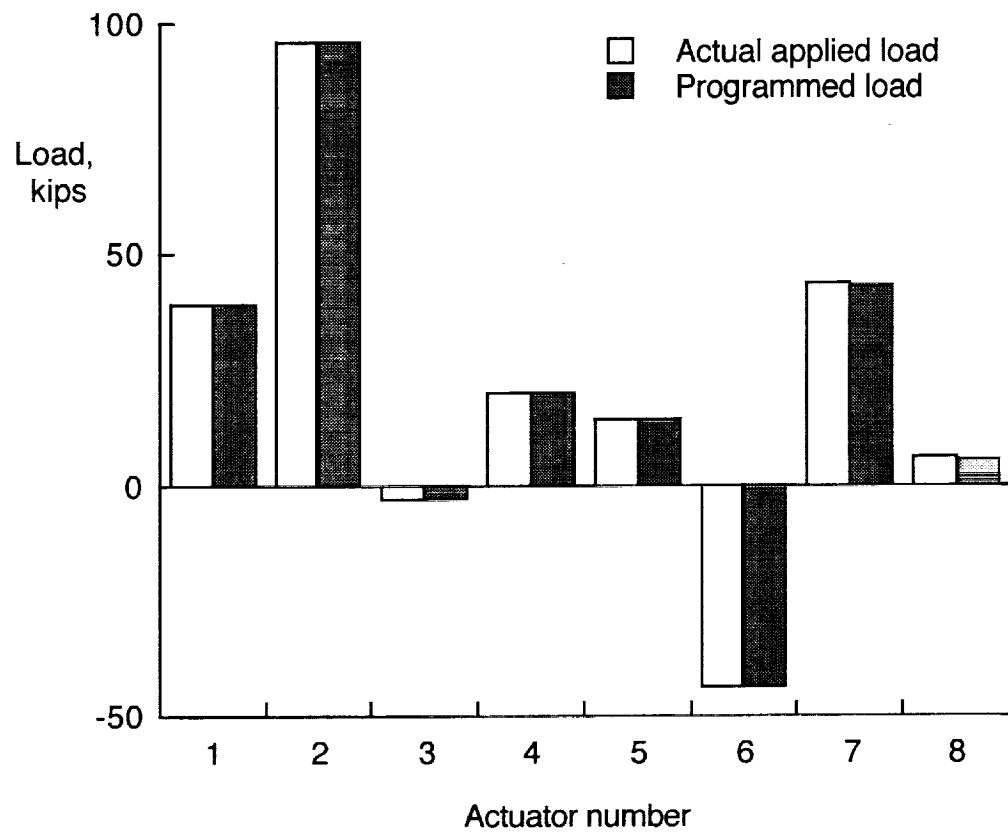
a) Programmed and actual applied load at actuator positions

Figure 45. Loading for test to DLL in the 2.5G load condition.



b) Error in applied load where P1= actual load, and P2=programmed load at DLL

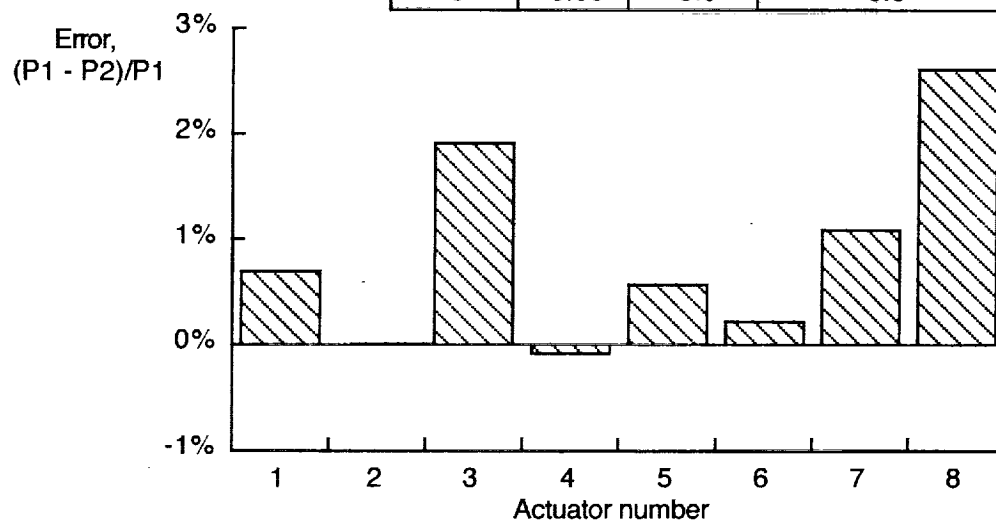
Figure 45. Concluded.



a) Programmed and actual applied load at actuator positions

Figure 46. Loading in test to failure in the 2.5G loading condition.

Actuator	DUL (kips)	Final test load (kips)	Corresponding programmed load (kips)	Error (%)
1	40.50	39.3	39.0	0.7
2	99.75	96.1	96.1	0.0
3	-3.00	-2.9	-2.9	1.9
4	21.00	20.2	20.2	0.0
5	15.00	14.5	14.5	0.6
6	-45.00	-43.5	-43.4	0.2
7	45.00	43.8	43.4	1.0
8	6.00	5.9	5.8	2.6



b) Error in applied load where $P1$ = actual load, and $P2$ =programmed load at failure

Figure 46. Concluded.

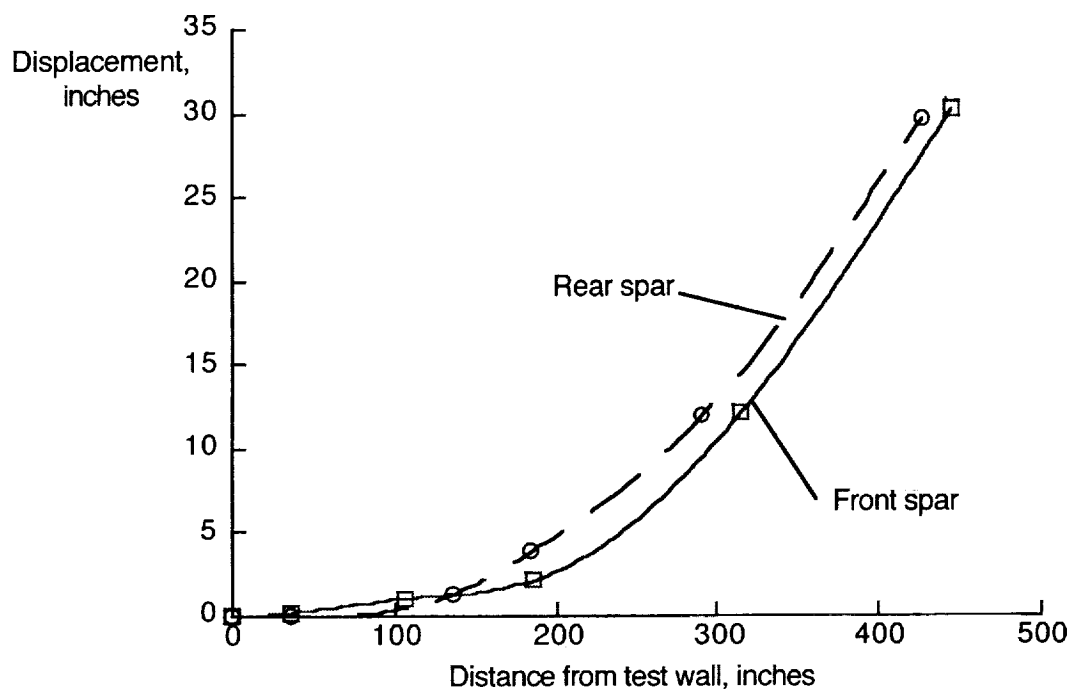


Figure 47. Displacement along front and rear spars of test article when loaded to DLL in the 2.5G condition.

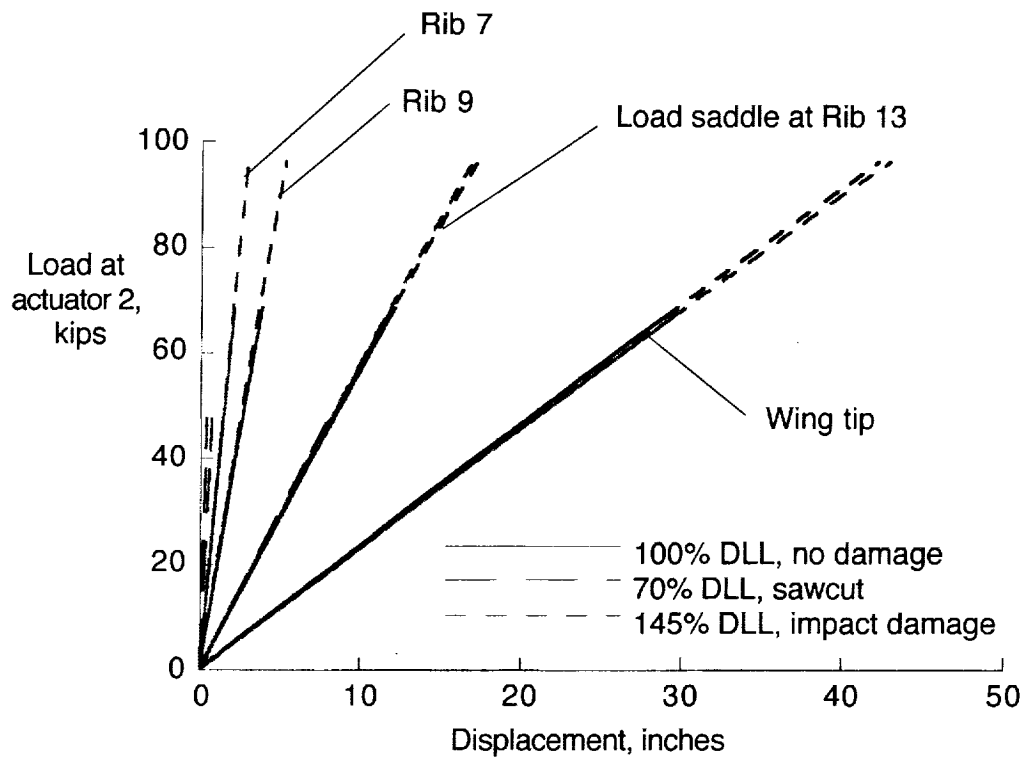


Figure 48. Comparison between displacement results in three different 2.5G loadings of structure: with no damage, with saw cut damage, and with impact damage and repair.

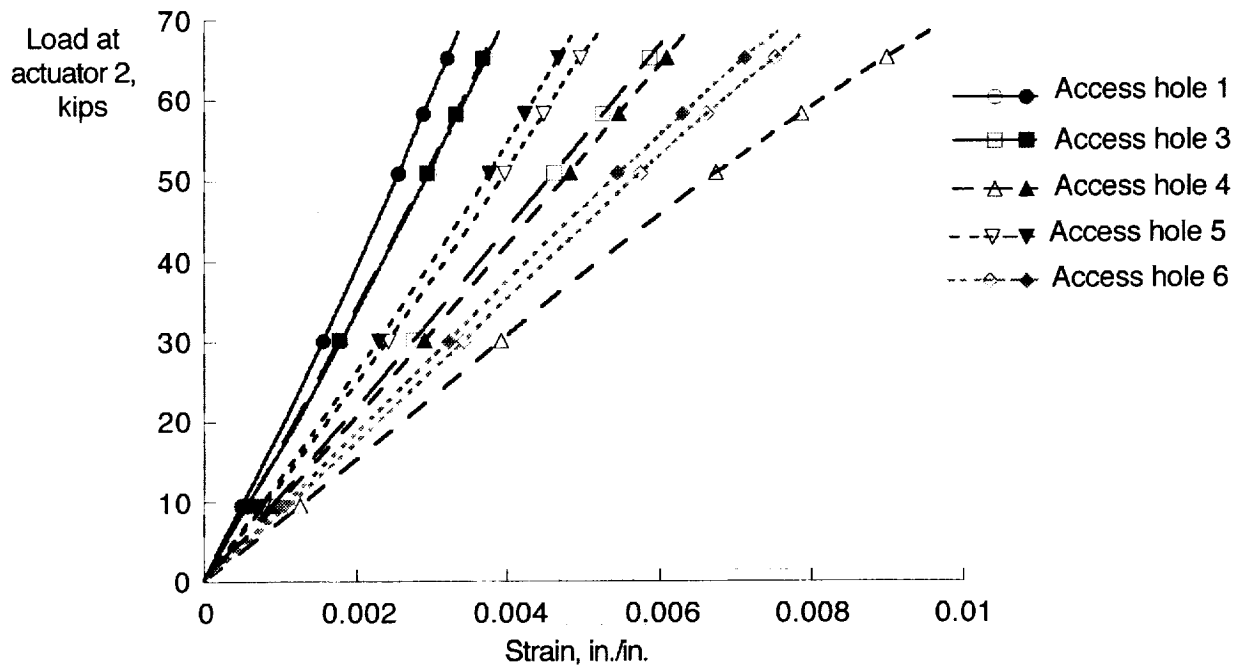
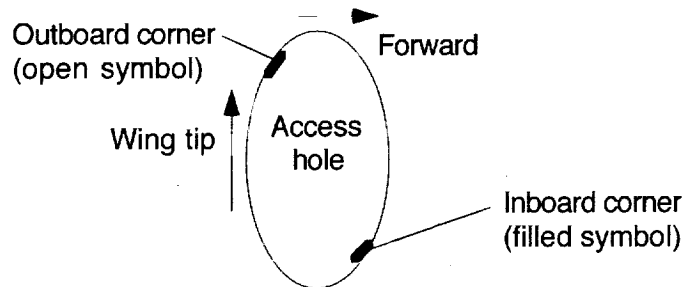


Figure 49. Measured strain at access hole edges for load to DLL in 2.5G load condition. Strain gage locations are shown in figure 7.

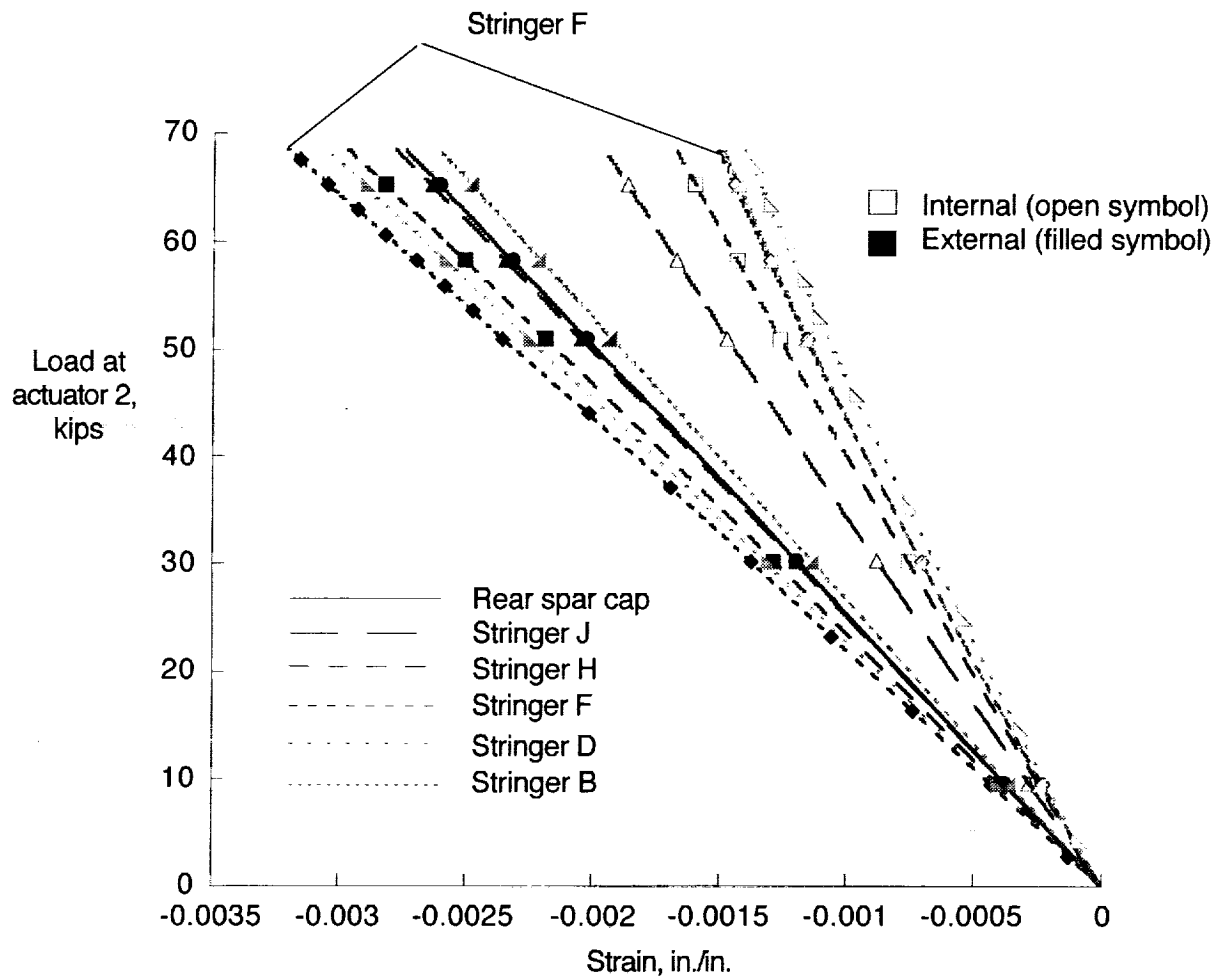


Figure 50. Bending in upper cover panel. Strain gage location are shown in figure 7.

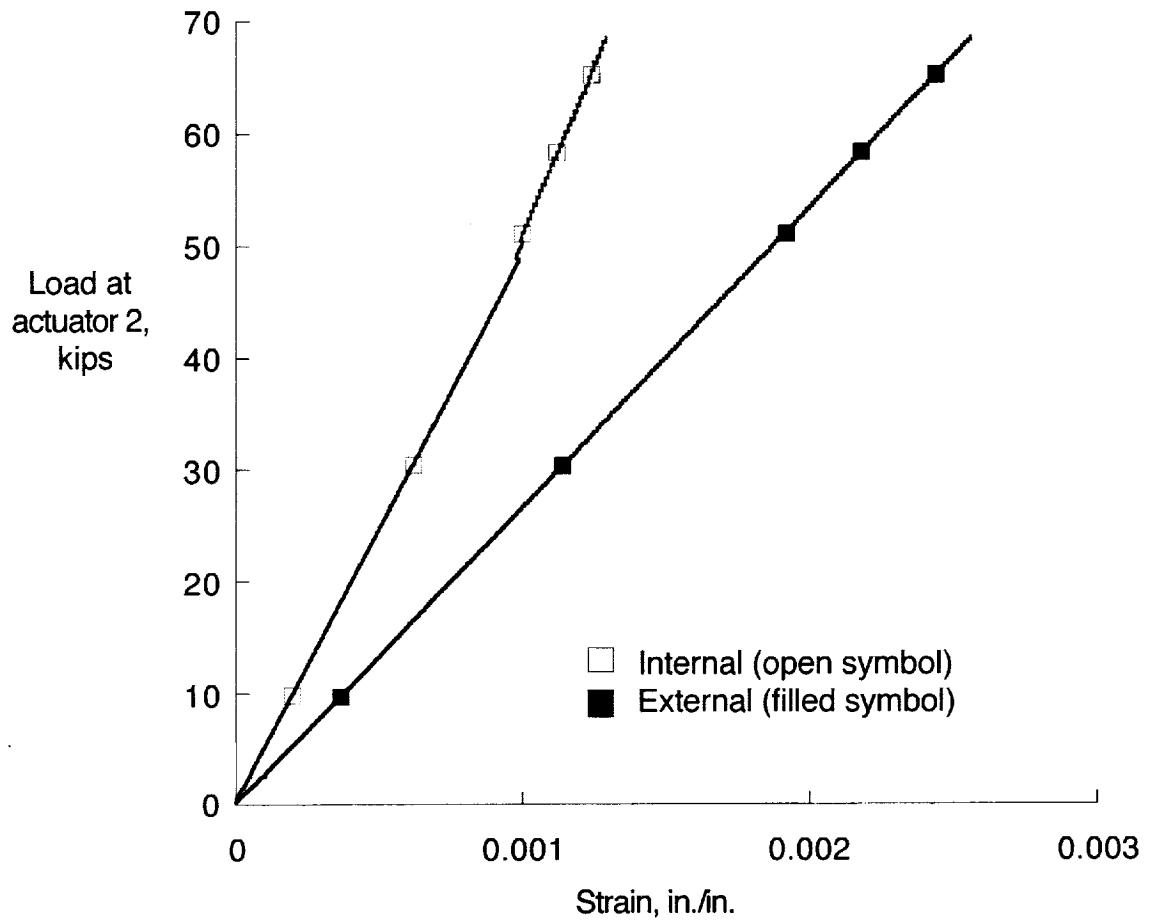


Figure 51. Bending in lower cover panel at stringer C between ribs 7 and 8. Strain gage locations are shown in figure 8.

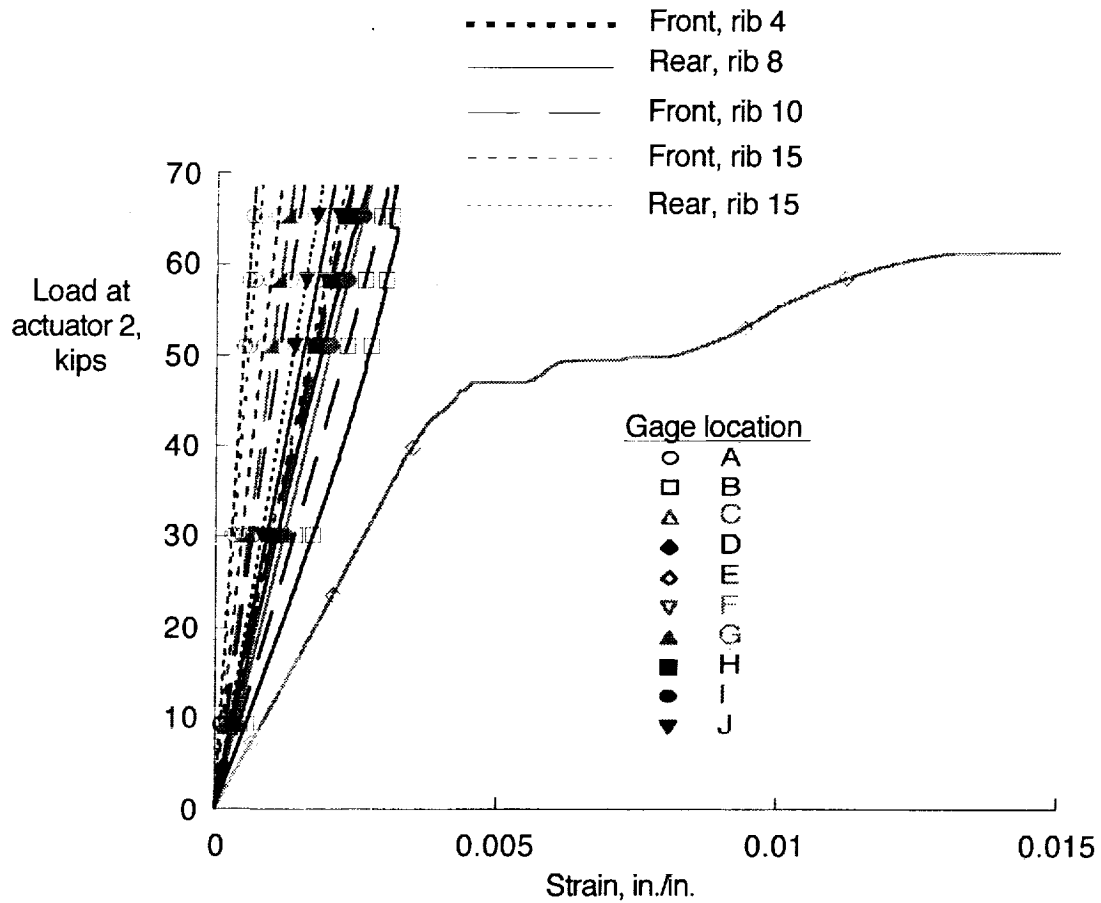


Figure 52. Measured strain at lower cover stringer runouts at DLL for 2.5G load condition. Strain gage locations are shown in figures 3 and 4.

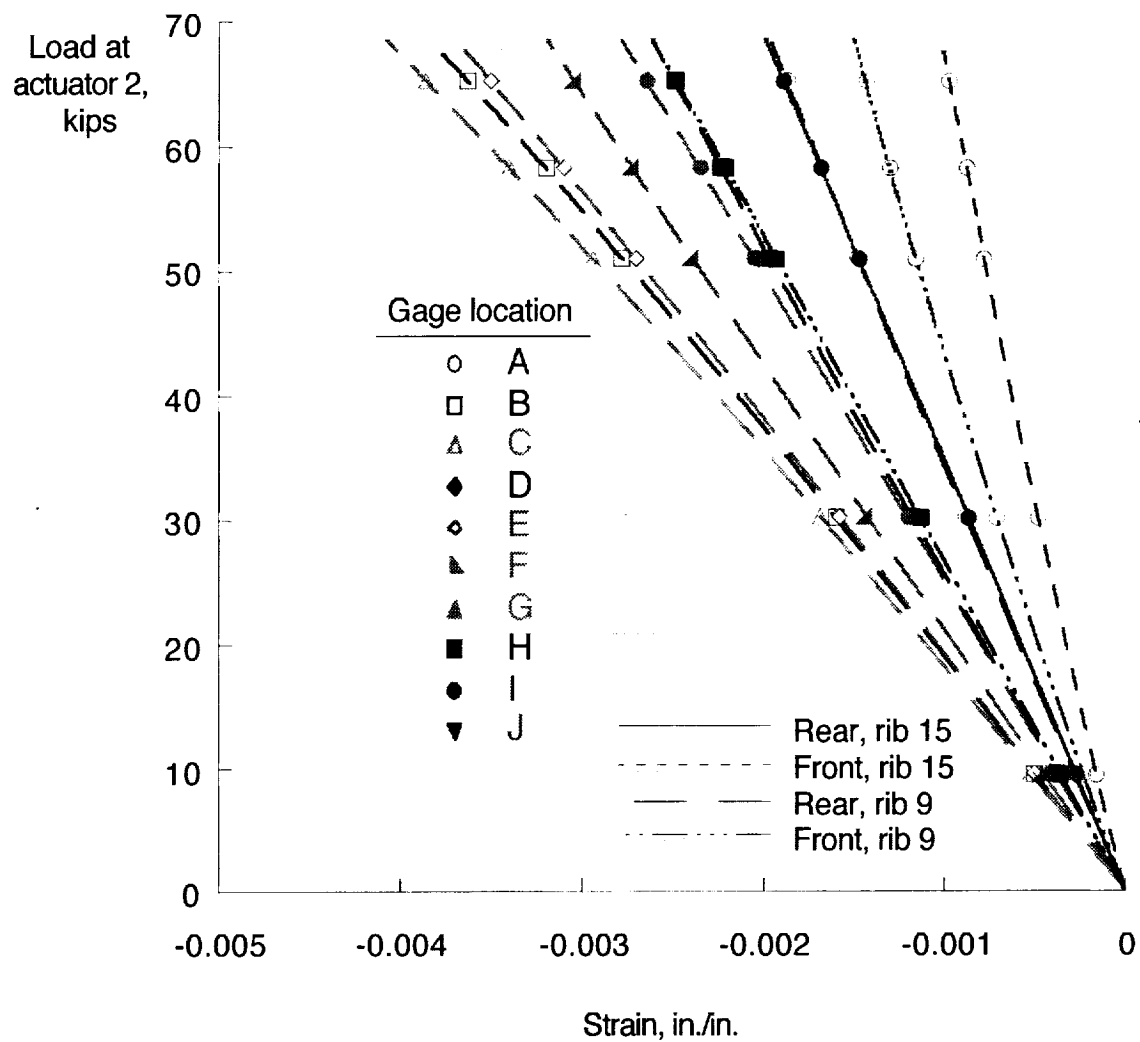
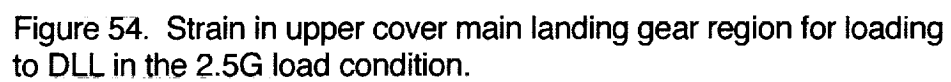


Figure 53. Strain in upper cover stringer runouts for loading to DLL in the 2.5G load condition. Strain gage locations are shown on figures 3 and 4.



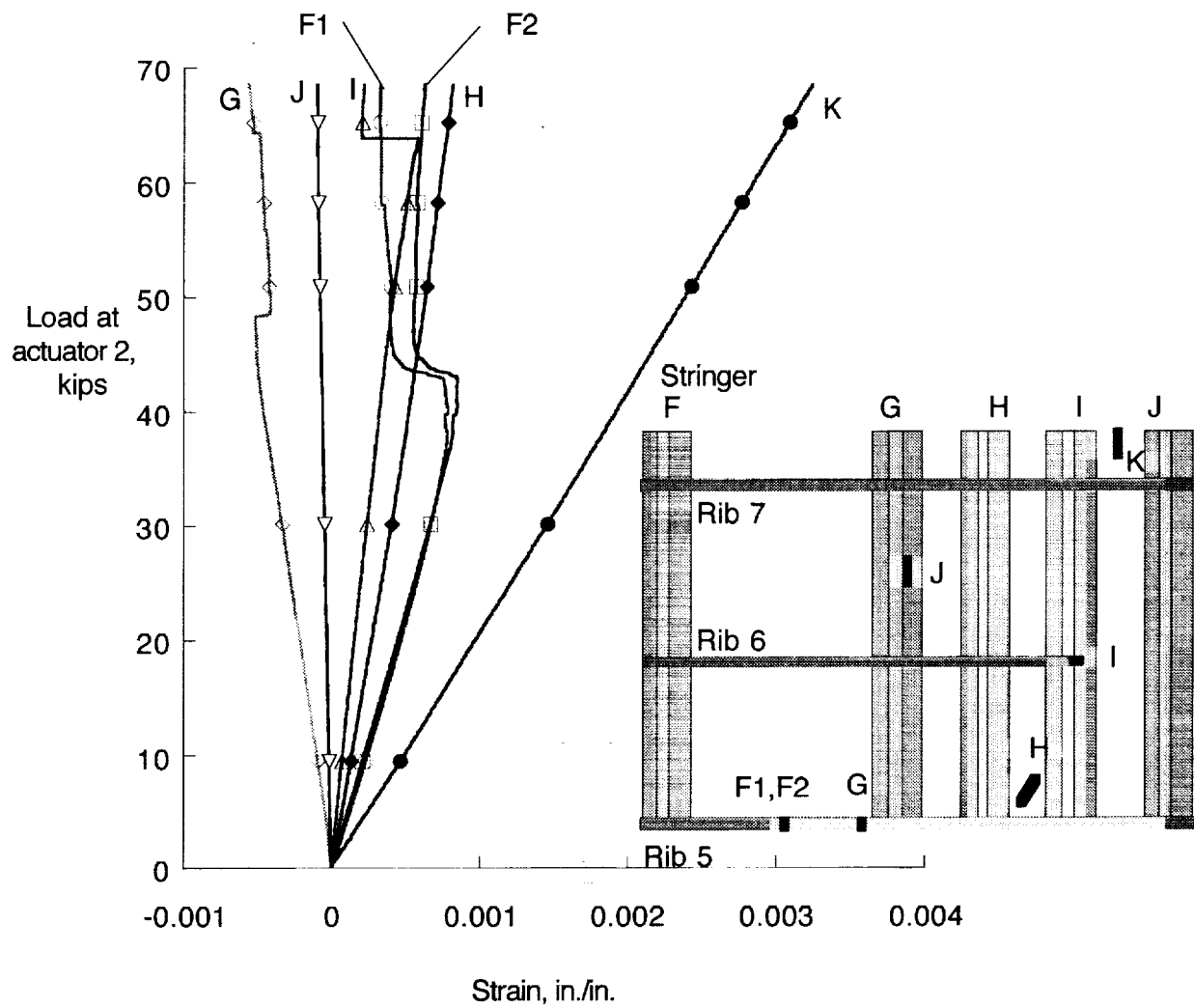


Figure 55. Strain in main landing gear area of the lower cover for loading to DLL in the 2.5G load condition. Strain gage locations are shown on figure 9.

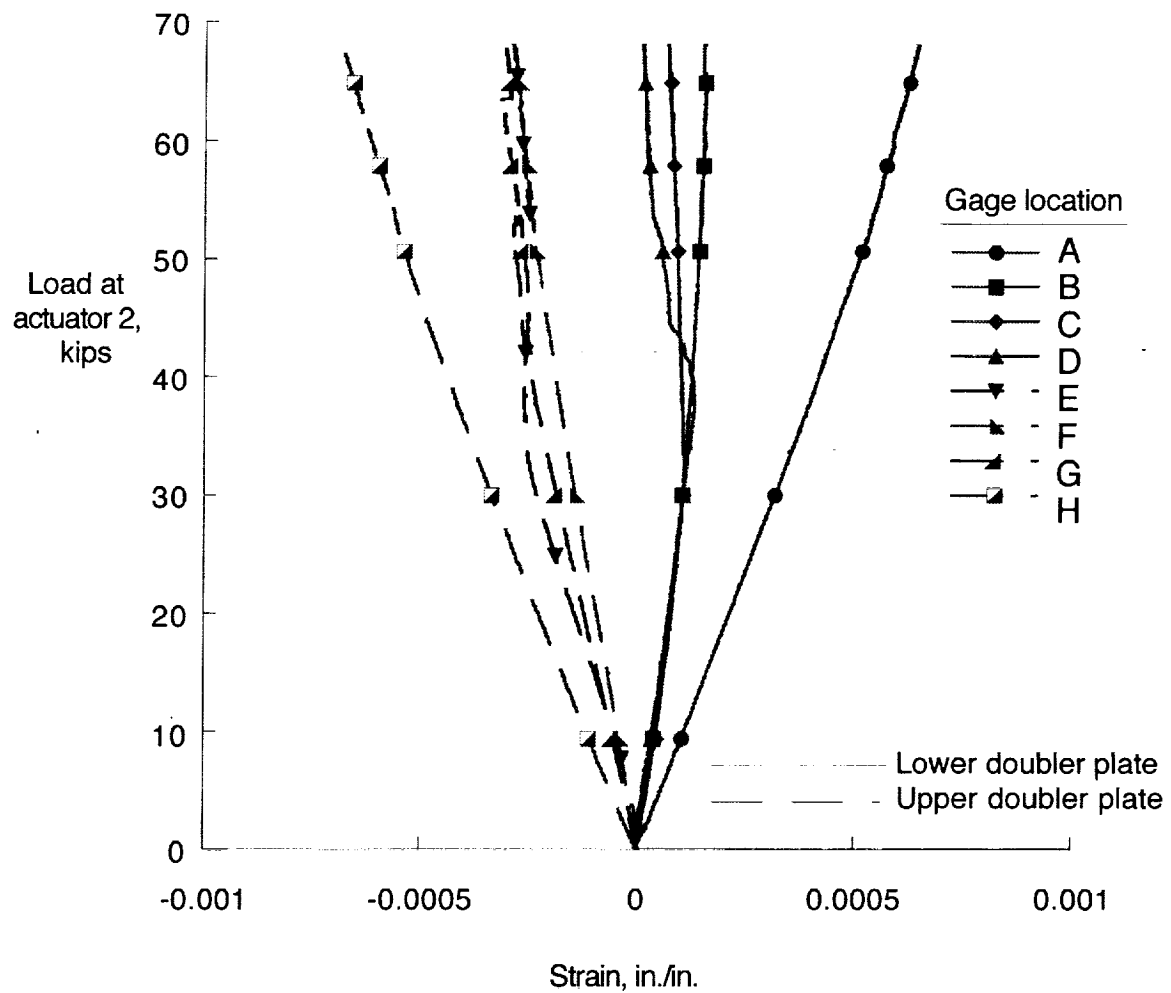


Figure 56. Strain in MLG doublers for loading to DLL in the 2.5G load condition. Strain gage locations are shown on figure 9.

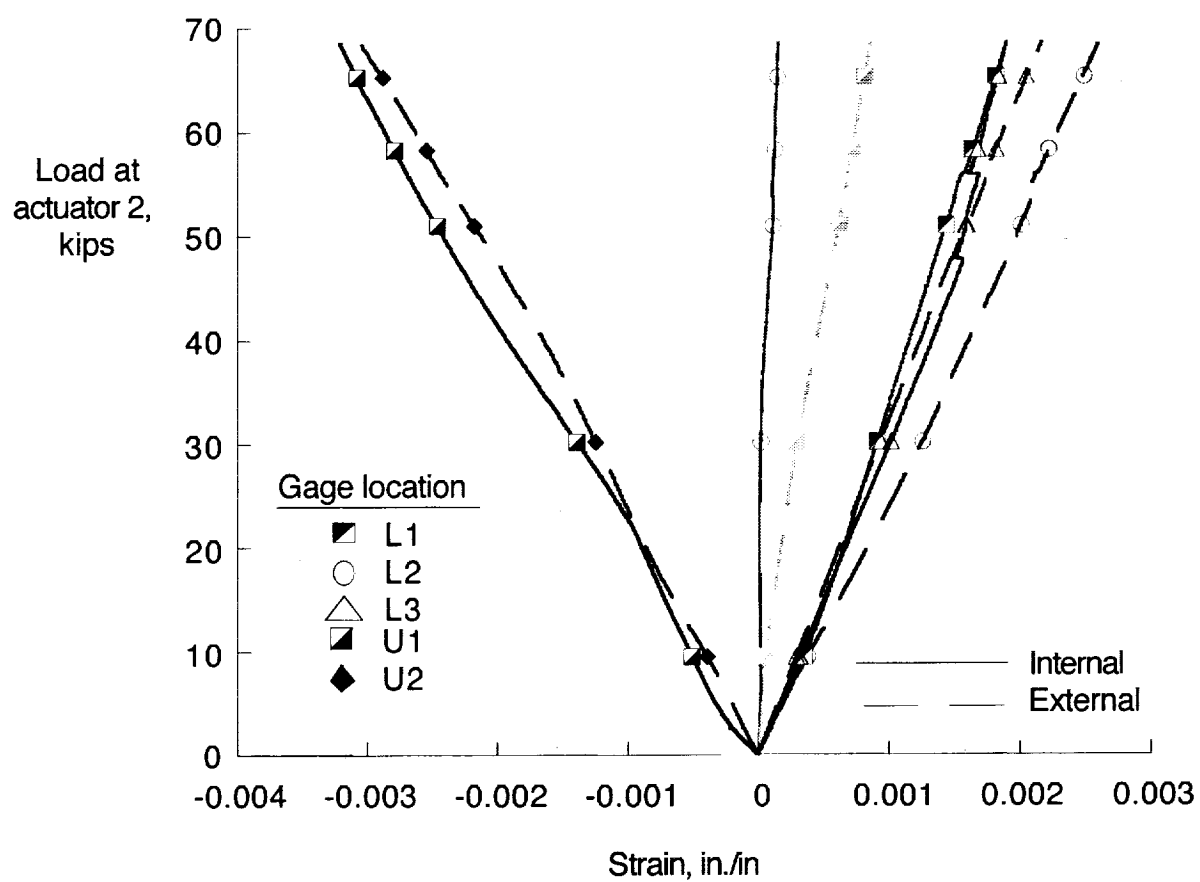


Figure 57. Strain in root region at DLL for 2.5G load condition. Strain gage locations are shown in figure 7 and 8.

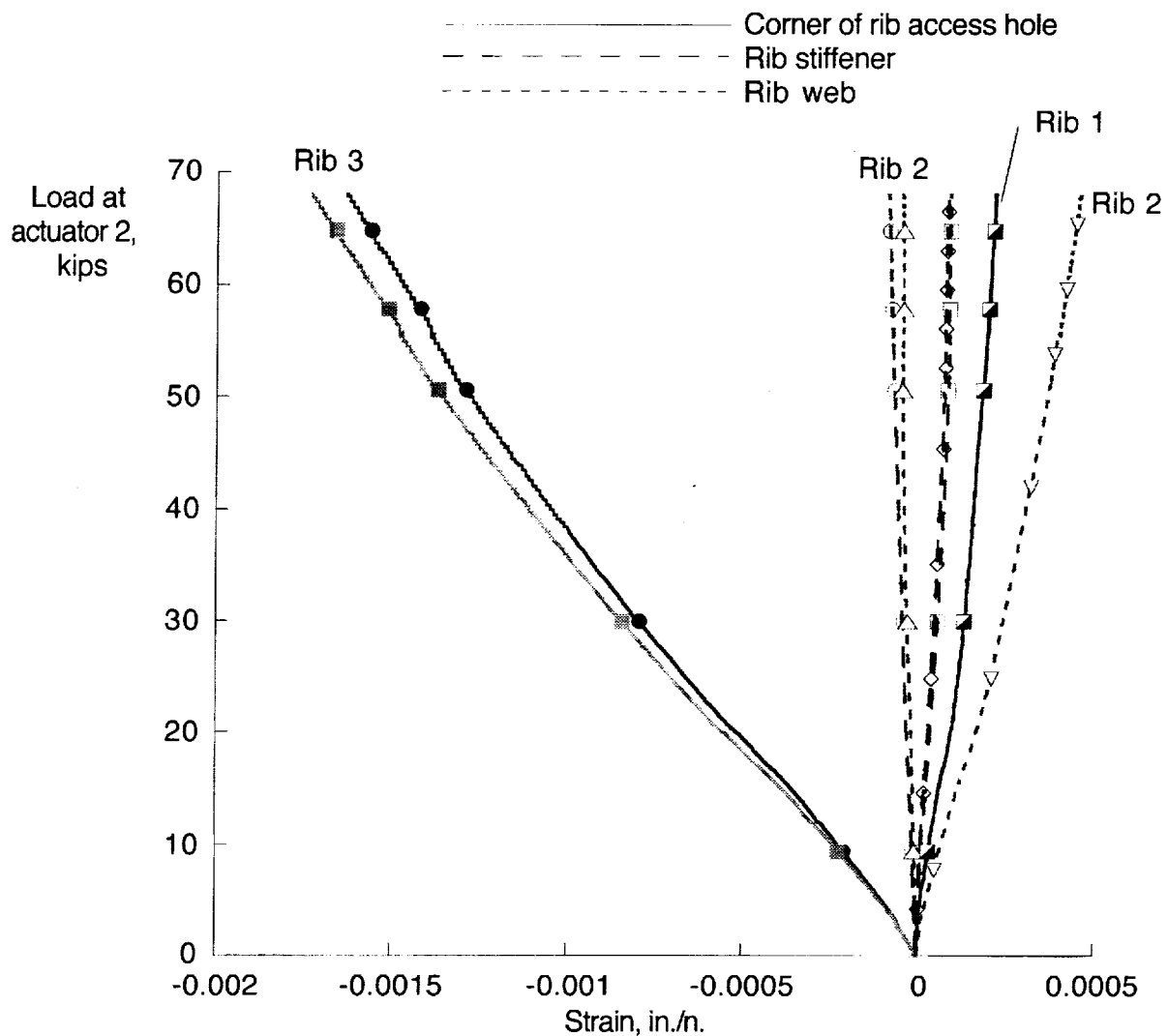


Figure 58. Measured strain in ribs 1, 2 and 3 for loading up to DLL for the 2.5G load condition. Strain gage locations are shown in figures 11a, 11b, and 11c.

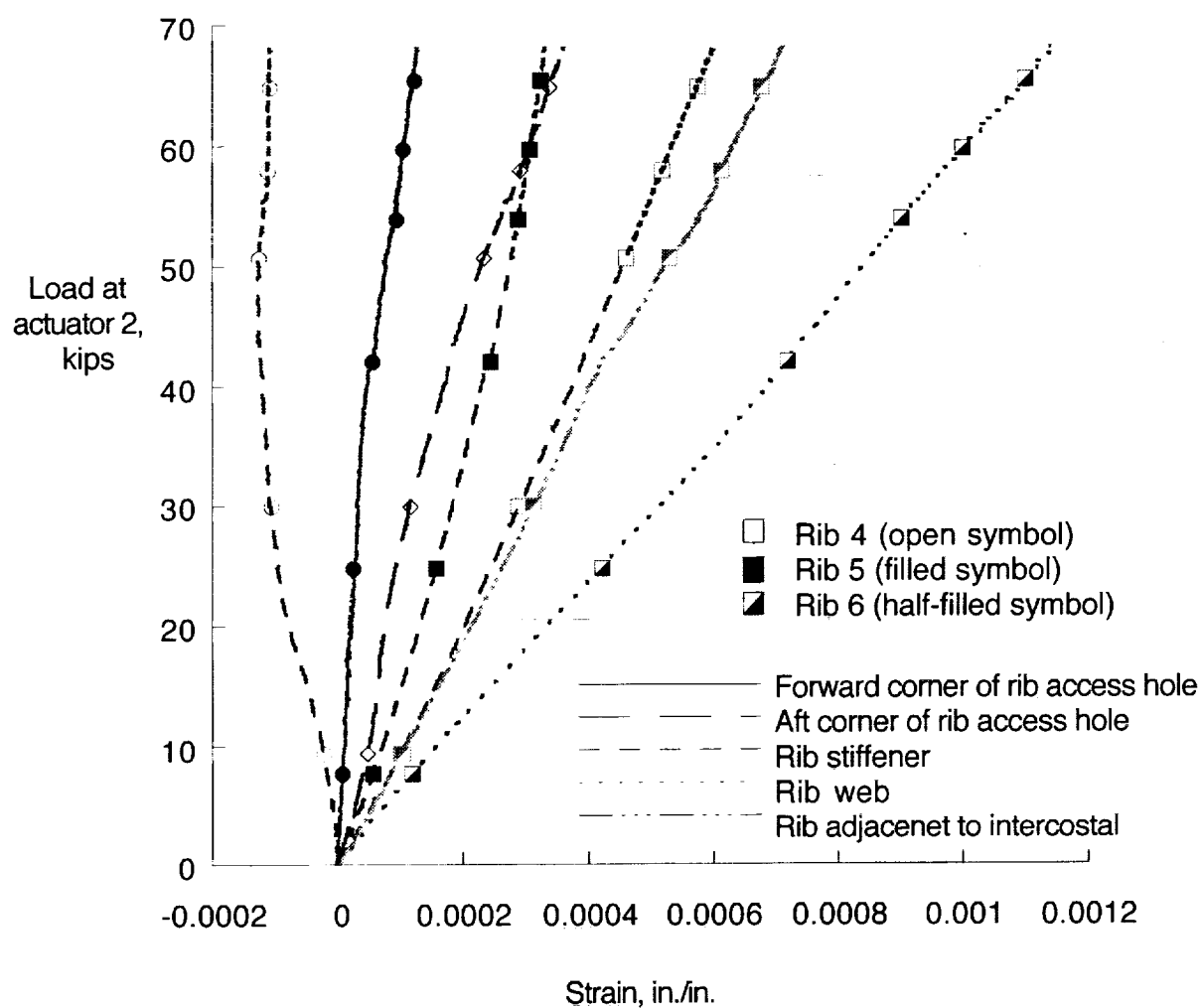


Figure 59. Strain in ribs 4, 5 and 6 for loading to DLL in the 2.5G load condition. Strain gage locations are shown in figure 11d and 11e.

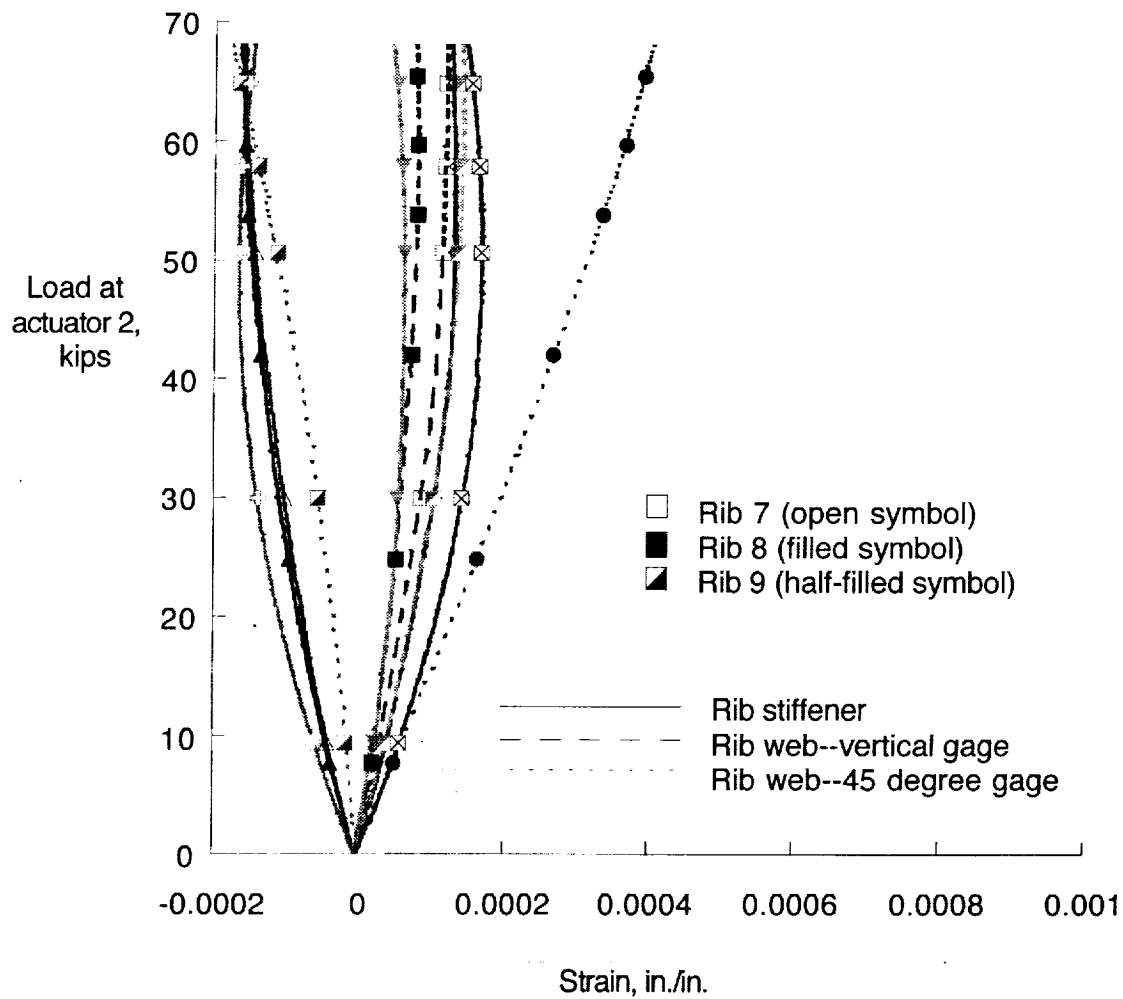


Figure 60. Strain in ribs 7, 8, and 9 for loading to DLL in the 2.5G load condition. Strain gage locations are shown in figure 11f.

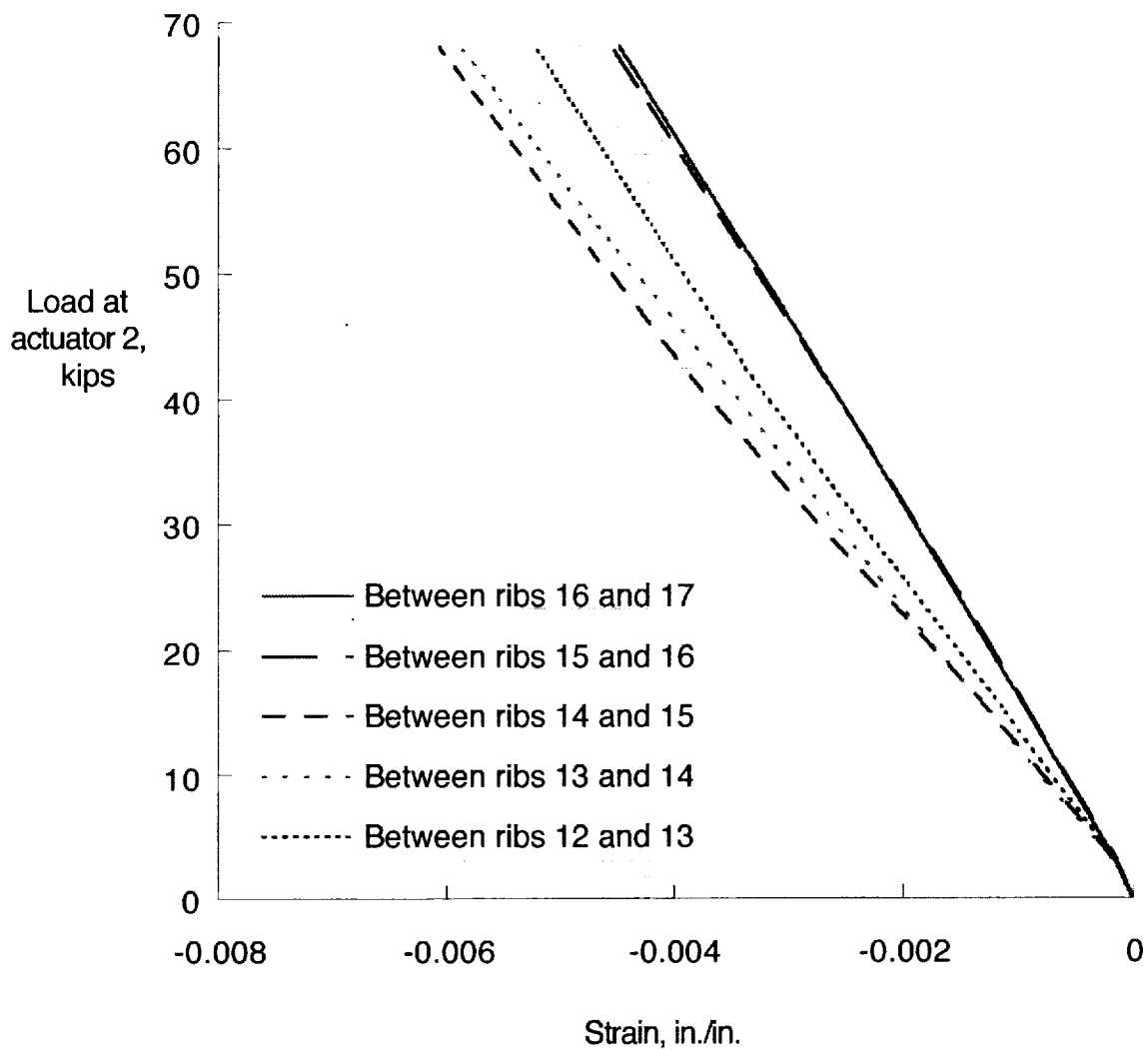
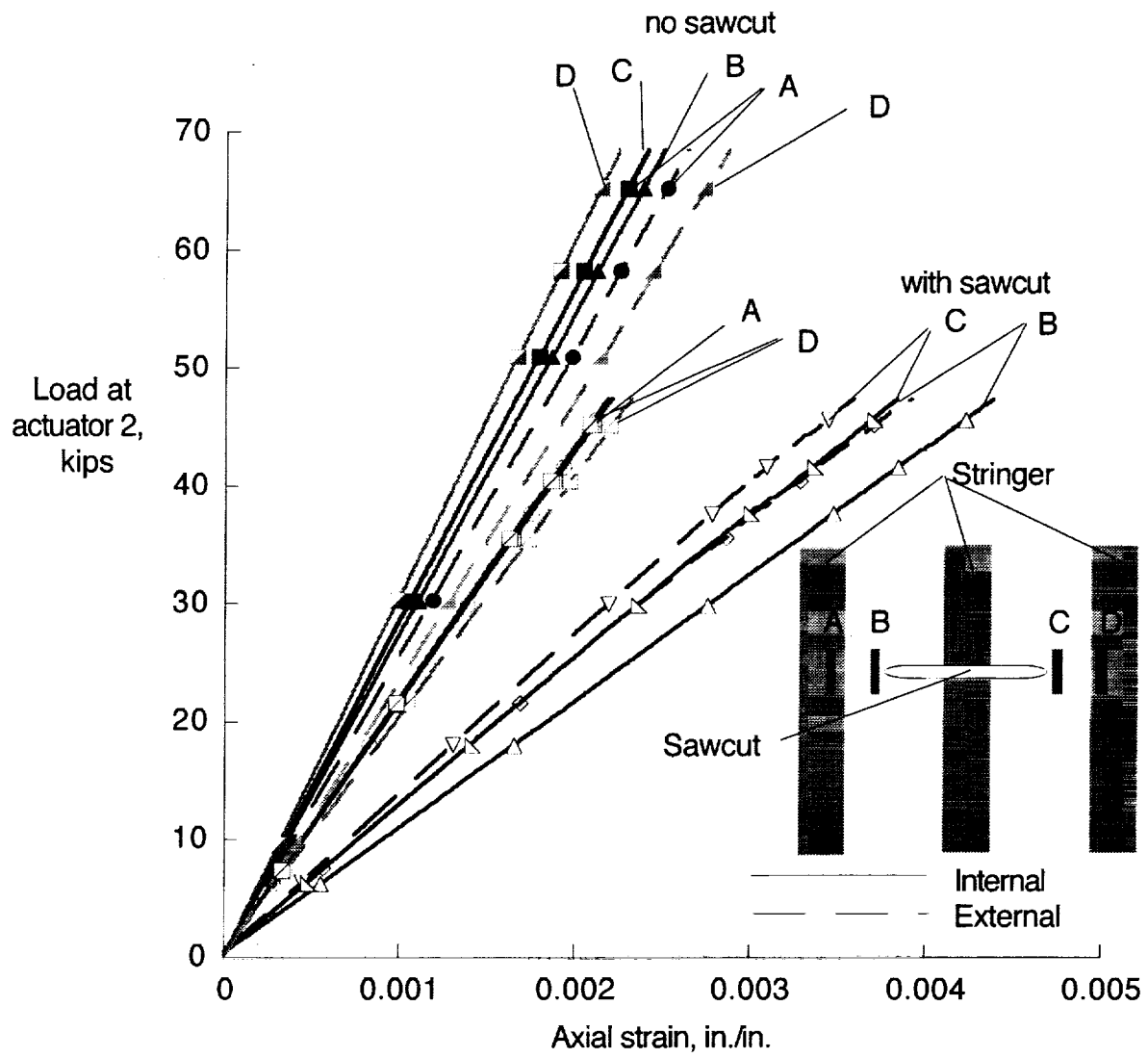
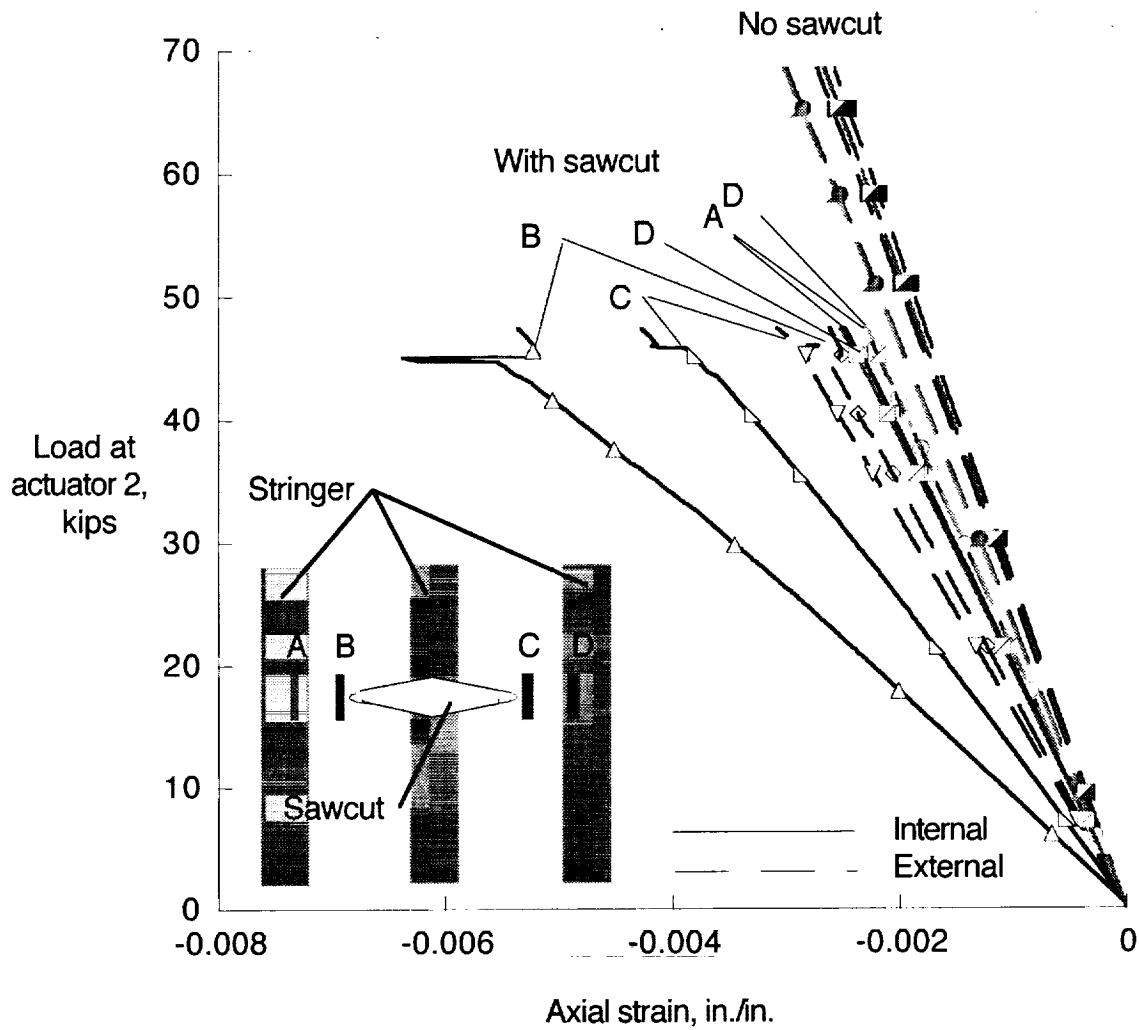


Figure 61. Strain in front spar for loading to DLL in the 2.5G load condition.



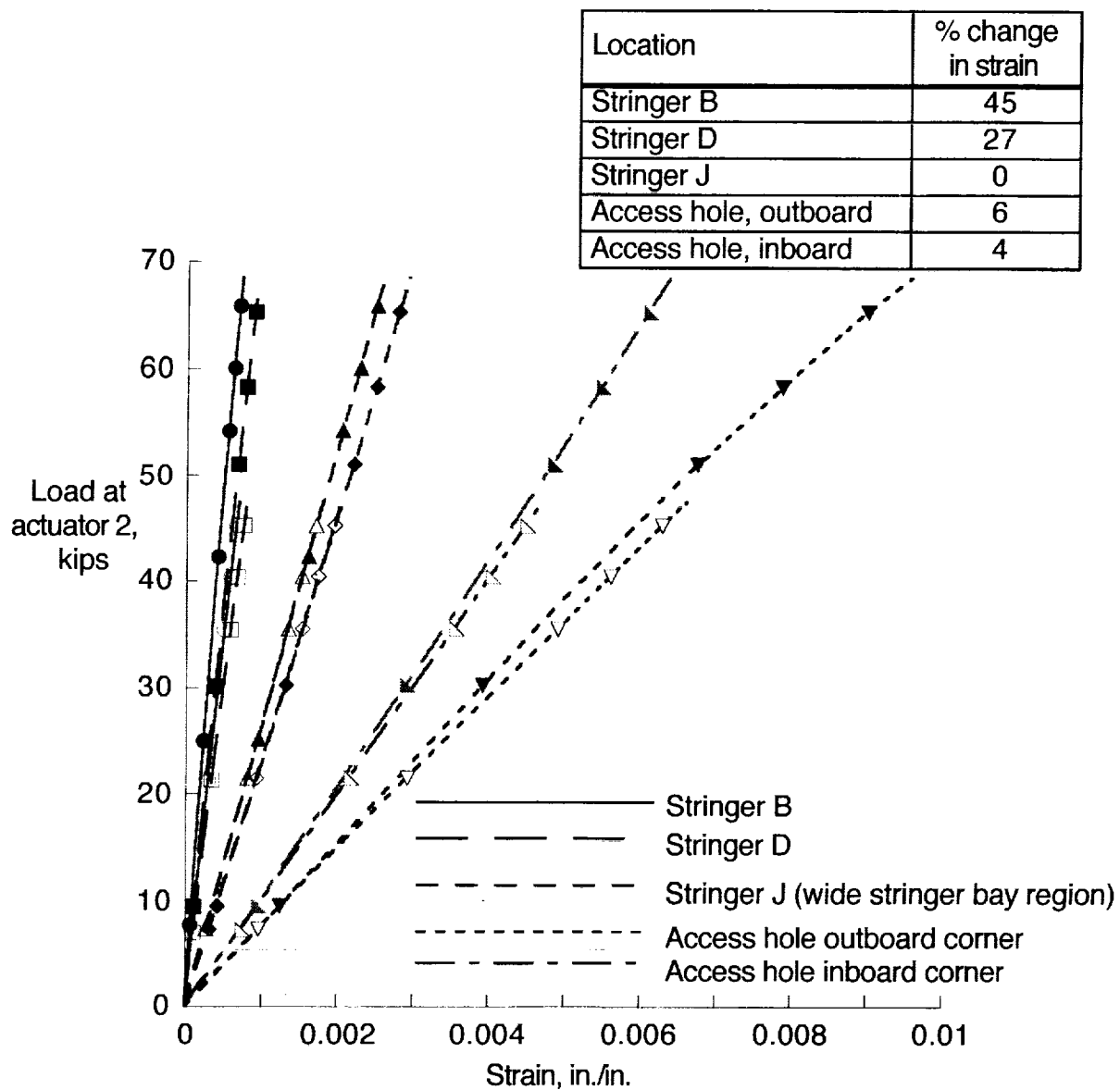
a) Lower cover panel

Figure 62. Strains in cover panels for loading to DLL with no sawcut and loading to 70% DLL with sawcut in 2.5G load condition.



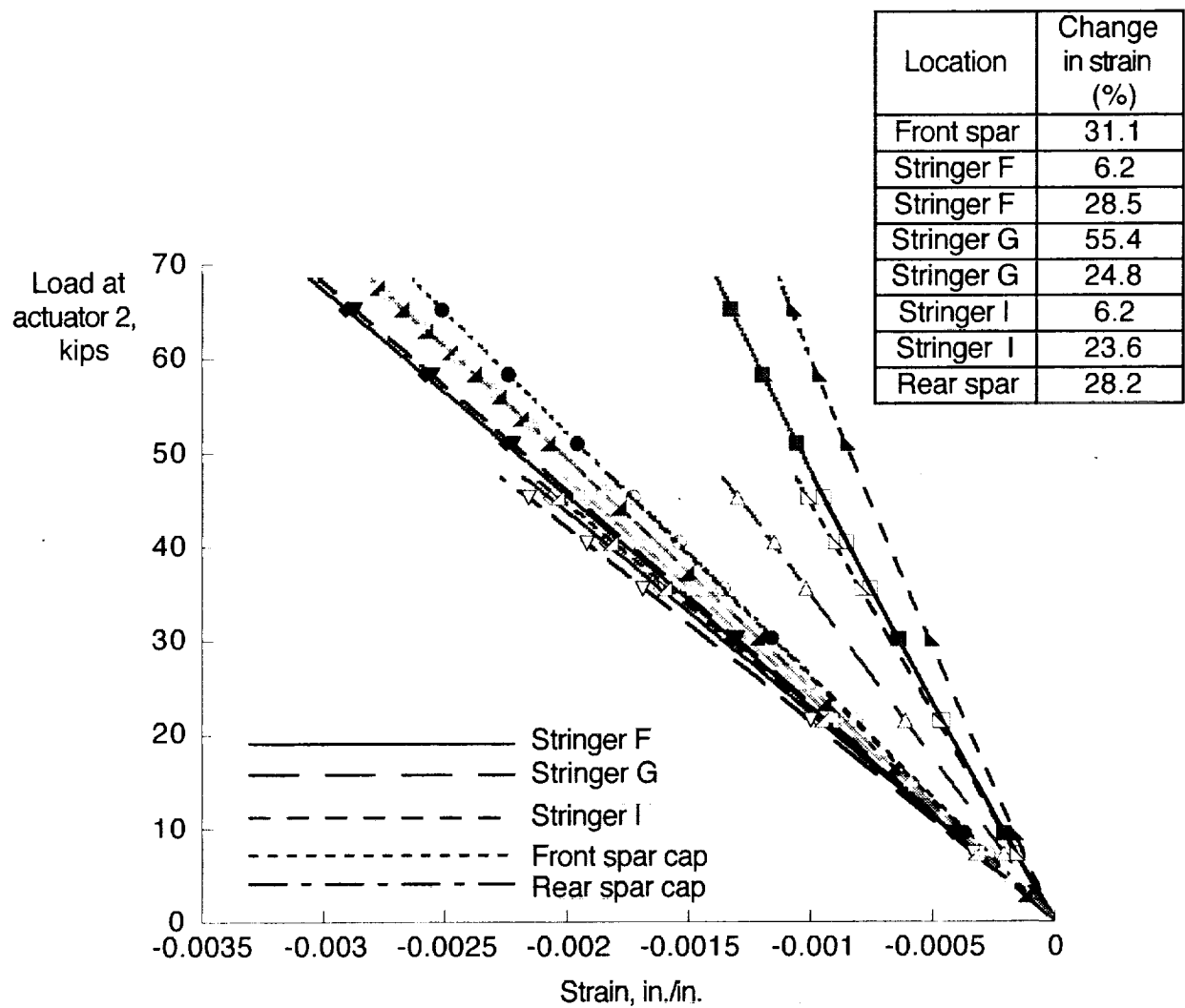
b) Upper cover panel

Figure 62. Concluded.



a) Measured strain in lower cover panel between ribs 8 and 9 away from damage site for sawcut and undamaged structure in 2.5G load condition

Figure 63. Effect of sawcut damage on panel strains.



b) Effect of sawcut on measured strains in upper cover panel between ribs 10 and 11

Figure 63. Concluded.

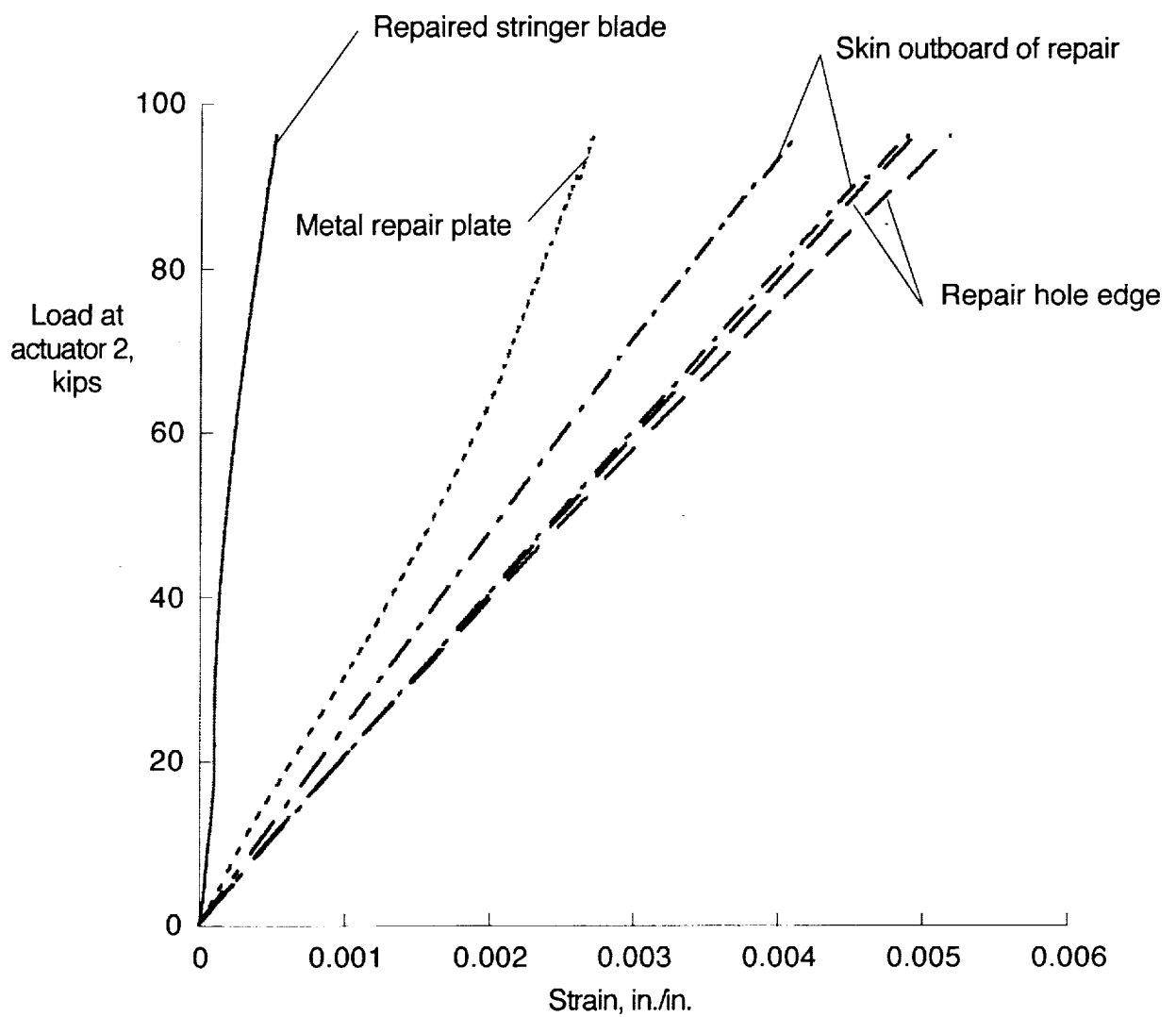


Figure 64. Strains in lower cover repaired region. Strain gage locations are shown in figure 14.

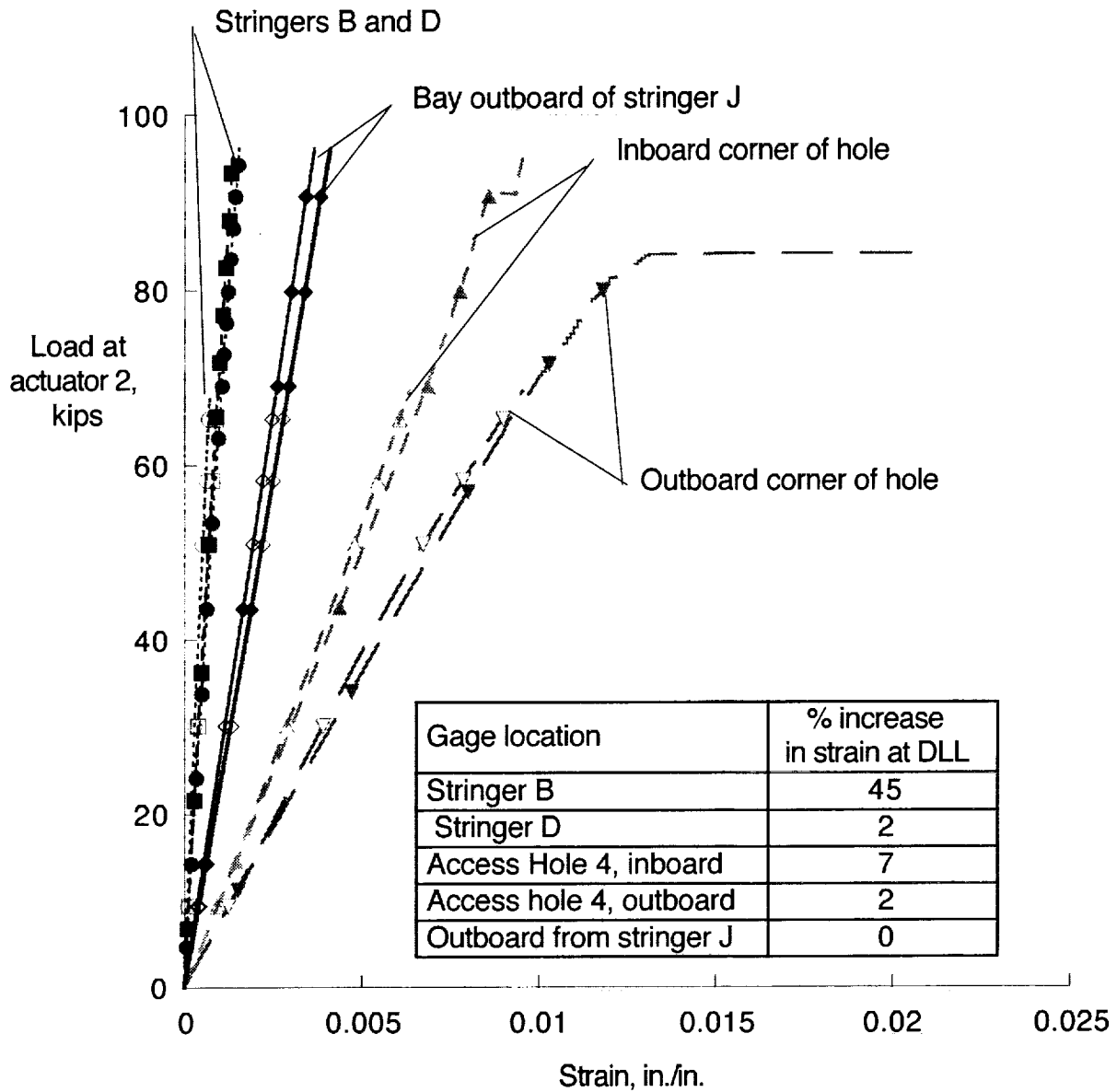


Figure 65. Strains in lower cover panel between ribs 8 and 9 for tests 6 and 8. Stringer identification shown in figure 2b.

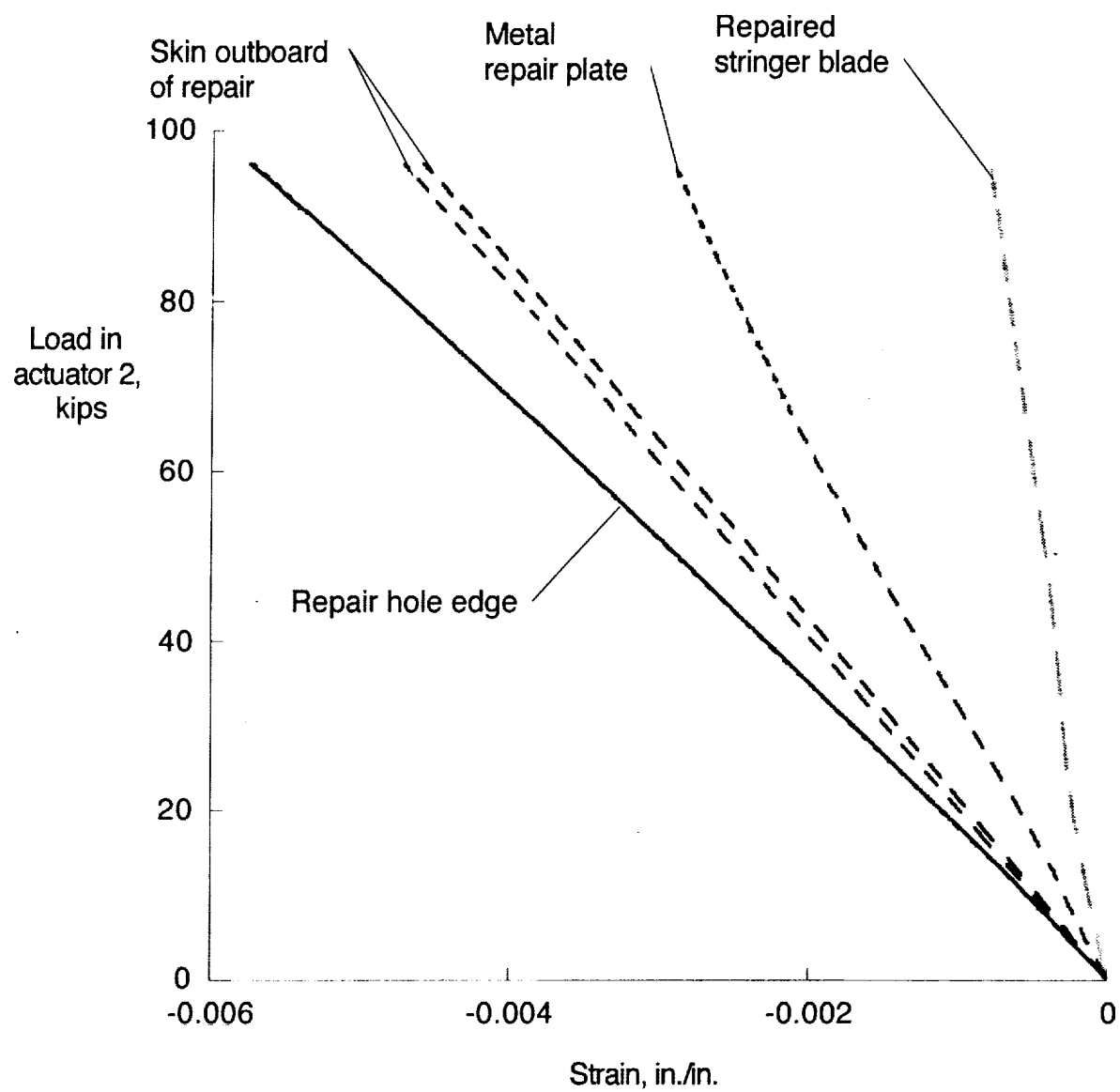


Figure 66. Strain in upper cover panel repair. Strain gage locations are shown in figure 14.

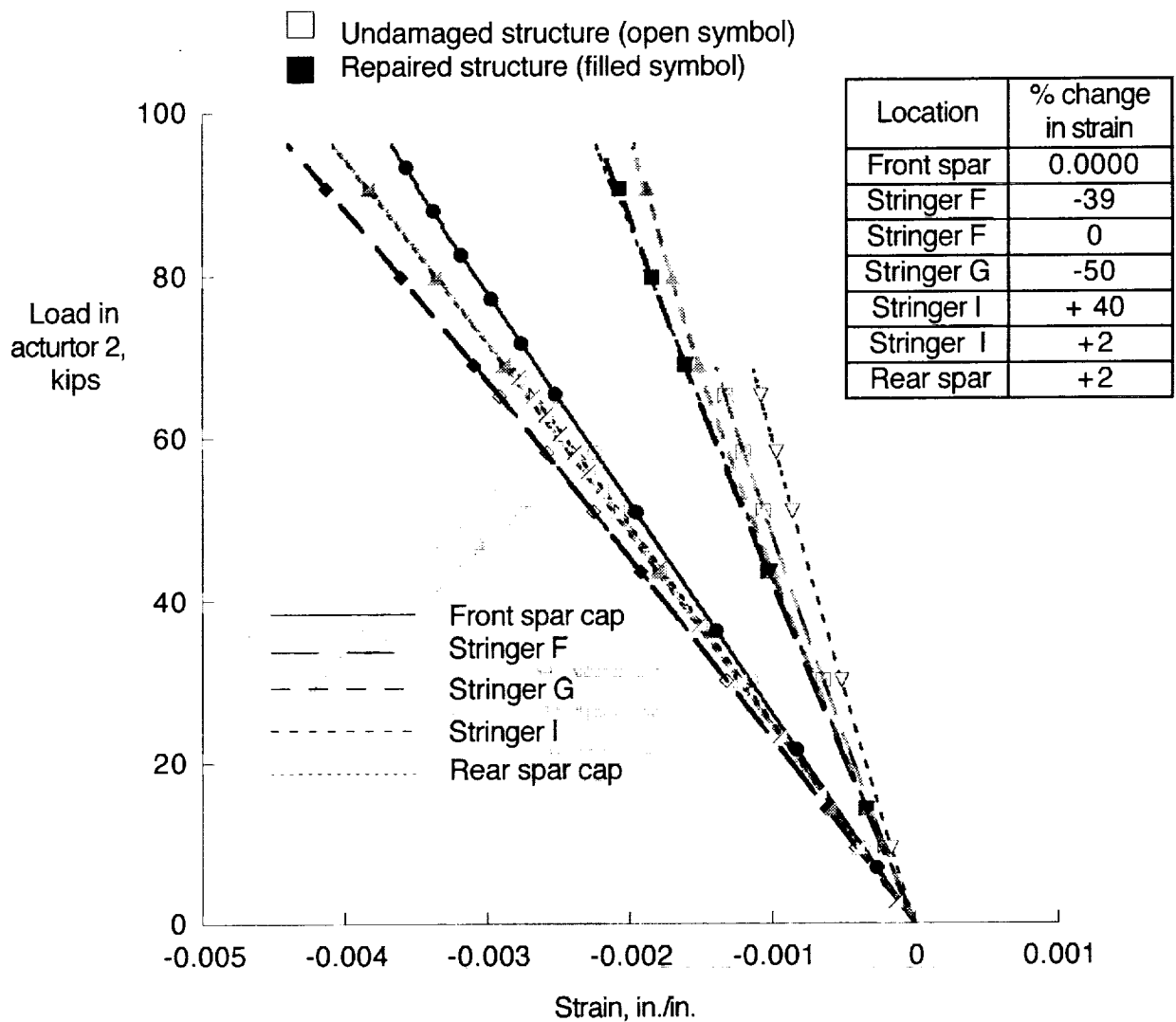


Figure 67. Effect of repair on measured strains in upper cover panel between ribs 10 and 11.

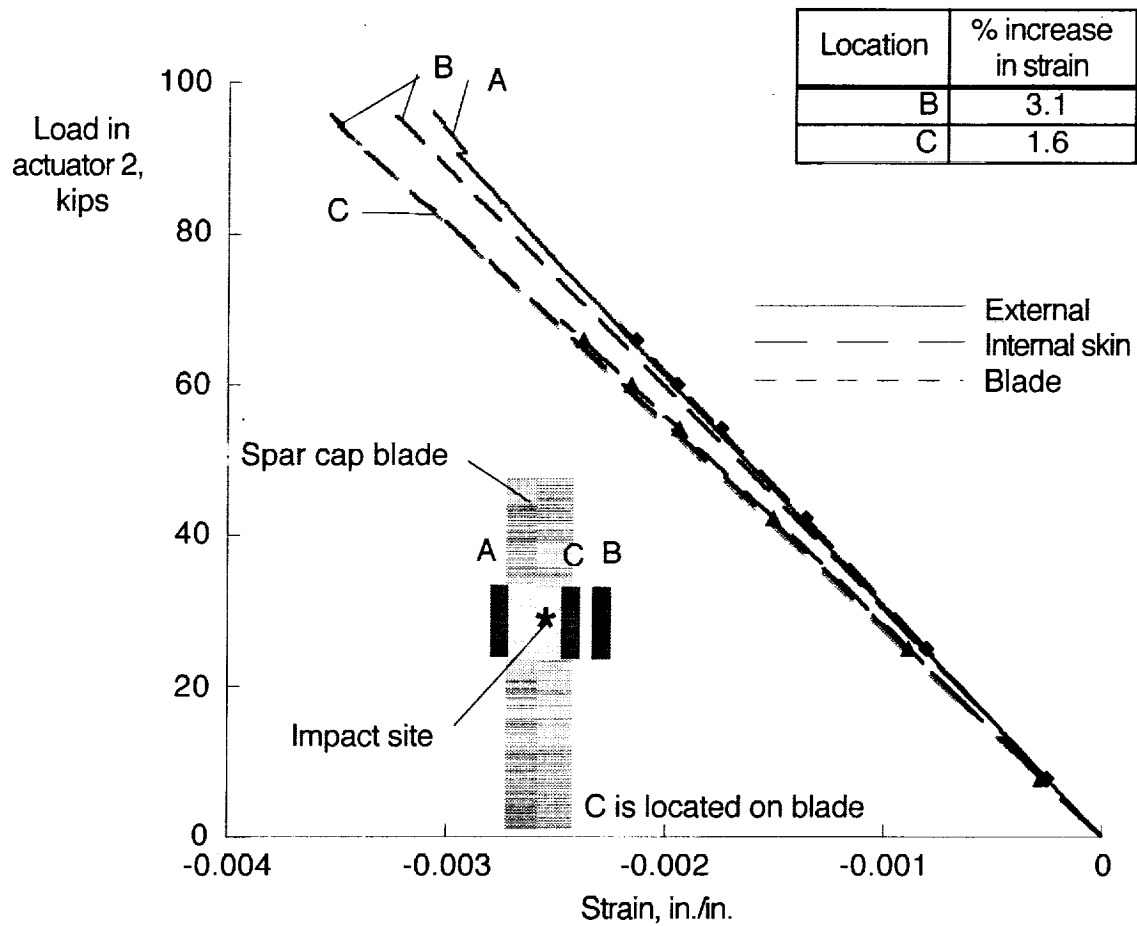


Figure 68. Effect of impact damage on strain at upper cover rear spar cap near rib 4. Gage and impact locations are shown in figure 13c.

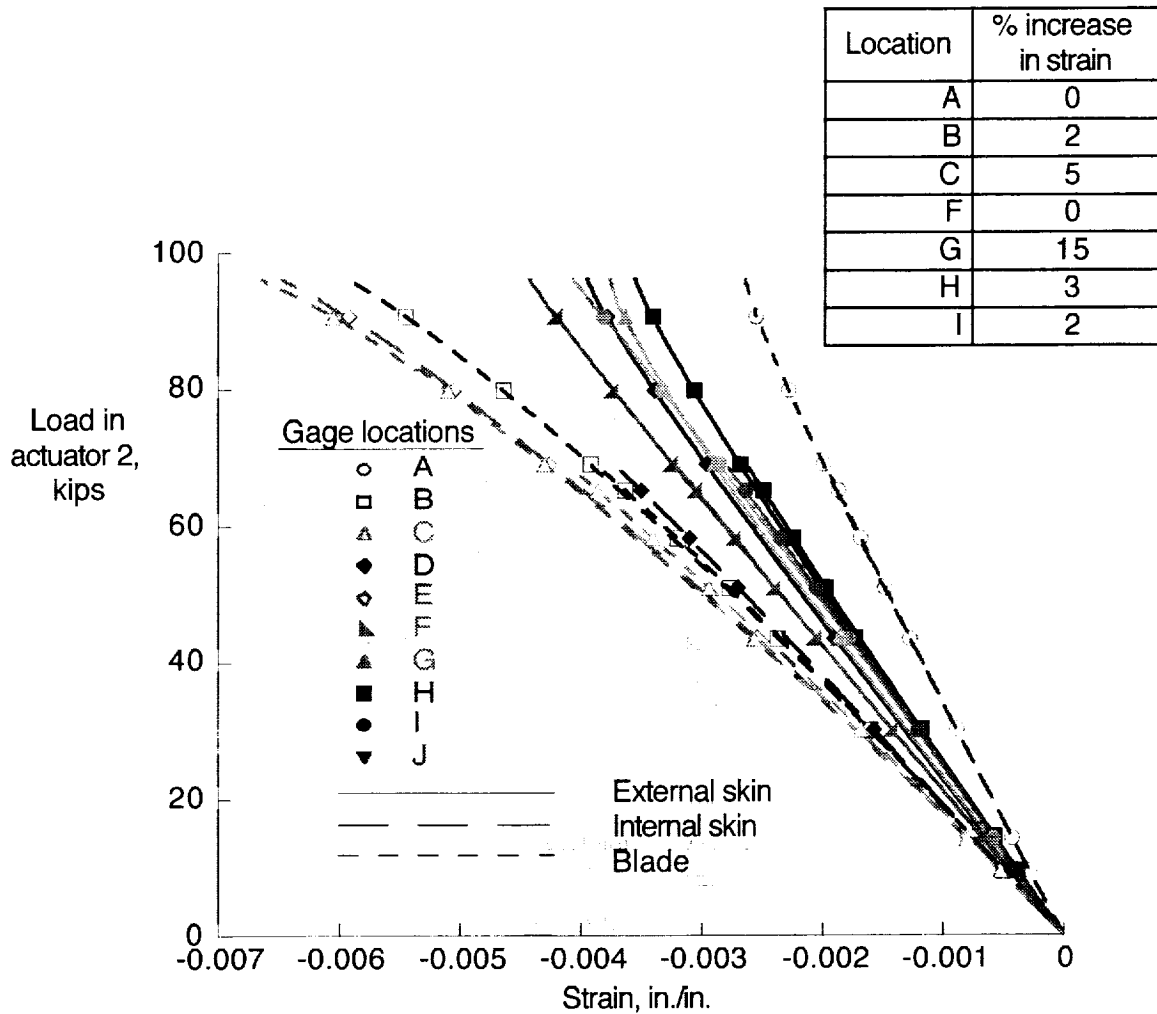


Figure 69. Effect of impact damage on strains at upper cover stringer runout at rib 9. Strain gage locations are shown on figure 3.

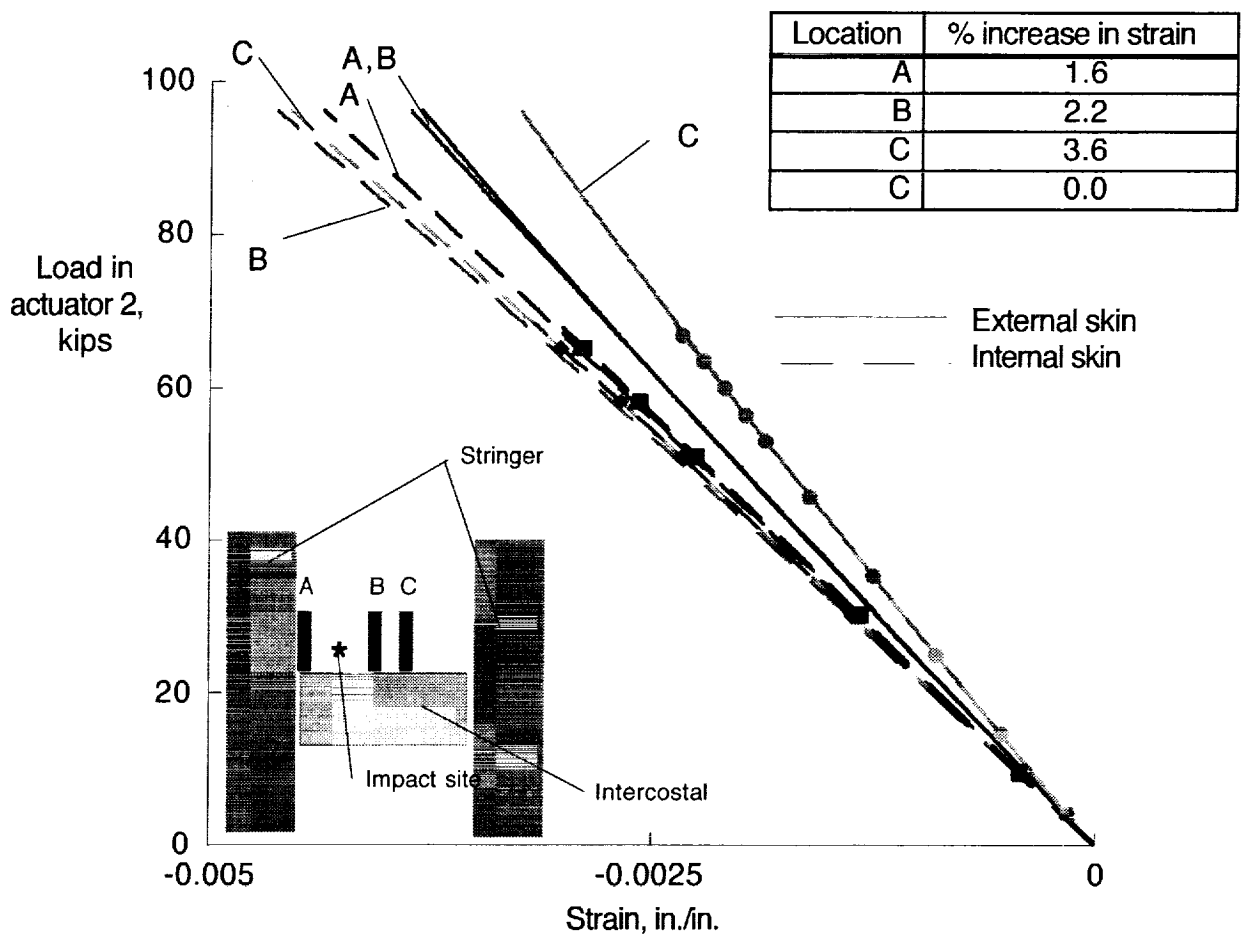


Figure 70. Effect of impact damage on strains in upper cover panel skin adjacent to rib 13. Strain gage locations and impact site are shown in figure 13a.

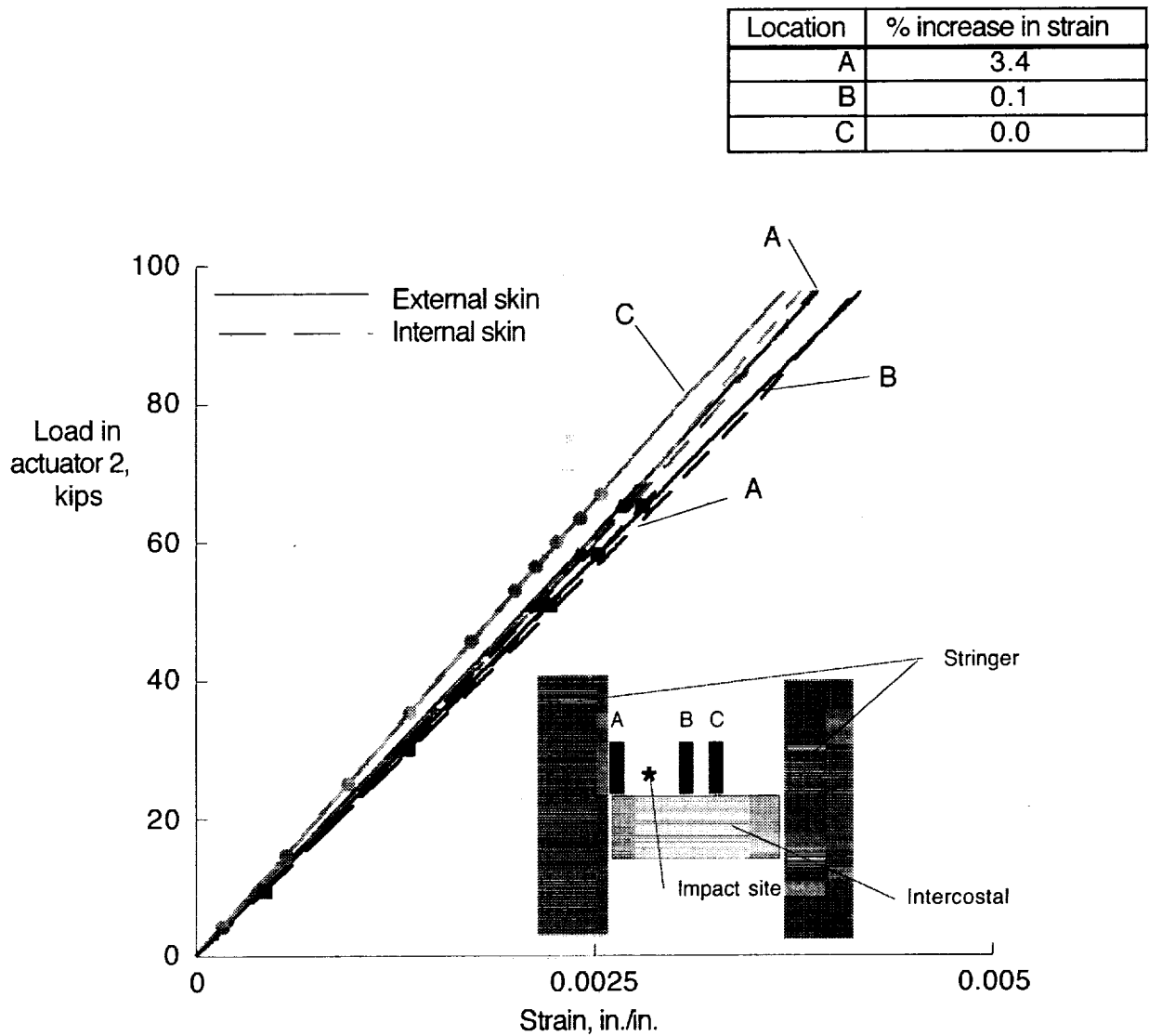


Figure 71. Effect of impact damage on strains in lower cover panel skin adjacent to rib 4. Strain gage and impact locations are shown on figure 13a.

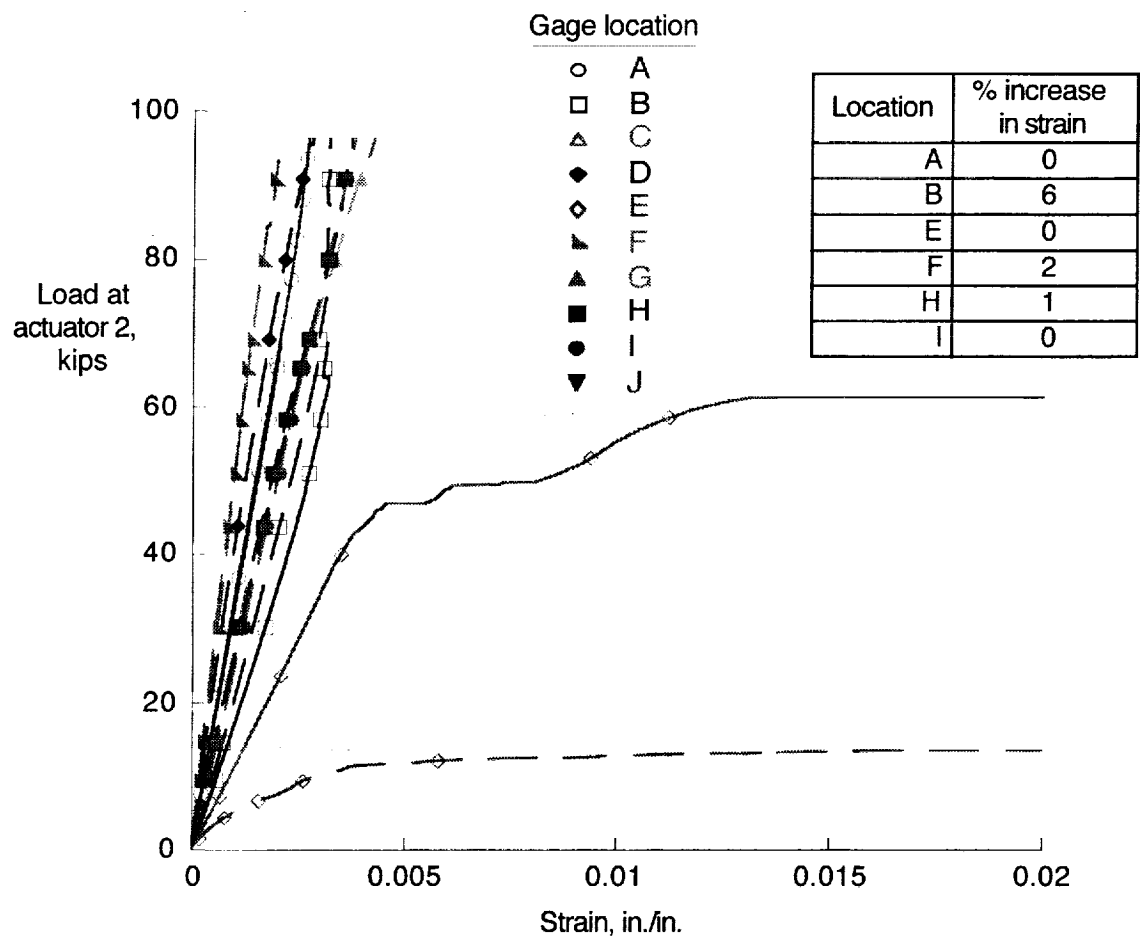


Figure 72. Effect of impact damage on strains at lower cover stringer runout at rib 8. Strain gage locations are shown on figure 3.

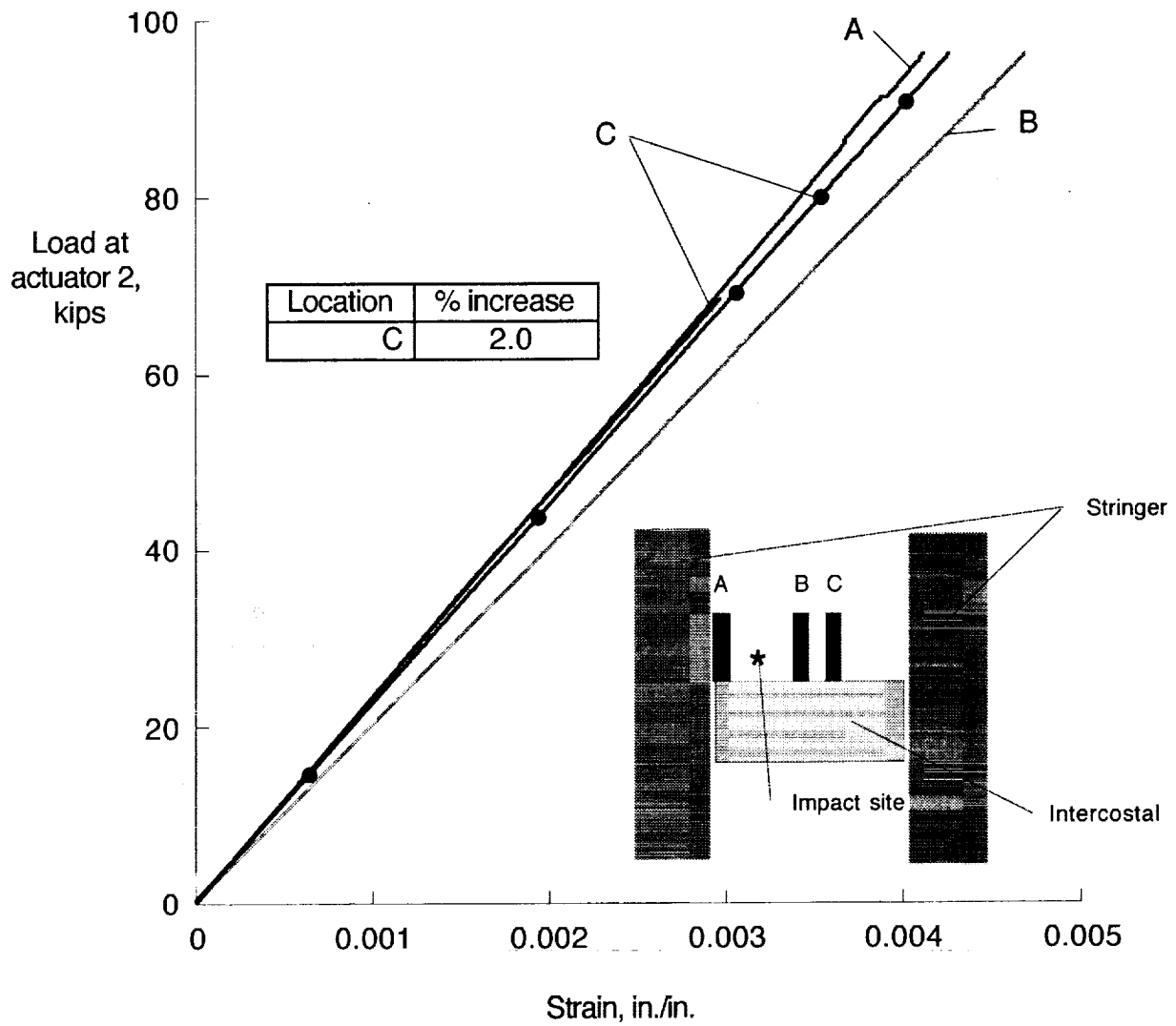
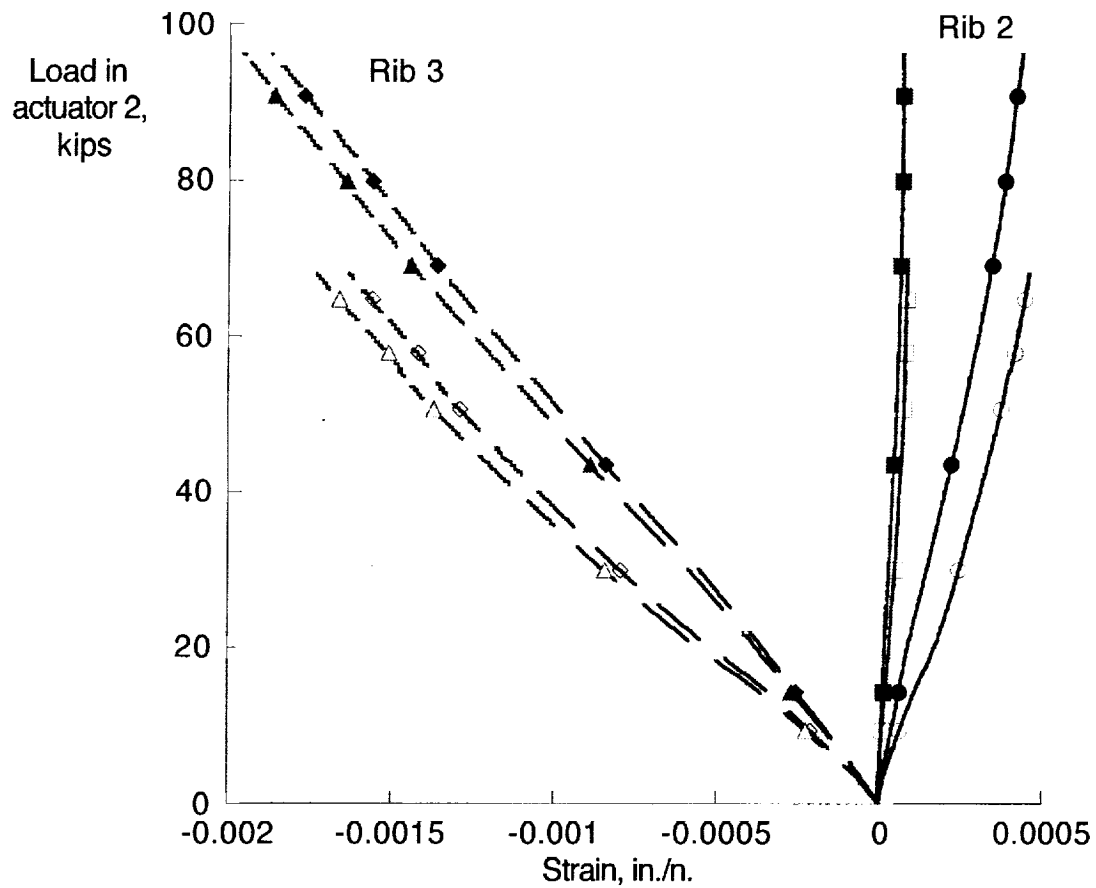


Figure 73. Effect of impact damage on strain in lower cover panel skin adjacent to rib 12. Strain gage and impact locations are shown on figure 13a.

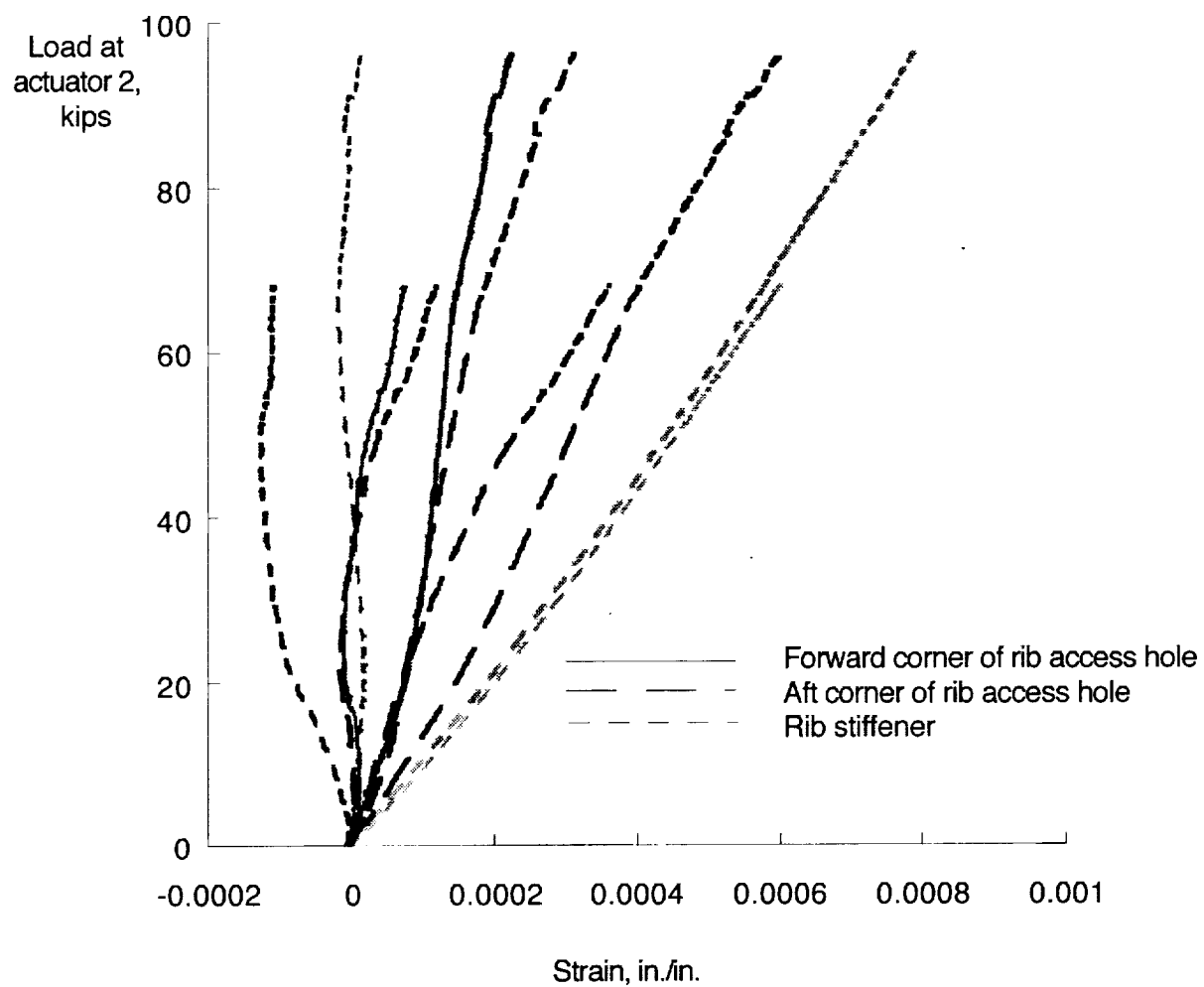
Location	% decrease in strain
Rib 2 web	26
Rib 3 access hole	18

— Rib web skin
 - - Rib access hole corner



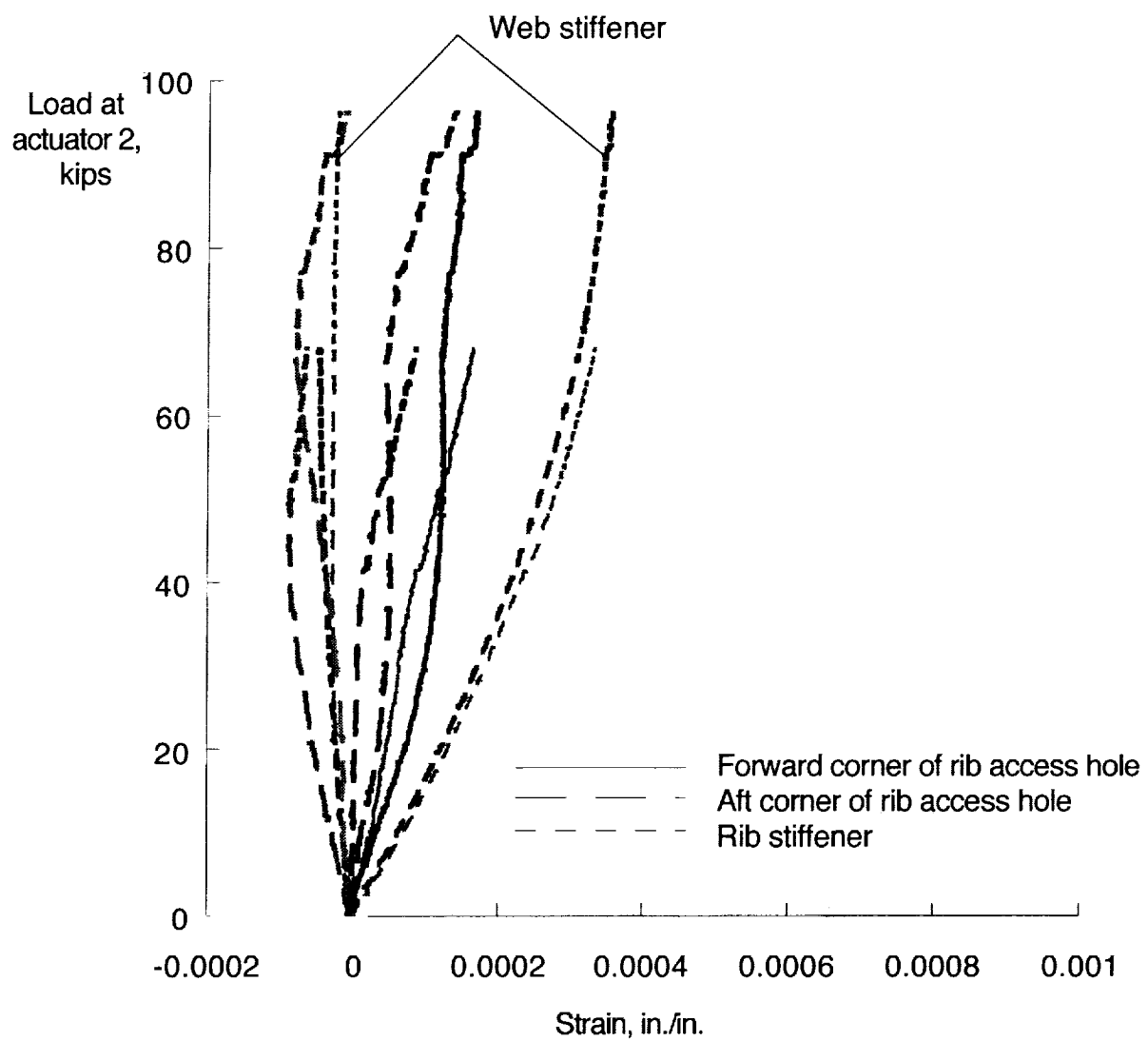
a) Ribs 2 and 3

Figure 74. Effect of repair on strain in ribs in 2.5G load condition. Strain gage locations are shown in figure 11.



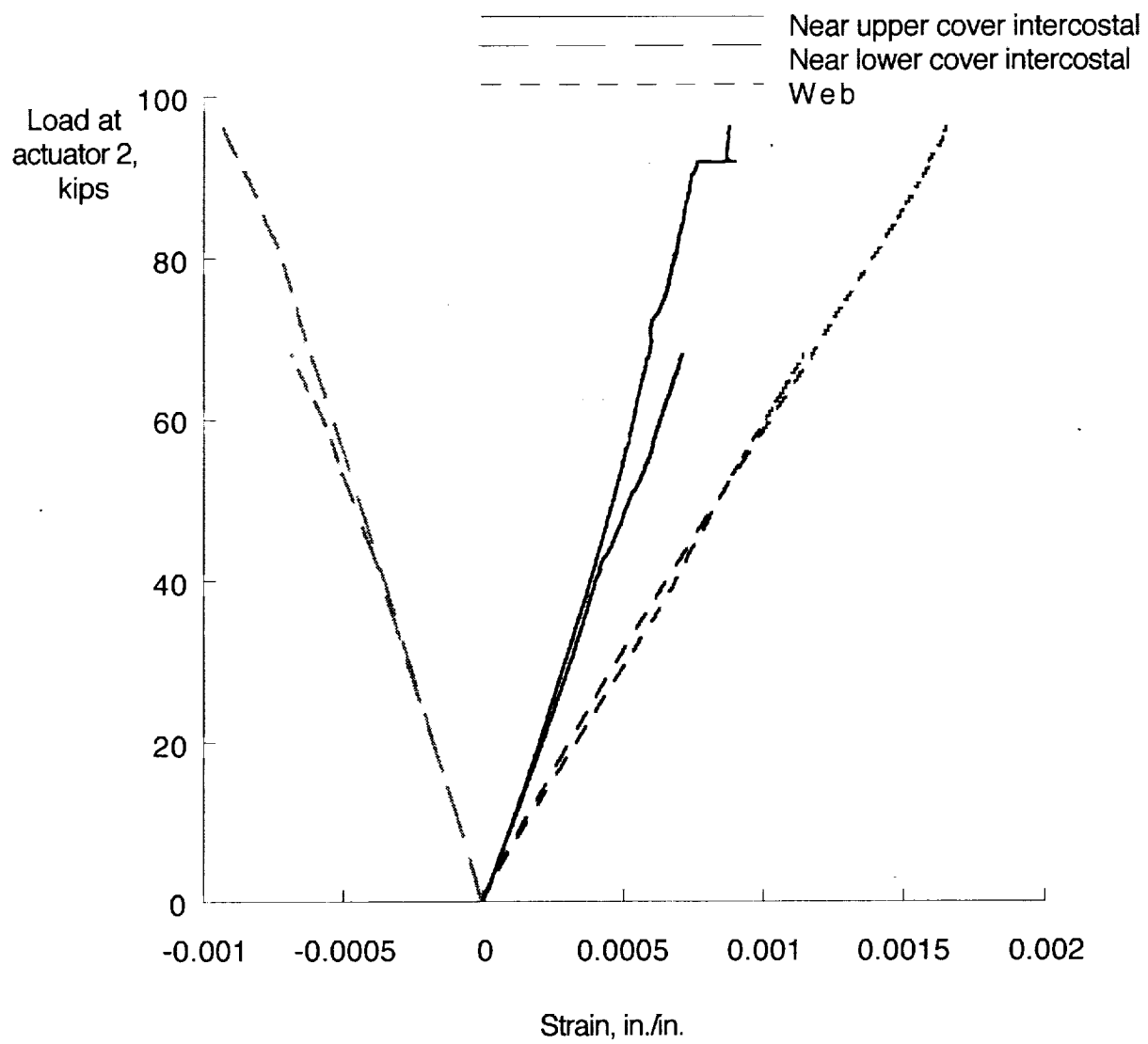
b) Rib 4

Figure 74. Continued.



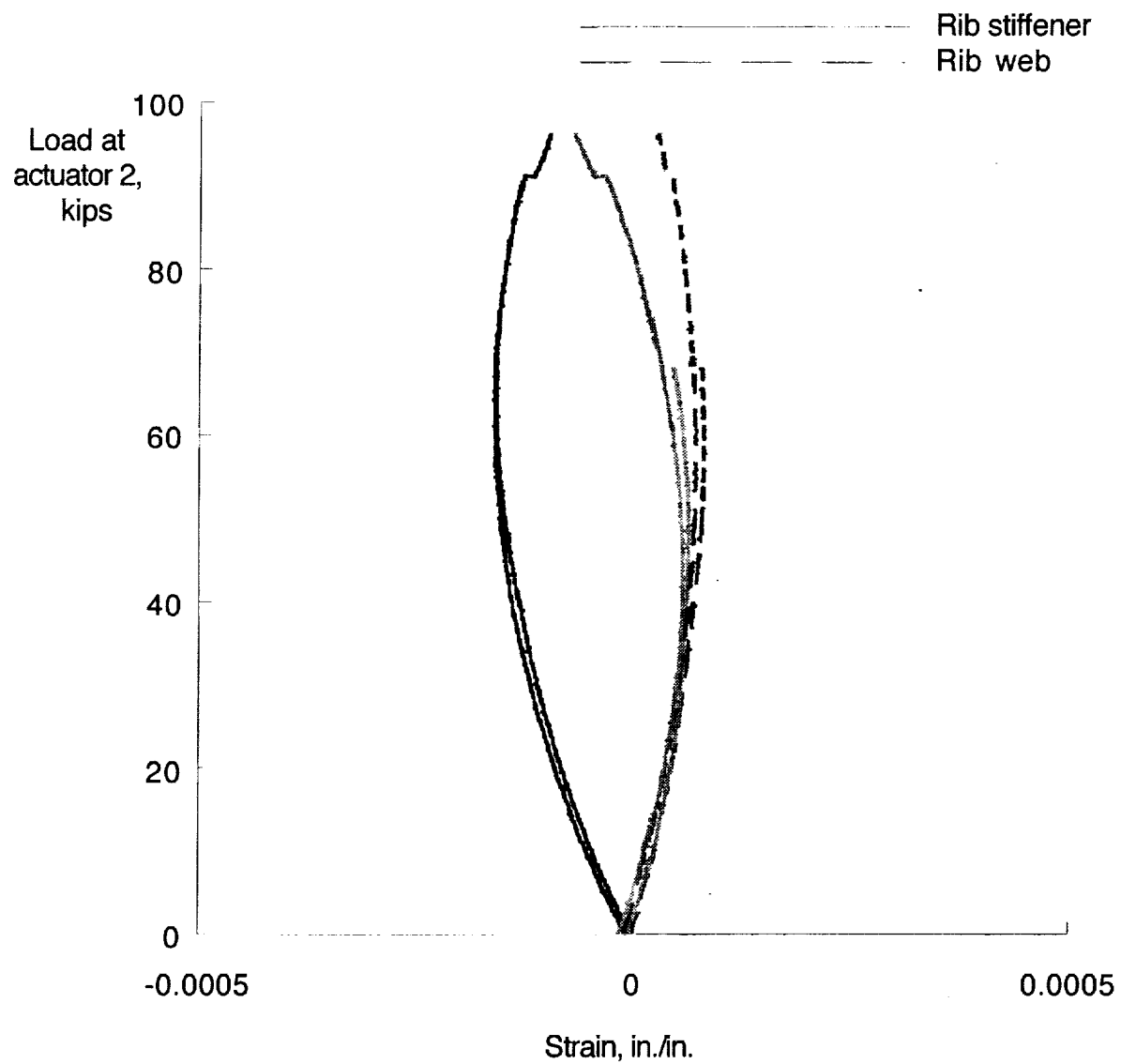
c) Rib 5

Figure 74. Continued.



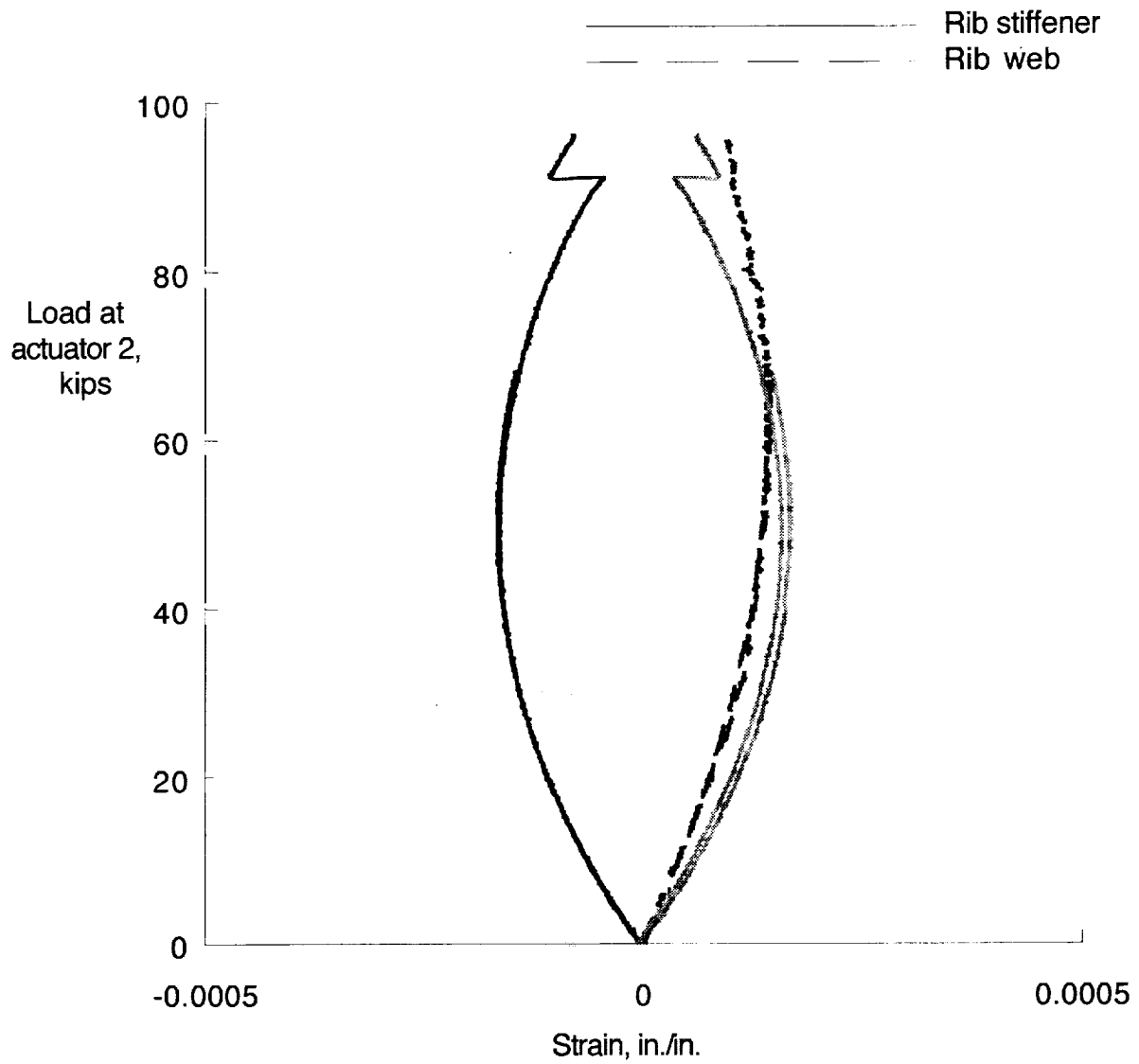
d) Rib 6

Figure 74. Continued.



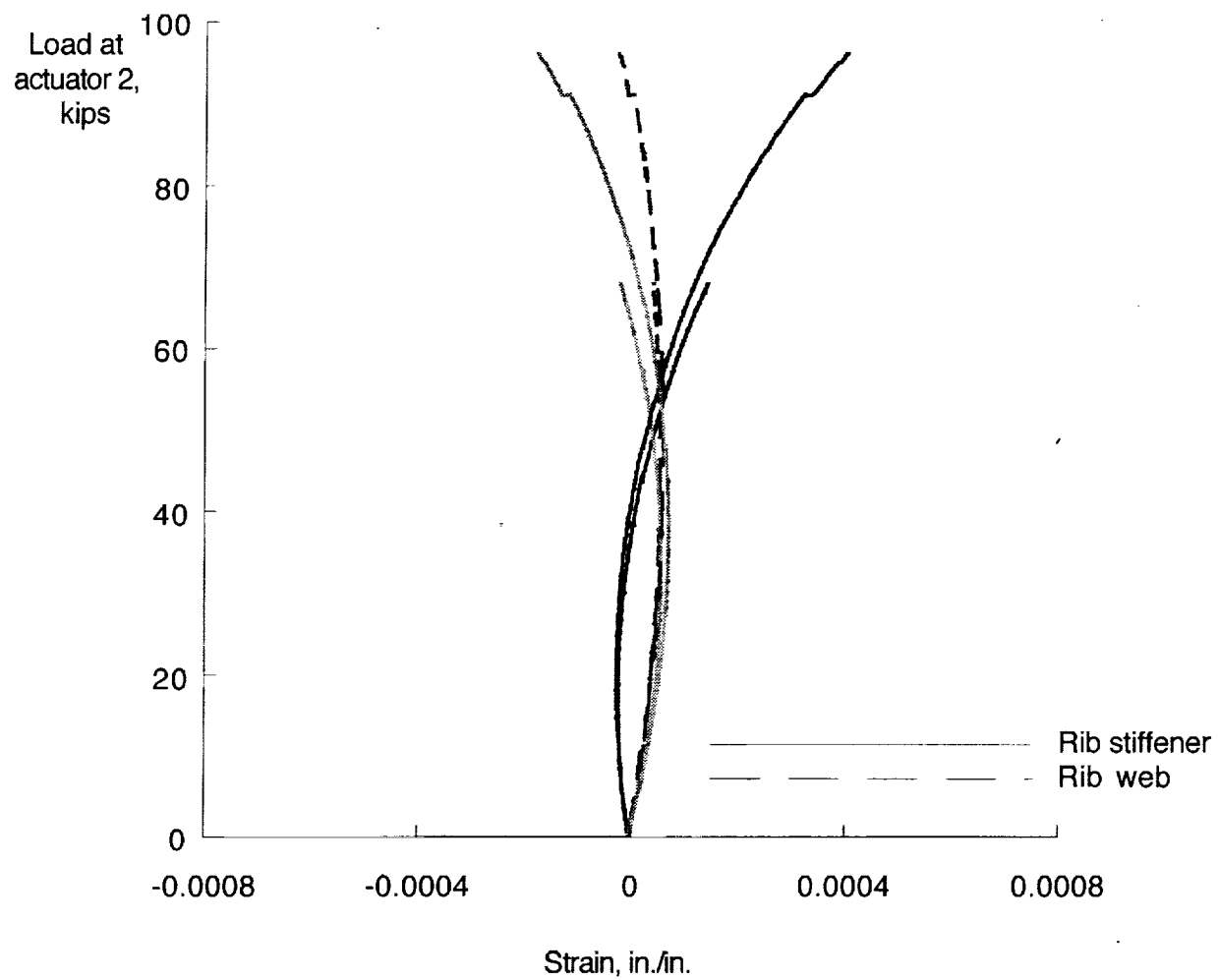
e) Rib 8

Figure 74. Continued.



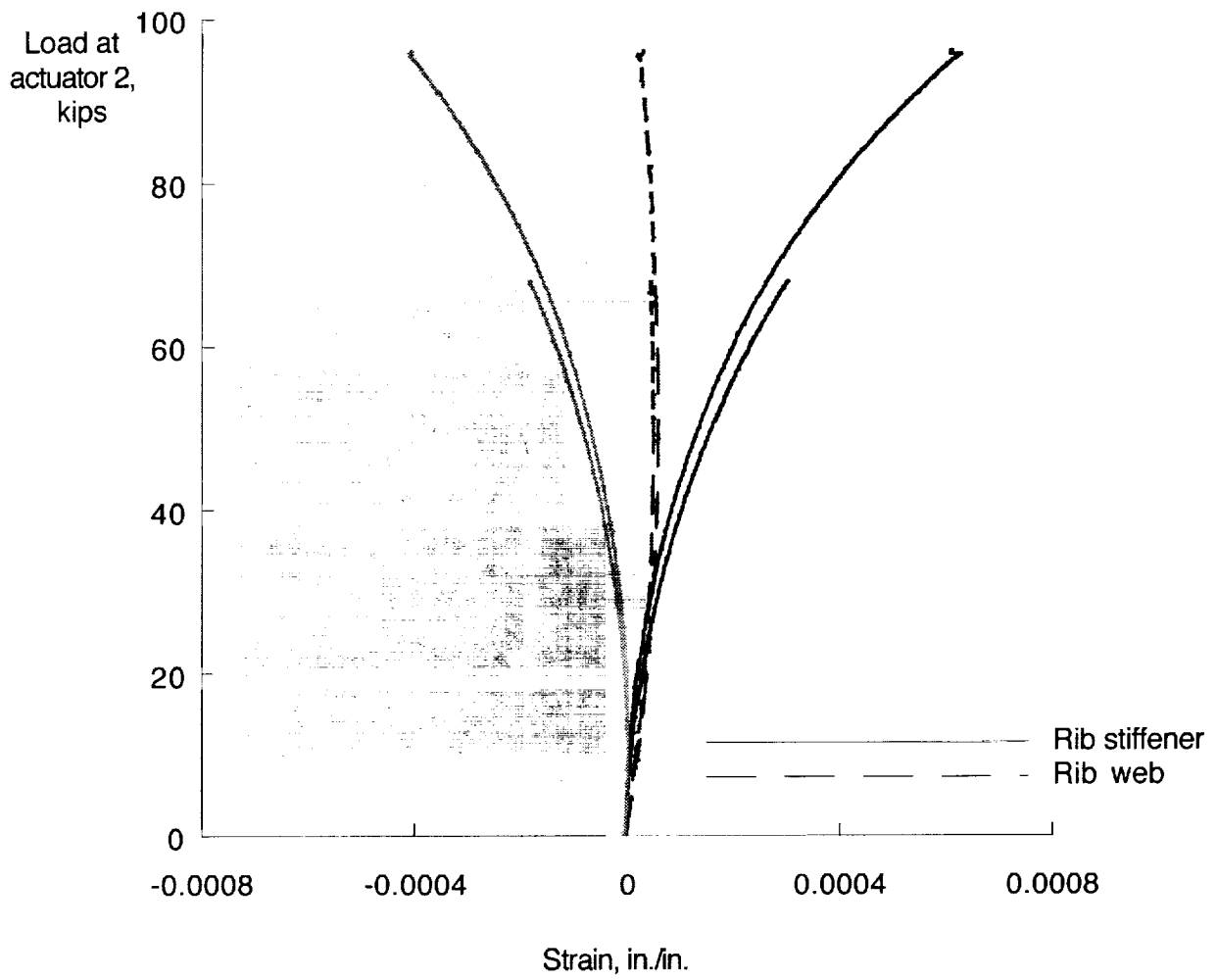
f) Rib 9.

Figure 74. Continued.



g) Rib 10

Figure 74. Continued.



h) Rib 11

Figure 74. Concluded.

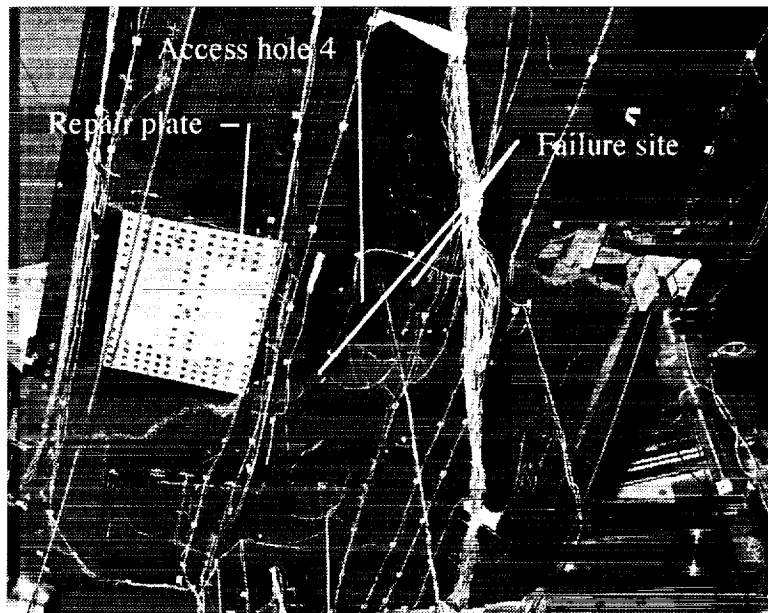


Figure 75. Failure across lower cover panel.

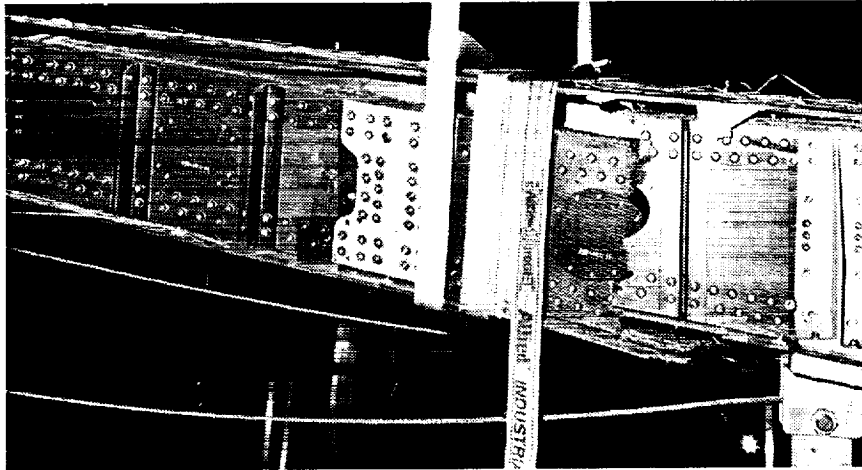


Figure 76. Rear spar after final test.

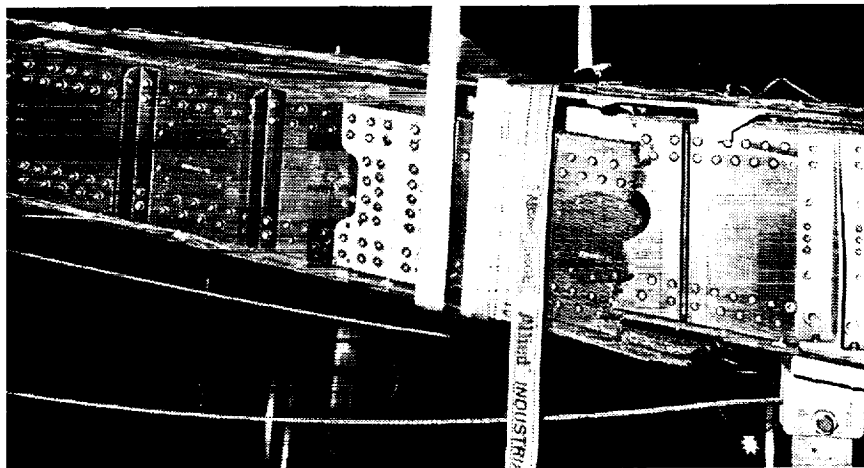


Figure 77. Front spar after final test.

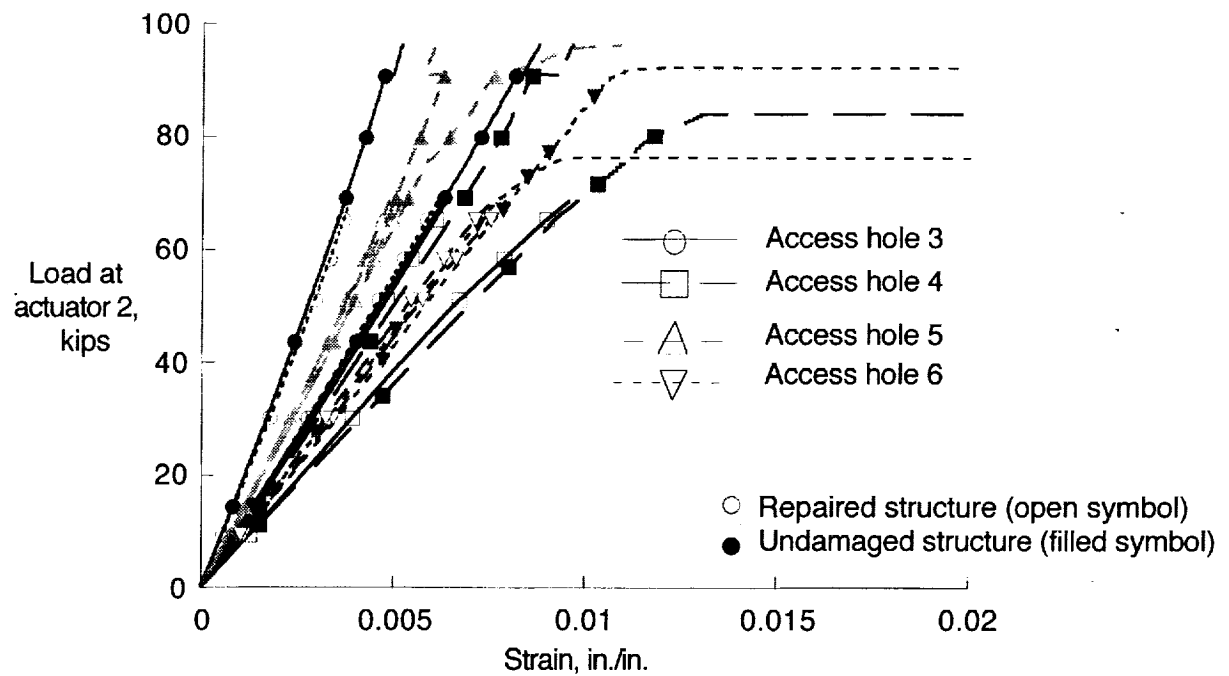


Figure 78. Measured strain at access hole edges for load to DLL and to failure in 2.5G load condition.

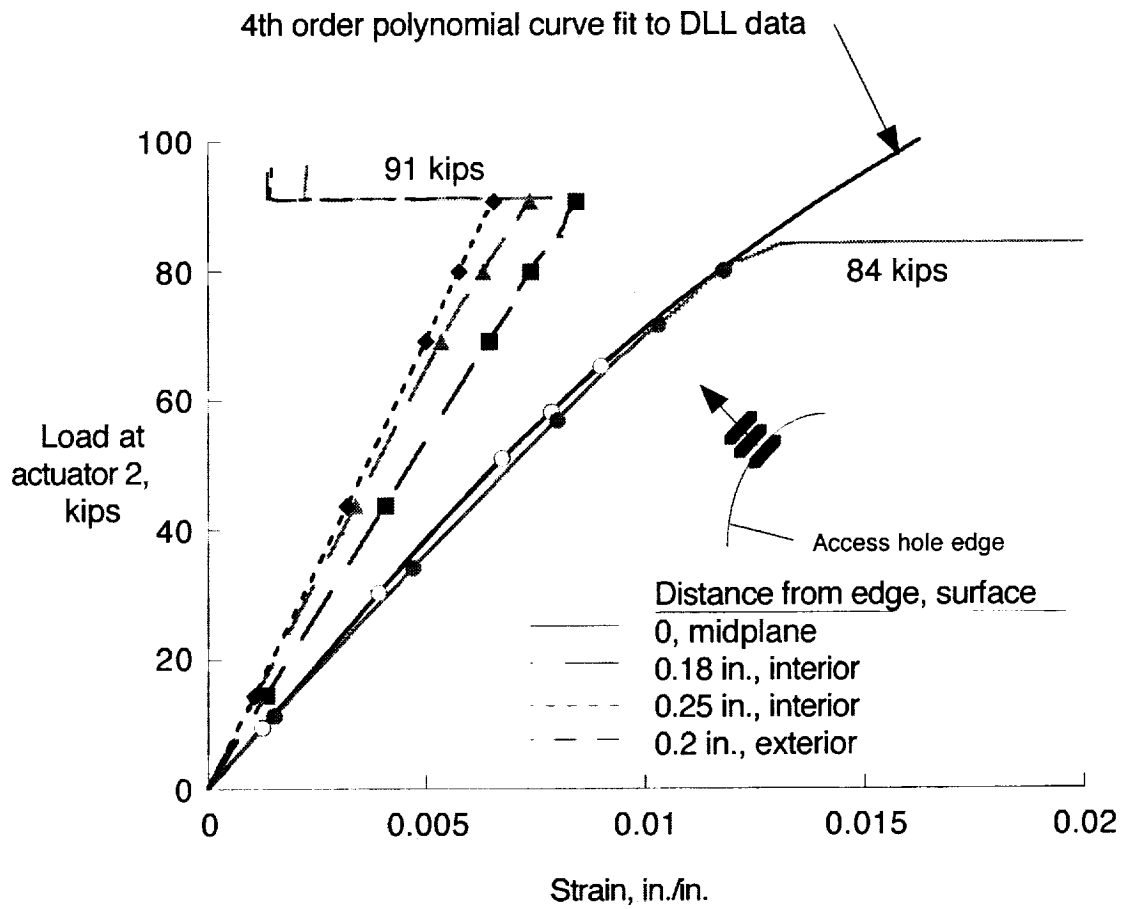


Figure 79. Strain at edge of access hole four.

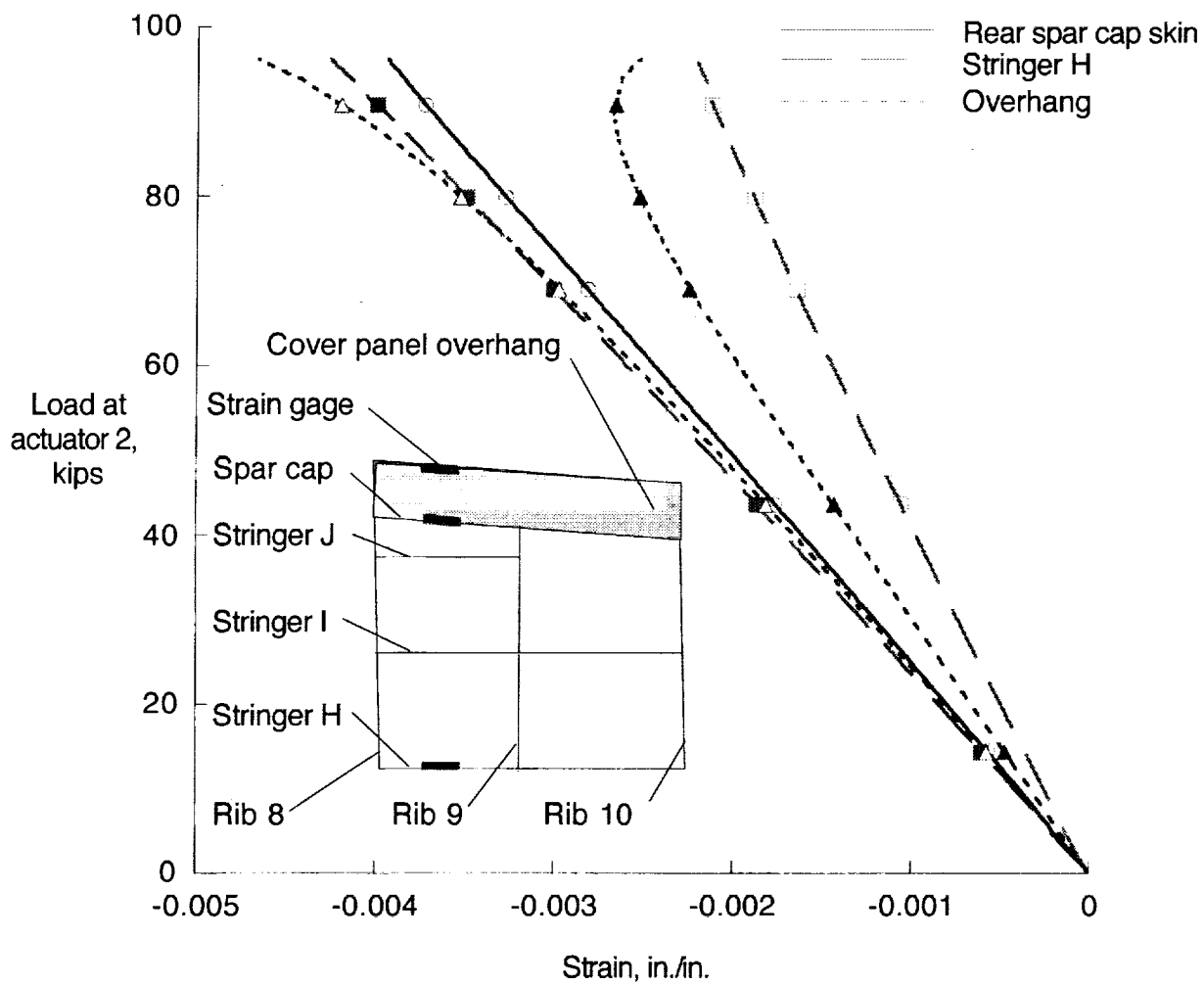


Figure 80. Strains in cover panel overhang region behind rear spar.

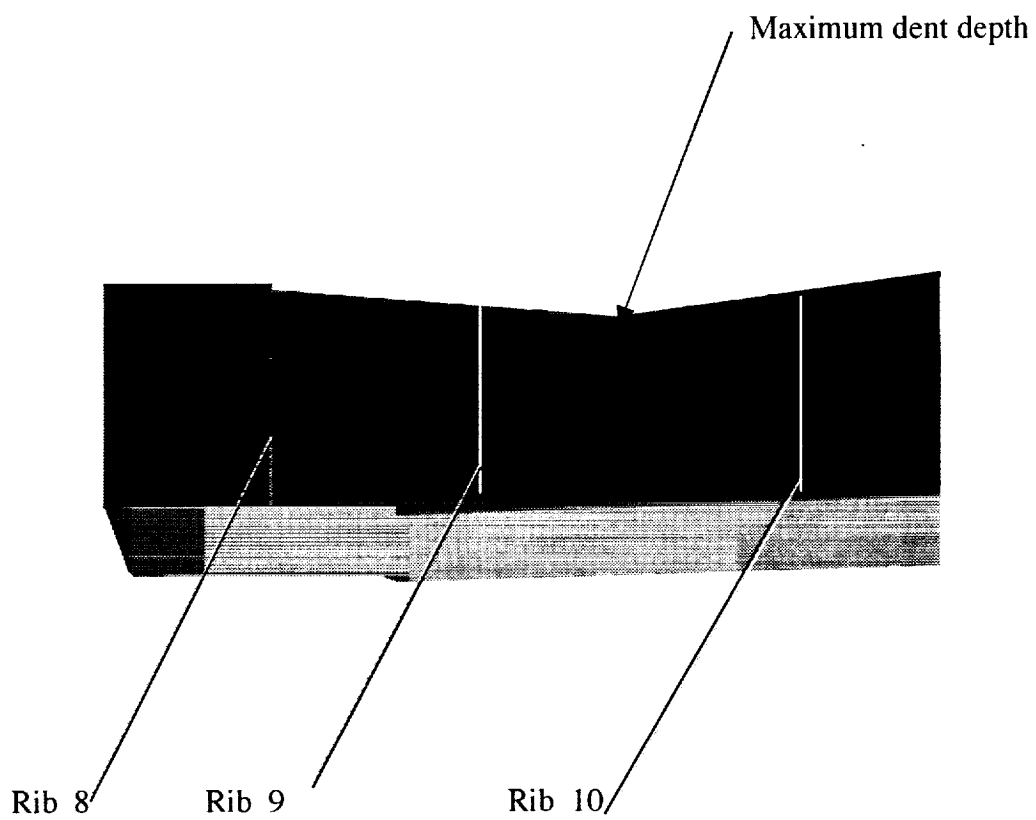


Figure 81. Imperfection in rear of upper cover panel.

REPORT DOCUMENTATION PAGE			Form Approved OMB No. 0704-0188	
Public reporting burden for this collection of information is estimated to average 1 hour per response, including the time for reviewing instructions, searching existing data sources, gathering and maintaining the data needed, and completing and reviewing the collection of information. Send comments regarding this burden estimate or any other aspect of this collection of information, including suggestions for reducing this burden, to Washington Headquarters Services, Directorate for Information Operations and Reports, 1215 Jefferson Davis Highway, Suite 1204, Arlington, VA 22202-4302, and to the Office of Management and Budget, Paperwork Reduction Project (0704-0188), Washington, DC 20503.				
1. AGENCY USE ONLY (Leave blank)		2. REPORT DATE April 2001		3. REPORT TYPE AND DATES COVERED Technical Memorandum
4. TITLE AND SUBTITLE Structural Testing of a Stitched/Resin Film Infused Graphite-Epoxy Wing Box			5. FUNDING NUMBERS 706-63-71-11	
6. AUTHOR(S) Dawn C. Jegley and Harold G. Bush				
7. PERFORMING ORGANIZATION NAME(S) AND ADDRESS(ES) NASA Langley Research Center Hampton, VA 23681-2199			8. PERFORMING ORGANIZATION REPORT NUMBER L-18071	
9. SPONSORING/MONITORING AGENCY NAME(S) AND ADDRESS(ES) National Aeronautics and Space Administration Washington, DC 20546-0001			10. SPONSORING/MONITORING AGENCY REPORT NUMBER NASA/TM-2001-210846	
11. SUPPLEMENTARY NOTES				
12a. DISTRIBUTION/AVAILABILITY STATEMENT Unclassified-Unlimited Subject Category 39 Distribution: Nonstandard Availability: NASA CASI (301) 621-0390			12b. DISTRIBUTION CODE	
13. ABSTRACT (Maximum 200 words) The results of a series of tests conducted at the NASA Langley Research Center to evaluate the behavior of an all-composite full-scale wing box are presented. The wing box is representative of a section of a 220-passenger commercial transport aircraft wing box and was designed and constructed by The Boeing Company as part of the NASA Advanced Subsonics Technology (AST) program. The semi-span wing was fabricated from a graphite-epoxy material system with cover panels and spars held together using Kevlar stitches through the thickness. No mechanical fasteners were used to hold the stiffeners to the skin of the cover panels. Tests were conducted with and without low-speed impact damage, discrete source damage and repairs. Up-bending, down-bending and brake roll loading conditions were applied. The structure with nonvisible impact damage carried 97% of Design Ultimate Load prior to failure through a lower cover panel access hole.				
14. SUBJECT TERMS graphite-epoxy, stitching, resin film infusion, impact damage, discrete source damage			15. NUMBER OF PAGES 121	
			16. PRICE CODE A06	
17. SECURITY CLASSIFICATION OF REPORT Unclassified	18. SECURITY CLASSIFICATION OF THIS PAGE Unclassified	19. SECURITY CLASSIFICATION OF ABSTRACT Unclassified	20. LIMITATION OF ABSTRACT UL	

NSN 7540-01-280-5500

Standard Form 298 (Rev. 2-89)
Prescribed by ANSI Std. Z-39-18
298-102